University of Cape Town
Department of Civil Engineering

CONVENTIONAL and NON-CONVENTIONAL STRESS PATH TESTING of MAGUGA CLAY

Patrick Beales

Bachelor of Science (Eng.)
University of Cape Town, 1999

A thesis submitted to the University of Cape Town in partial fulfilment of the requirement for the Degree of Master of Science in Civil Engineering.

June 2002

Declaration

I, Patrick Beales hereby declare that this thesis that I submit to the Department of Civil Engineering, University of Cape Town, in partial fulfilment of the requirements for the Degree of MSc (Civil Engineering), is my own work, except where otherwise indicated, and has not, to the best of my knowledge, been submitted for a degree at any other university.

Patrick David Beales

June 2002

Synopsis

The research work undertaken in this Master's dissertation focused on the soil behaviour of Maguga clay in terms of stress-strain-strength characteristics. The behaviour of the clay is investigated from two different testing perspectives, namely conventional and non-conventional stress path testing.

Comparisons are drawn from conventional triaxial compression testing investigating undisturbed and remoulded clay specimens. Marginal differences with respect to conventional stress-strain characteristics and shear strength are observed. The conclusion is drawn that, where possible, undisturbed triaxial testing should be undertaken because the *in-situ* soil structure cannot be adequately simulated in the laboratory using remoulded samples. The conventional triaxial results are incorporated with consolidation tests in order to compile the critical state concept, which enables a conventional back-prediction to be compiled. The back-prediction simulated the undisturbed test results more effectively than the remoulded test results.

The non-conventional stress paths consisted of sequential combinations of various common stress paths. The non-conventional paths simulated a stress history, which preconditioned the remoulded soil structure before failure was induced. Different soil responses for the non-conventional stress path tests are observed in the triaxial test results. The remoulded soil structure responded as in a stiff manner when various combinations of stress paths are applied and as a plastic material when the soil structure integrity is destabilised by pore water dissipation. There are no experimental specifications and sparse research literature regarding non-conventional stress paths even though such paths do realistically occur in geotechnical structures.

The non-conventional stress path results are incorporated into the critical state concept, although the model is limited to formulation from standard triaxial test applications. The critical state analysis of Maguga clay shows that no matter what or how many stress paths are simulated, they all tend to follow various yield surfaces. These yield surfaces approach the critical state surface from different states of applied stress, suggesting that perhaps the non-conventional stress paths can be applied to the many models that are based on the prediction of the reliability of experimental test results.

Table of Contents

List of Illustrations and Tables

Figures

Tables

Table of Nomenclature

B	-	Skempton saturation factor
c'	kPa	cohesion of soil in terms of effective stress
G_s	-	specific gravity of soils
K	-	coefficient of lateral stress
K_o	-	coefficient of earth pressure at rest
M	-	critical state stress ratio
N	-	specific volume intercept of isotropic normal compression line defined at $p' = 1$ kPa
p'	kPa	effective mean stress
p'_f	kPa	effective mean stress at failure
p'_e	kPa	equivalent mean stress in terms of effective stress
q	kPa	deviator stress
q_f	kPa	deviator stress at failure
u, u_w	kPa	pore water pressure
v	-	specific volume
v_λ	-	specific volume of critical state line defined at $p' = 1$ kPa
v_κ	-	specific volume of unloading line defined at $p' = 1$ kPa
ε_{axial}	%	axial strain
ϕ'	degrees	angle of internal friction in terms of effective stress
η	-	stress ratio factor (q/p')
κ	-	unloading gradient of consolidation compression curve
λ	-	gradient of critical state line
$\sigma_1, \sigma_2, \sigma_3$	kPa	major and minor principal stresses in terms of total stress
σ'_v, σ'_h	kPa	vertical and horizontal effective stress
τ	kPa	shear stress
Γ	-	specific volume intercept of critical state line defined at $p' = 1$kPa
Λ	-	critical state consolidation parameter

CHAPTER 1

INTRODUCTION

1.1 Introduction

Maguga Dam is situated 15 km north of Piggs Peak in Swaziland and is the fourth largest earth embankment in Southern Africa. Maguga Dam is a dry core rockfill dam 750m long and 115m high. Rockfill and core material were extracted from areas behind the dam within the inundation zone of the basin area. The UCT geotechnical laboratory was awarded a contract to test the shear strength properties of various core materials. The core materials consisted of brown, sandy-silts and red, slightly silty clays, which were tested in the conventional (standard) triaxial compression manner. The term 'conventional' has long been associated with the typical isotropically consolidated, undrained triaxial compression test. The conventional triaxial compression test has been conducted in standardised triaxial cells, whereby cell pressure is kept constant while the axial pressure is increased.

In recent years developments in geotechnical equipment, control and data acquisition have allowed the simulation of non-conventional triaxial tests in stress space that was previously only attainable in a 'theoretical' context. In reality, the soil is in general exposed to specific or several successive stress conditions in its stress history; obviously the stress conditions will naturally depend on the geotechnical application in question. Following a so-called stress path attains these stress conditions. Each stress path has its own distinct stress characteristics, which was previously unable to be simulated in the triaxial test apparatus. The progression of developments in the field of triaxial testing in the laboratory has not only enabled soil testing to advance into the more complex areas of soil research, but provides an insight into future stress changes within soil masses.

The attributes of the 'modern' triaxial system is noticeably justified by the diversity of worldwide research currently undertaken in geotechnical laboratories in the United

Kingdom, Brazil, Italy, Norway, Portugal, Singapore and South Africa. Geotechnical laboratories are now capable of undertaking advanced stress path testing, but such tests are deemed too complicated for practical application and therefore restricted to research investigations. Unfortunately South African geotechnical laboratories have been restricted to standard testing procedures because of the cost of more advanced and highly sensitive equipment.

The control methodology of non-conventional triaxial testing requires a thorough theoretical understanding of stress states in soil mechanics as well as the experimental technique. The prerequisite to efficient testing is, however, that the experimenter has to gain a competent knowledge of the theoretical fundamentals and is familiar with the control philosophy of the specialised triaxial testing system.

1.2 Research Objectives

As highlighted earlier, developments in geotechnical equipment and data acquisition has enabled reliable stress path simulations of what the soil may experience in the field. Real in-situ soils should be regarded as inelastic, anisotropic and history-dependent materials whose shear strength behaviour cannot be adequately analysed in conventional triaxial testing. It will be shown that conventional stress-strain-strength relationships are a good approximate solution to analysing soil behaviour, but do they really describe the condition of the soil adequately?

The fact that most conventional triaxial tests are undertaken at 100% saturation conditions is in fact itself questionable. The degree of saturation of soil elements in the field are varied, hence the corresponding stress-strain-strength characteristics are in fact different (varied saturation conditions were not investigated in this thesis). Other aspects such as changes in stress path direction, previous stress path history, anisotropic stress preconditioning, and failure characteristics are going to be investigated and shown in this research work.

During the conventional testing period, one of the Maguga test materials (identified as a red clay-MECC765) exhibited 'interesting difficulties' that were attributed to the natural stress history of the material. It was of interest to the research work to see how the material would react to an applied stress 'history', especially as the tests were undertaken on remoulded material. The research work consisted of undertaking non-conventional testing procedures, on the remoulded test material, to investigate whether or not different shear strength characteristics could be attained from different stress 'histories'.

The thesis envisages that there may be different responses from soil that is tested from undisturbed material and that consisting of remoulded material. In fact, the very method of compaction to prepare remoulded material may determine the failure characteristics that will be observed. The differences between undisturbed and remoulded material may be influential from a test result perspective and a soil modeling perspective.

The results of the conventional test configurations of undisturbed and remoulded specimens are analysed to determine the most adequate test, suitable for incorporating into the critical state model. As the initial concept of critical state is based on observations from the behaviour of saturated remoulded clay, an attempt is made to decide if the undisturbed triaxial results would be successfully integrated into the critical state concept. The critical state parameters would then be used to predict the response of undisturbed or remoulded samples.

It is further suggested that remoulded soil subjected to 'stress preconditioning' alters the soil structure of the material to accommodate that particular stress application. The preconditioning of the remoulded soil serves the purpose of applying a past stress history and noting the affect on stress-strain-strength characteristics as different stress paths are followed.

In Figure 1.1 the idealised stress-strain characteristics of soil whose particles are in a plastic or stiff arrangement are shown. No matter what sort of stress history a soil was or is subjected to or to what state of compaction effort the material was prepared, the stress-strain response of the soil always tends to approach a steady state characterised by a critical void ratio, the indicator of the particle packing.

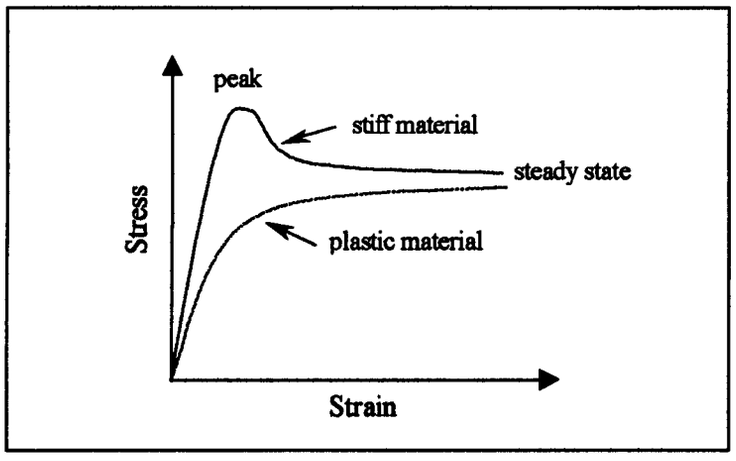

Figure 1.1 Idealised stress-strain characteristics of particulate soil

This steady state is commonly referred to as a residual state of granular or cohesive material. This residual state is of interest in this thesis as it represents the measure of strain after which plastic shearing continues indefinitely without changes in volume or effective stress. The steady state is a common state that all soil material tends to; therefore this similarity in clay can be modeled to assist the understanding of soil behaviour.

The theoretical model that unifies shear strength and volume characteristics is known as critical state concept. The research work will focus on critically analysing the undisturbed conventional triaxial compression test in conjunction with the consolidation test and formulating the critical state parameters.

Critical state assists the geotechnical engineer in predicting undrained as well as drained response by simplifying the representation of different stress/strain conditions into a

single diagram. The compilation of this single diagram for this research work will emphasise, in terms of effective stress, the different modes of stress path testing.

1.3 Research Overview

In this research work, a theoretical review of the stress path method is provided, in terms of how the method has developed. The review is initiated in *Chapter 2* by first considering the chronological development of the stress path method and then discussing the likely field applications of selected non-conventional stress paths in an earth embankment scenario. With this initial basis in place it is of importance that the test material is introduced in *Chapter 3*, firstly from a geological perspective and secondly from a soil mechanical perspective so as to demonstrate the test material properties and gain familiarisation for the test material. Details of the experimental procedure and program for all of the triaxial compression tests are presented in *Chapter 4*, as well as the triaxial control philosophy. *Chapter 5* contains all of the triaxial compression test results, discussions and comparisons with respect to conventional and non-conventional stress path testing. Evaluation of critical state parameters and the back prediction of the conventional stress path analysis are presented in *Chapter 6*. Finally, in *Chapter 7*, conclusions are drawn from the research work and the recommendations for further research are given.

CHAPTER 2

STRESS PATH REVIEW AND APPLICATION

2.1 Introduction

Chapter 2 is divided into two sections. The chronological review of the stress path concept is introduced in the first section. The discussion regarding the stress path method provides clarity to the stress parameters that are used in this thesis. The stresses that are referred to are, namely, the deviator stress (q) and the effective mean stress (p'). The use of the stresses q and p' facilitate a fundamental approach to understanding the shear behaviour of soil as the stress state varies due to conditions of loading and unloading. The variation of stress application, often complex in structural performance, can be analytically approached using the stress path method and expressed in the most convenient terms, namely in q and p', to the geotechnical engineer. The stress path method therefore provides the basis for understanding the concept of a stress path.

The stress path theory introduced in this chapter should be regarded as a helpful method that assists the geotechnical engineer to identify underlying geotechnical situations and, which may allow to some extent, the anticipation of the performance of the soil in the particular structure.

In the second section of *Chapter 2*, some relatively non-conventional stress paths are highlighted, which were experienced and followed in the triaxial tests for this research work. The non-conventional stress path equivalence in the context of field application, within an earth embankment, is simulated using common stress paths that do and could realistically occur. The selected stress paths were specifically undertaken on a test material (clay) that was associated in the construction of an earth dam in Swaziland (Komati Joint Venture, 2000). Some details about the dam, the description of the test material and the soil mechanical properties will be presented in *Chapter 3*.

Stress paths that occur beneath or within earth embankments were previously unable to be simulated in a standard triaxial compression device in the geotechnical laboratory. Simulation of those stress processes is now capable with the development of sophisticated testing equipment, the hardware and the software for data acquisition. The developments over the last decades have enabled triaxial testing to progress to stress/displacement zones that were only known to be theoretically possible. The identification of the specific stress paths is presented in acronym fashion to facilitate the easy and quick demonstration and reference of the stress paths in these stress/strain zones.

2.2 Stress Path Theory

2.2.1 Introduction

The stress path method was described by Lambe (1967) and Lambe & Marr (1979), Pender (1980) and Fredlund & Rahardjo (1993) as an important tool in geotechnical engineering as it investigates the changes in stress state that a soil structure undergoes in its historical development and the consequences in the field application. The stress states in the stress path method can be represented by Mohr circles in the τ-σ diagram.

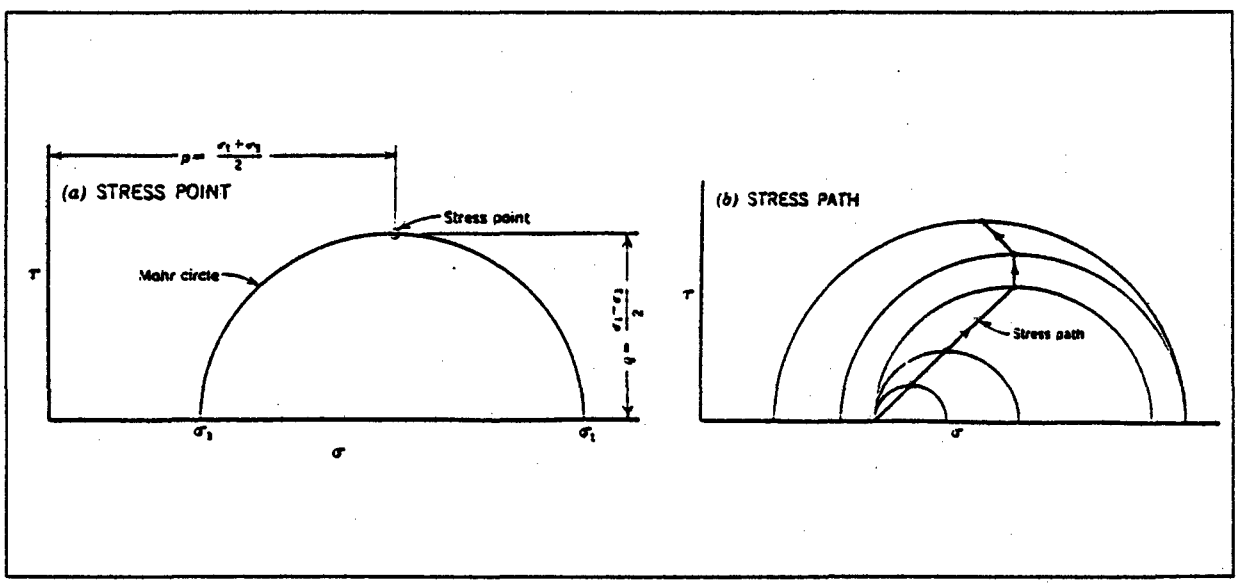

Figure 2.1 Mohr circle diagram in terms of selected stress points (Lambe, 1967)

In Figure 2.1 the basic illustration of typical Mohr circles in a τ-σ diagram in terms of a selected stress point governed by the stress parameters defined as q and p are shown (all stresses are at this stage shown in total terms). The peak stress point represents the point of maximum shear stress at a specific stress state comprising of principal stresses σ_1 and σ_3. This peak point itself is defined by the stresses q and p. These shear strength parameters will be elaborated in more detail in the coming sub-sections. In a conventional triaxial compression test σ_3 is kept constant and σ_1 varies as the loading is increased. The result is that a number of different stress states (each represented by a Mohr circle starting at an initial mean stress p) are passed through. If the peak stress points of the circles were joined, a path is identified representing the different stresses applied to a soil element in the process of a test. This line of interconnected stress points is known as the stress path.

The construction of Mohr circle plots is cumbersome to derive for non-conventional triaxial tests in terms of plane strain situations. The fact that Lambe & Marr (1979) choose to ignore the principal stress σ_2 (due to plane strain considerations), suggests that the influence of the intermediate principal stress is of less importance and has been neglected in the method. Lambe & Marr (1979) concluded that the contribution of the principal stress σ_2 was small in a number of geotechnical stress/strain situations, but Pender (1980) amongst others, demonstrated a case where intermediate principal stress σ_2 influenced the quantity an engineer predicts and cannot be ignored. In his research it is further illustrated that the influence of the intermediate principal stress σ_2 could be captured by using a three-dimensional representation of stress that is conveniently portrayed in terms of q and p. This formed the basis of representation of a stress state in the q-p' diagram.

2.2.2 Effective Stress Principle

The geotechnical engineer generally applies the limit equilibrium analysis in the field to calculate stresses and loads. Hence he is concerned with stress in the stress path method, and thus not strain. Stresses and forces can be approximated with a degree of accuracy in the field, while strain can be regarding as an undefined variable. The fundamental basis

for understanding the behaviour of saturated soils, in terms of stresses, is accepted in geotechnical engineering as the Effective Stress Principle. The principle of effective stress was first stated by Terzaghi (1936) and is attributed with being the catalyst of modern soil mechanics. The principle requires that all measurable effects associated with changes in stress, such as straining and changes of strength, occur as a consequence of a change of effective stress.

In the triaxial compression context, the transmission of stresses in saturated soil under an applied load originates from the cell confining pressure σ, which applies a total stress σ normal to the triaxial sample boundaries. The pressure of the water in the void spaces, the pore water pressure, acts equally in all directions in the test sample. This pressure is referred to as the pore water pressure (u_w) and exerts a pressure u_w normal to the triaxial sample boundaries. Thus, the difference between the total stress and the pore pressure is transmitted across the boundary to the soil grains and is known as the 'effective stress' (σ'). The equation defining the effective stress is:

$$\sigma' = \sigma - u_w \tag{2.1}$$

2.2.3 Cambridge Stress Field Method

Lambe & Marr (1979) introduced the concept of 'stress paths', ignoring the principal stress σ_2. Roscoe et al (1958) developed the use of the mean of the three principal stresses (σ_1,σ_2, σ_3) instead of the mean of the major and minor principal stresses (σ_1,σ_3). This method became known as the Cambridge Stress Field method. The effective mean stress p' and deviator stress q are defined in terms of effective stress by the following equations:

$$p' = \frac{\sigma'_1 + \sigma'_2 + \sigma'_3}{3} = \frac{\sigma'_1 + 2\sigma'_3}{3}$$

$$q = \sigma'_1 - \sigma'_3 = \sigma_1 - \sigma_3 \tag{2.2}$$

Graphical representation of the stresses q and p'

The stresses q and p' can be illustrated from a set of triaxial compression tests by using stress paths. In Figure 2.2 the three effective stress paths from a conventional triaxial compression test in the Cambridge stress field is shown. The stress paths rise at a slope of 3:1 from effective mean stress σ'_3 and terminate on the failure line.

The Cambridge or MIT stress plot is fundamentally advantageous as it presents the state of stress with regard to the mode of failure conveniently better than other methods, such as the Mohr circle method. The behaviour of elastic soils is also a particular property associated with the Cambridge Stress Plot method. The term 'elastic' refers to the recoverable states that can be attained from particular soils at low stress-strain regions. The undrained effective stress path for such an elastic soil consists of a constant p' stress path by definition of the method (Head, 1986). This particular stress path will be discussed in the non-conventional stress path section.

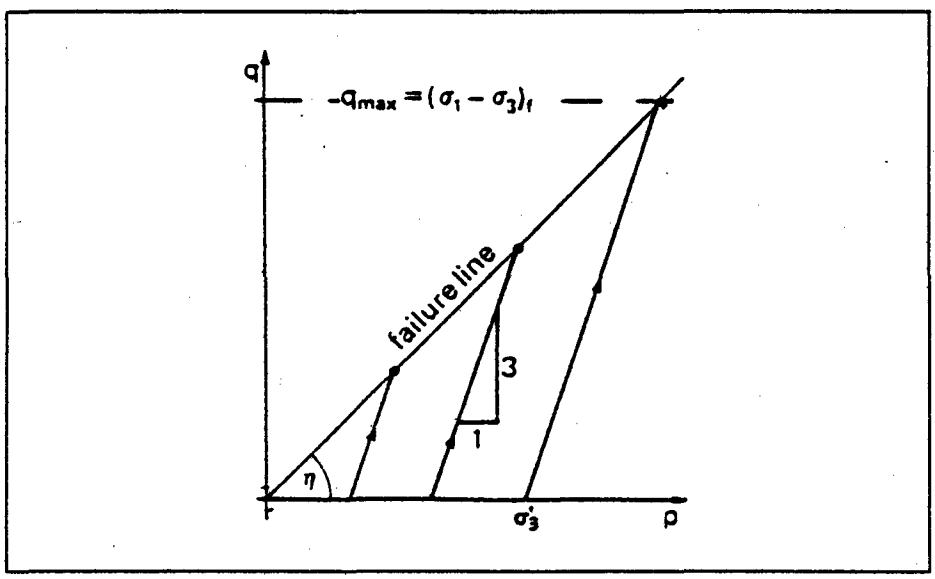

Figure 2.2 Cambridge stress field with stress paths (Head, 1986)

The Cambridge stress plot can be expanded by plotting volume changes, in terms of void ratio or specific volume in a plane perpendicular to the q-p' plane. A three-dimensional space representing stresses and deformation is obtained. Such three-dimensional

stress/deformation fields have been used extensively in 'critical state' formulation. The critical state concept will be presented in *Chapter 6*.

Derivation and conversion of the shear strength parameters ϕ' and c'

Triaxial tests are performed on axisymmetrical samples and the response of the sample is exposed to a state of stress according to the respective stress path application. In Figure 2.3 a Cambridge shear strength diagram with effective stress paths (ESP) at selected mean effective pressures (p'_o) are shown. The initial p'_{oi} are equal to the principal effective stress σ_3'. The line drawn through the set of peak points representing failure (i.e. maximum q and maximum p' values) identifies the failure line or failure surface.

Although q-p' diagrams are presented in terms of effective stresses in this thesis, there are other paths associated with the Cambridge Stress Plot method, namely the total stress path (stress paths expressed in q versus p) and the path of total stress minus static pore pressure (where q versus $\{p-u_s\}$). These stress paths are not shown in Figure 2.3.

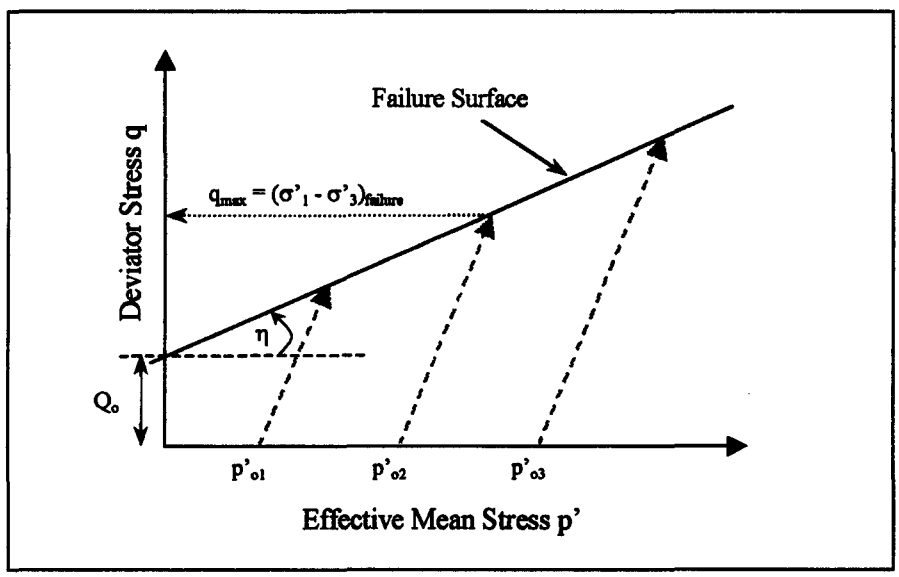

Figure 2.3 Cambridge shear strength diagram with stress paths at selected p'_o

The failure surface can be formulated in terms of q-p' values as $q = p'.\tan\eta + Q_o$. The Mohr-Coulomb shear strength parameters (ϕ' and c') can be calculated from this

relationship where η is the inclination and Q_o the intercept of the failure line. The angle of internal friction ϕ' and cohesion c' in effective terms are calculated using the following conversion equations:

$$\sin\phi' = \frac{3\tan\eta}{6+\tan\eta}$$

$$c' = \frac{3-\sin\phi'}{6\cos\phi'}(Qo) \qquad (2.3)$$

2.2.4 Representation of stress paths in principal stress space

Elements of soil are subjected to loading or unloading in vertical and horizontal direction during their stress history. At different locations in the vicinity of a structural element the soil elements are exposed to different stress paths. For the purposes of predicting the behaviour of soil, it is imperative that all the major stress paths that are experienced in reality are known and simulated in the laboratory. Desai & Siriwardane (1984) identified the most common stress paths in terms of principal stress space. In Figure 2.4 those paths are projected into the triaxial plane. Each stress path has a name according to principal loading direction. The respective acronyms are given.

Stress Path Acronyms:

PL = Proportional Loading
RTC = Reduced Triaxial Compression
TC = Triaxial Compression
SS = Simple Shear
CTC = Conventional Triaxial Compression
HC = Hydrostatic Compression
CTE = Conventional Triaxial Extension
TE = Triaxial Extension
RTE = Reduced Triaxial Extension

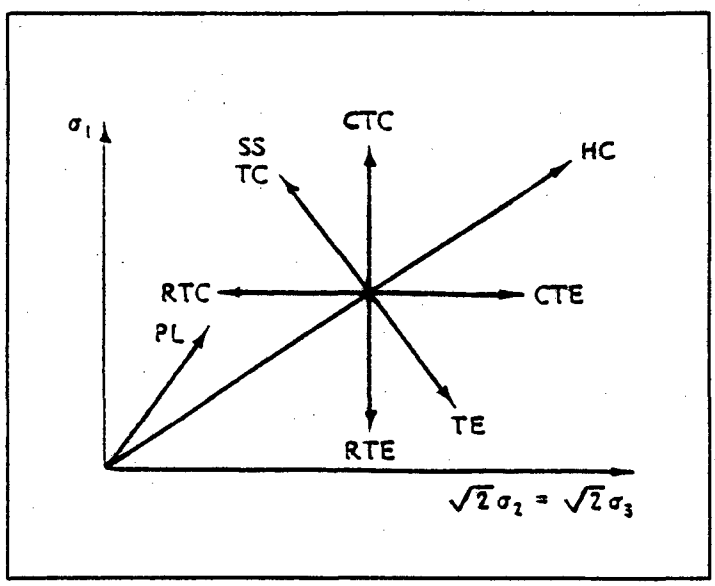

Figure 2.4 Schematic representations of common stress paths in the triaxial stress space (Desai & Siriwardane, 1984)

The stress paths discussed in this thesis are presented in the Cambridge q-p' diagram, however they are identified in accordance with the respective stress paths in principal stress space. The identification of the common stress paths forms an important component in the following section on non-conventional stress paths. Explanations defining the non-conventional stress paths are represented in the subsequent section. The simulation of the non-conventional stress paths and the effect on some selected field application where stress paths of that nature will occur, is discussed.

2.3 Non-Conventional Stress Paths

Non-conventional stress paths consist of combinations of common stress paths that are applied in a particular sequence, so that a simulated stress history can be represented. State-of-the-art triaxial testing is capable of fully automated control in an unlimited range of non-conventional stress paths. The operation of computers in conjunction with specialised triaxial cells has improved the stress/strain application of stress paths. The *in-situ* stress path of any particular soil can be followed in the laboratory, therefore allowing the simulation of complex loading and unloading processes in the field.

As this research work in its first phase focused on the simulation of stress conditions and to compile meaningful data for the subsequent modeling exercise, it was essential that major stress paths, which could be experienced in reality in a particular situation, be followed and investigated.

This was undertaken in two distinct initial load applications, namely, starting at an isotropic stress state (consolidation) creating an isotropic stress condition, which corresponds to standard or conventional test approach. The other starting point was a zero all-round pressure ($p_o = 0$), followed by an anisotropic load application creating anisotropic stress conditions in the test sample. Different simulated stress histories were applied to the test samples to produce non-conventional stress paths.

Conventional triaxial compression tests are either undertaken in drained or undrained conditions, which are easily distinguishable in the standard context. Specific non-

conventional stress paths are undertaken in a controlled 'drained' condition, which consists of a controlled or 'locked-in' pore water pressure. The 'locked-in' pore water pressure is undertaken at a relatively high pressure so that the dissolved air in the water does not dissolve out of solution. This controlled 'drained' condition is described as a quasi-drained condition in the non-conventional triaxial tests. The relevant quasi-drained conditions will be recognised as a controlled 'drained' condition for this research work.

The details of the non-conventional stress paths are discussed in the subsequent sub-sections.

2.3.1 Proportional Loading (PL) in conjunction with Conventional Triaxial Compression (CTC) and Reduced Triaxial Compression (RTC)

The starting point of the stress path for soil samples subjected to anisotropic compression or proportional loading (PL) is at the zero (isotropic) stress condition ($p'_o = 0$). The diagonal movement in stress space is achieved by means of incremental loading of the effective mean stress and the deviatoric stress. The incremental loading is applied as a ratio of principal stresses σ'_1 and σ'_3 (or q and p') so that it remains constant during the loading. In Figure 2.5, the PL stress path or anisotropic compression path of a ratio K_o of 0.50 is shown.

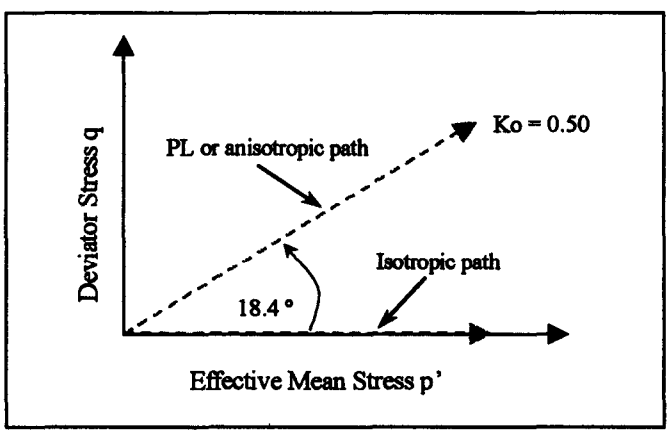

Figure 2.5 Anisotropic compression or PL stress path

According to the theory of lateral earth pressure it is generally assumed that at any point in a soil deposit, the horizontal effective stress σ'_h (σ'_3) is different from the vertical effective stress σ'_v (σ'_1). The ratio of these stresses is known as the coefficient of lateral stress (K). If the lateral stress condition is at 'rest', the soil experiences no lateral strain. The ratio is denoted as the 'coefficient of earth pressure at rest' (K_o) and is expressed as:

$$K_o = \sigma'_h/\sigma'_v = \sigma'_3/\sigma'_1 \qquad (2.4)$$

The value of K_o adopted in this research work was based upon the expression given by Jaky (1944) and suggested by Wood (1990) as an approximate value for soil materials with an internal angle of friction ϕ' between 20° and 45°. The empirical expression for K_o is:

$$K_o = 1 - \sin\phi' \qquad (2.5)$$

In Figure 2.6(a) a 'drained' proportional loading (PL) stress path is shown, followed by a conventional undrained triaxial compression (CTC) stress path. The CTC stress path is a conventional path where the major principal stress σ_1 is incrementally increased during the final stage of the triaxial compression test, while the minor principal stresses σ_2 and σ_3 are kept constant. The straight line drawn through the maximum points of the CTC path represents the failure surface.

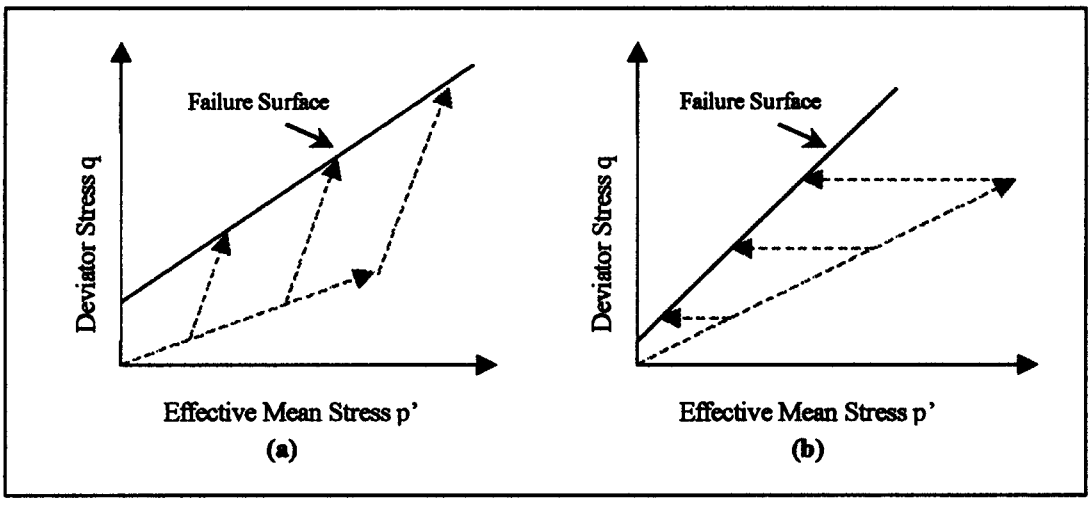

Figure 2.6 (a) PL-CTC stress paths; (b) PL-RTC stress paths.

In Figure 2.6(b) a 'drained' PL stress path that precedes an undrained reduced triaxial compression (RTC) stress path is shown. All stress paths shown in Figure 2.6 are initiated and preconditioned along the K_o line (with K_o = 0.50), until predetermined effective mean stresses are achieved. The RTC stress path is followed by incrementally reducing the confining stresses while the axial stress is kept constant.

2.3.2 Field applications of PL-CTC and PL-RTC stress paths

It is accepted that stress paths could be followed in various combinations and implemented in different applications, however since the test material originates from an earth embankment, embankment applications will be considered. Soil elements within an earth embankment are assumed to have had sufficient time for consolidation. The soil has 'settled' and a state of equilibrium exists. At this stage there is no lateral deformation and the value of the stress ratio K would be equal to the coefficient of lateral earth pressure K_o.

The K_o preconditioning within the soil element can be a rather complex process, considering the many stress conditions that the soil can be exposed to. Any choice of applied stress condition can be applied. For simplicity only two common stress paths, (namely the CTC and RTC paths), are followed starting at the K_o line.

Stress interventions that affect soil behaviour are characterised in two manners, namely a physical intervention by man and a natural process. A selected physical intervention represented by the PL-CTC stress path is shown in Figure 2.7.

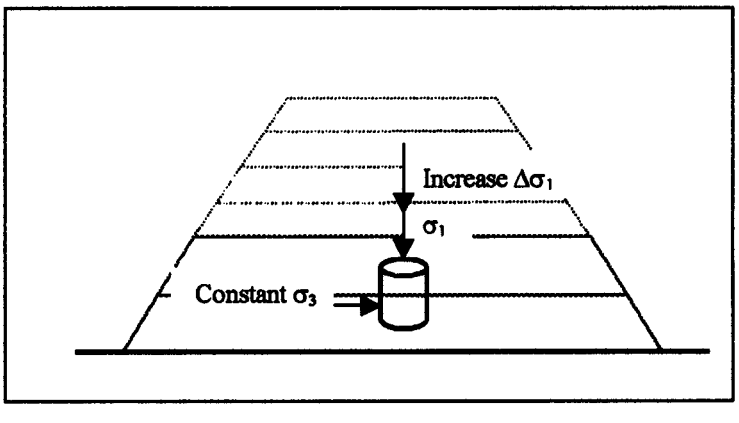

Figure 2.7 Field application of PL-CTC stress path

In the schematic of Figure 2.7, a K_o condition has been reached and the soil is in equilibrium in the existing embankment. As the upper embankment layers are compacted into position, the soil undergoes an increase in the major principal stress by $\Delta\sigma_1$. It is assumed that the minor principal stresses σ_2 and σ_3 are kept constant while the loading is increased (i.e. as the new layers are placed on the embankment).

With respect to a natural context, the process involves the dissipation of pore water pressure, associated with seepage or the infiltration of precipitation. The pore pressure in the soil element makes the effective mean stress p' lower than the total mean stress p while maintaining constant deviator stress. A reduced triaxial compression stress path (RTC) is characterised as a low strength stress path. The recognition of low strength zones within earth embankments is ignored probably because such paths are unable to be simulated in standard triaxial cells. Although the effects on the stability of the embankment are questionable, it will be shown that the RTC stress path influences the magnitude of the shear strength parameters ϕ' and c' and thus affects the factor of safety specified by the designer.

Fell et al (1992) undertook an investigation into the major causes of embankment failure. The researcher attributed the failure of embankments to low strength stress conditions or zones within the embankment and the incorrect design of drainage systems (drainage filters).

It is accepted that Figure 2.8 represents just one natural application of pore pressure dissipation, namely the infiltration of rainfall and subsequent seepage. Pore pressure dissipation may also occur if there is a sudden lowering in the water table due to remedial work after a blockage of the drainage system within the embankment.

In Figure 2.8 a typical natural application representative of the PL-RTC stress path is shown.

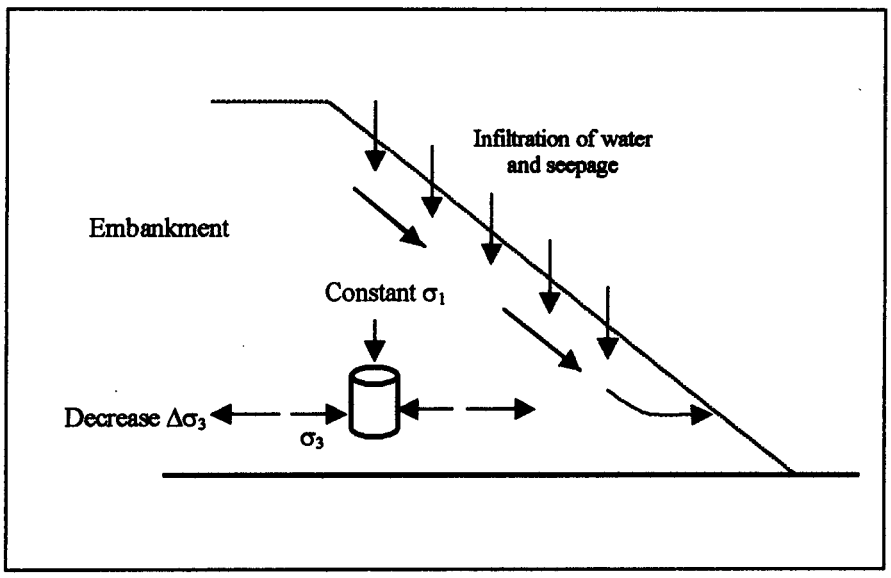

Figure 2.8 Field application of PL-RTC stress path

The soil element is in equilibrium with respect to the initial stress conditions. The stress changes in the soil element are characterised by a decrease in the minor principal stress ($\Delta\sigma_3$), while the major principal stress σ_1 is kept constant. The soil element remains confined by the soil mass, but as the pore pressure decreases and water passes through the soil mass, the soil structure may change from a stiff matrix to a more plastic consistency. In this case, it can be visualised that the bonds between the soil particles are 'lubricated' by the infiltration of water. Stability (especially of the side of the embankment) will be affected by the reduction of pore water pressure combined with the subsequent seepage action.

The following subsection investigates the behaviour and application of HC-TC-PL-CTC and HC-TC-PL-RTC stress paths.

2.3.3 Hydrostatic Compression (HC) - Triaxial Compression (TC) - Proportional Loading (PL) in conjunction with Conventional Triaxial Compression (CTC) and Reduced Triaxial Compression (RTC)

This testing procedure is initiated from an isotropic stress condition to precondition the soil to an assumed isotropic effective mean stress. The HC-TC-PL-CTC stress path approaches the failure surface following a sequence of common stress paths. The stress paths will be initiated from predetermined initial conditions of p'_{oi} on the effective mean

stress axis. From these p'_{oi} points the TC and PL stress paths will be propagated until pre-selected stress points on the K_o line (with $K_o = 0.50$) are reached. The HC-TC-PL stress paths are undertaken in a controlled 'drained' or quasi-drained condition, while the final CTC and RTC stress paths are initiated in an undrained condition, taken to failure.

In Figure 2.9(a), a combination of HC-TC-PL-CTC stress paths is schematically shown.

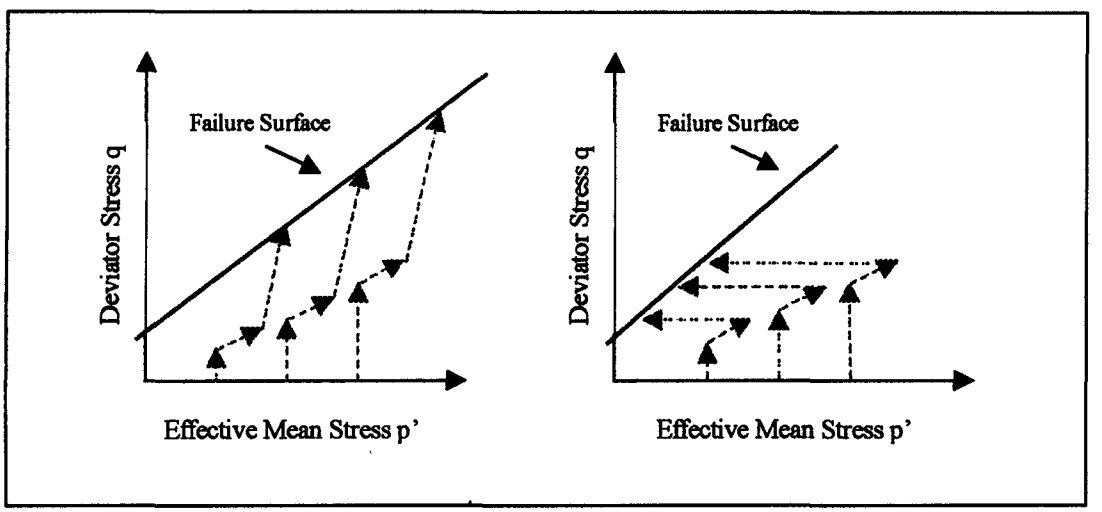

Figure 2.9 (a) HC-TC-PL-CTC stress paths; (b) HC-TC-PL-RTC stress paths.

The hydrostatic compression (HC) stress path starts from a zero isotropic stress state in a controlled 'drained' condition and follows the effective stress application in terms of the q-p' diagram until the pre-selected initial stress state (p'_{oi}) is reached. These stress points are equivalent to effective mean stresses 75 kPa, 200 kPa and 300 kPa on the effective mean stress (p') axis.

The triaxial compression (TC) stress path is a special case of triaxial compression (also in a controlled 'drained' condition). In the TC stress path the applied stress is such that the stress state always remains on an octahedral stress plane in principal stress space. By definition, the octahedral stress is given as (Desai and Siriwardane, 1984):

$$\sigma_{oct} = (\sigma_1 + \sigma_2 + \sigma_3)/3 \qquad (2.6)$$

The octahedral stress equation is equivalent to the effective mean stress p'. In terms of the Cambridge method (see equations 2.2), it is representative of the axisymetrical situation $\sigma_{oct} = (\sigma_1 + 2\sigma_3)/3$. In the TC stress path σ_{oct} or p' remains constant during loading.

The TC stress path is followed by a PL stress path (anisotropic loading path), which again is programmed to follow the K_o line to predetermined stress points. The non-conventional triaxial test is concluded with a conventional triaxial compression (CTC) stress path in undrained condition, taken to failure.

In Figure 2.9(b) the schematic of the HC-TC-PL stress paths are shown exactly the same as previously illustrated (see Figure 2.9(a)). However, instead of a CTC stress path a RTC stress path concludes the test in undrained condition. Initiation of the RTC stress path was taken from the same predetermined stress points as in the previous HC-TC-PL-CTC tests.

2.3.4 Field application of HC-TC-PL-CTC and HC-TC-PL-RTC stress paths

Selection of a suitable geotechnical application for such stress paths is difficult, but the combination of such stress paths is realistically possible. Again, various stress paths of mixed composure can simulate physical 'man-made' and natural interventions. The TC stress path is generated from relatively large increases of deviator stress (q), which gives rise to deformation due solely to shear straining in a particular compression plane.

Under varying axial and lateral loading conditions, elements of soil undergo different paths of loading (stress paths). The combination of stress paths that a particular soil element is subjected to in its short and long-term stress history is different in many respects.

The stress conditions below or within embankments are complex and no stress path combination occurring within such a structure is unique. In Figure 2.10 a schematic of a field application, based on the Golillas Dam in Tasmania (Fell et al, 1992) is shown.

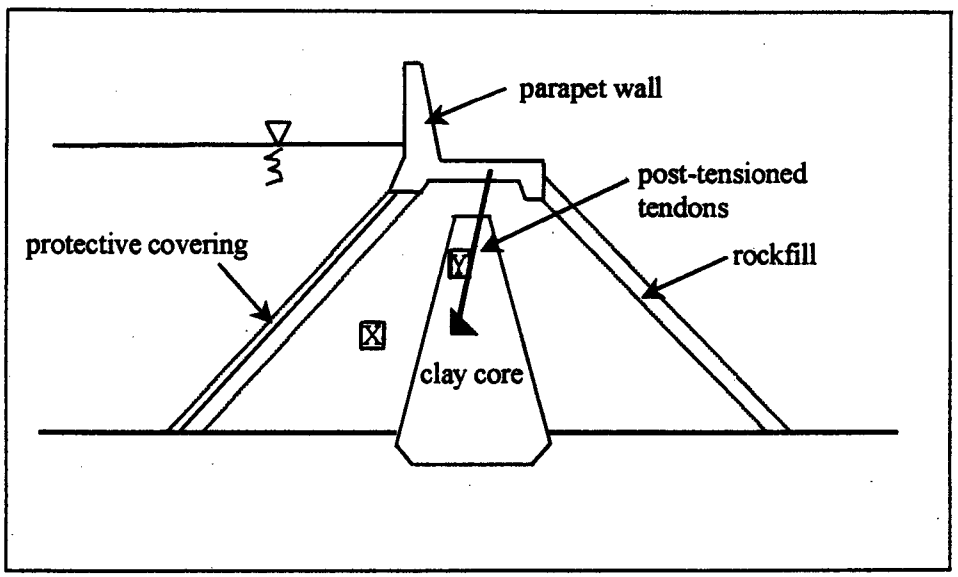

Figure 2.10 Golillas Dam application representative of HC-TC-PL-CTC and HC-TC-PL-RTC stress paths

The Golillas Dam consists of a reinforced concrete parapet wall at the crest of the dam, which reduces the volume of rock fill needed during construction. The parapet wall is anchored by post-tensioned tendons, which are embedded in the core of the dam. A protective covering usually consisting of a concrete face slab is cast and impervious clay layers placed underneath, as a security measure should the concrete ever crack.

The stress history of soil elements in positions X and Y (see Figure 2.10) may be hypothetically represented by the simulation of HC-TC-PL-RTC and HC-TC-PL-CTC paths in the laboratory.

The soil in position Y is assumed to have isotropically consolidated to a particular effective stress equilibrium. The post-tensioning of the tendons results in a relatively large increase in deviator stress (shear stress) within soil elements in proximity to the anchorage system. The triaxial compression (TC) stress path is generated from the shear stresses and the initial effective mean pressure p' remains constant. As the upper layers are compacted by say, the construction of the deck super structure, the K_o condition may apply and the PL stress path follows on from the TC stress path. Normal soil response

is then assumed to occur and the conventional triaxial compression (CTC) stress path is generated in an undrained condition.

The soil element in the vicinity of position X undergoes similar HC-TC-PL stress paths in the 'drained' condition. However, should the protective covering be damaged in the vicinity of position X, the soil element will undergo the reduced triaxial compression (RTC) stress path (which has already been discussed in Section 2.3.2).

The selected test material in all standard and non-conventional stress path investigations was subjected to stress 'preconditioning', isotropically and anisotropically to enable a simulation of a specific soil stress 'history'. The following chapter focuses on the nature of the test material and is essential to understanding the behavioural responses of the clay material.

CHAPTER 3

RESEARCH MATERIAL

3.1 Introduction

In *Chapter 3*, the test material used in this thesis is discussed. The selected material formed part of the core material of Maguga Dam. The Maguga Dam is a dry core rockfill dam situated in Swaziland on the Komati River, approximately 12 km south of Piggs Peak. The core material was excavated from the dam basin and is of colluvial origin.

The test specifications and procedures are taken from the geotechnical manual of soil laboratory testing (Head, Volumes 1 to 3, 1980 to 1986). At times, referral to the ASTM book of standards (ASTM, 1982) is also made for comparative reasons that will be discussed in *Chapter 4*, where the investigation itself is addressed.

In order to fully identify the type of material, the properties and soil behaviour of Maguga clay, a geological review and soil mechanical tests were conducted. The soil mechanical tests will illustrate the geotechnical properties that were attained and the difficulties that were experienced throughout the test period. The classification tests will include a grading analysis, the Atterberg limits and the Proctor compaction characteristics. Consolidation of the clay was investigated in an oedometric analysis. The undrained triaxial compression characteristics are not mentioned in this chapter, they will be presented in *Chapter 4*. The geological review taken from Brink (1985) discusses the pedological class in terms the degree of alteration of the parent material and the emplacement of the erosional remnants as a result of colluvial processes. The geological review addresses certain material characteristics of the clay attributed to the colluvial formation of the clay.

A summary of the geotechnical properties is presented and the relevant data listed at the end of this chapter.

3.2 Geological Classification of Maguga clay

The main criterion used for differentiating the geological groups is the degree of alteration of the original parent material. The parent material may be a residual soil formed by the weathering of the bedrock or a transported soil such as colluvium. The main process, through which this differentiation is achieved, is by the movement of water through the parent material. Colluvium is a term, which includes all soils on hill or mountains slopes, which have moved down slope under the influence of gravity and water action to form fine or coarse hillwash soils (Brink, 1985).

Maguga clay is a ferrallitic soil derived from sediment deposits of the Post-Gondwanaland Period (Brink, 1985). Ferrallitic soil occurs in areas where the mean rainfall is above 800mm, such as the case in Swaziland. The Maguga clay probably developed from highly weathered transported soil (colluvium material). The fact that the clay content was high (68%, see Section 3.3) and that the clay-coated quartz particles consisted of various sizes suggests that the clay originated from residual igneous rock such as granite. Igneous rock such as granite contains the mineral feldspar (often in large quantities) as well as quartz particles. It is the weathering of mineral feldspar that produces clay. The red colouration of the ferrallitic soil is derived from the mobilisation of iron oxides during weathering of the transported soil.

3.2.1 Properties of Ferrallitic Clays

The ferrallitic clays are of the 1:1 crystalline lattice type and are mainly red in colour due to the lattice being mixed with quantities of free iron oxides and occasionally with aluminium oxides. The clay mineral is composed of strong ionic bonds, which result from the electrostatic attraction between positive ions (silica tetrahedrons-Si^{+}) and negative ions (iron oxide-Fe^{-} and aluminium oxide-Al^{-}). As a result of the strength of these primary ionic bonds and the formation of a flocculated structure, these clays are considered well suited to the construction of both cuts and fills. Ferrallitic clays are neither expansive nor dispersive.

3.3 Geotechnical Classification of Maguga Clay

The Maguga clay was chosen as the test material because it displayed typical and, at times, interesting geotechnical characteristics. These characteristics are imperative to understanding and interpreting facets of result analysis that are discussed in this chapter as well as in *Chapter 5*.

3.3.1 Grading

The specifications for the grading analysis are BS1377:1975, Test B and BS1377:1975, Test 7 D. The particle size analysis was conducted by Ninham Shand Geotechnical Laboratories (2001).

In Figure 3.1, the grading curve of the Maguga clay is shown. The particle size distribution consisted of a clay component equal to 68% by mass, while silt and sand components made up approximately 17% and 15% by mass, respectively.

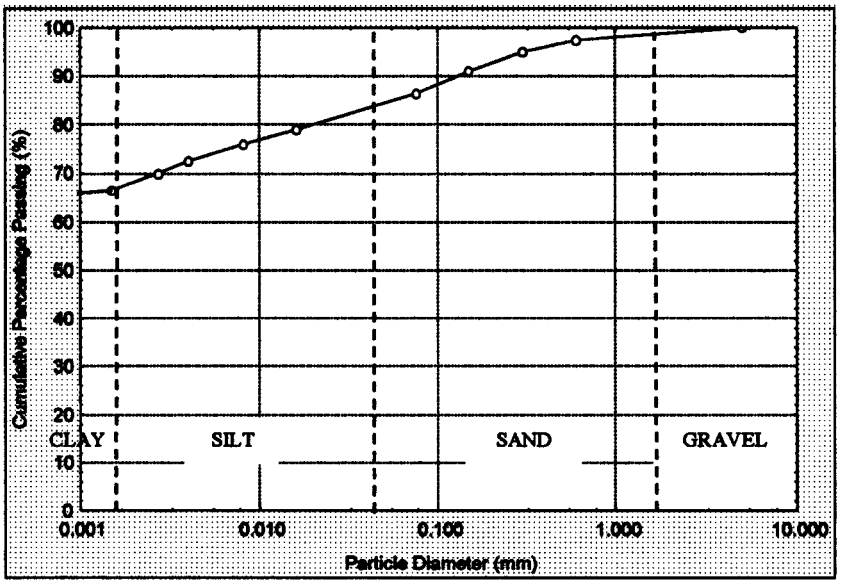

Grading Analysis

CLAY	SILT	SAND
%	%	%
68	17	15

Figure 3.1 Grain size distribution for Maguga clay

The specifications for earth embankments in terms of particle size distribution are rather varied because of the diversity associated with the source of the embankment, the quantity and quality of the material available in the borrow area. The specifications given by Australian authorities such as the Public Works Department of Western Australia (PWD) suggest that a full grading envelope should be undertaken with 55% of the material passing through the 0.075mm sieve (Fell et al, 1992). The Maguga clay satisfied these requirements with approximately 80% of the test material passing through the 0.075mm sieve.

3.3.2 Atterberg Limits

The specifications for the Atterberg limits analysis are BS1377: 1975, Test 2 B and BS1377: 1975, Test 3. The procedures for the Atterberg limits undertaken in this research work are shown in Appendix A-3.

The liquid limit test results are shown in Figure 3.2. According to the Casagrande test method procedures, a liquid limit of 60.1% is determined. The plastic limit was found to be approximately 36.9%. The difference in the liquid limit and the plastic limit is the plasticity index value of 23.2.

In comparison with the liquid limit result attained from the cone penetrometer test, which is a liquid limit equal to 78% (van Koersveld, 2001), the difference was considerable. On-site laboratory tests conducted in Swaziland attained a value of 60% for the liquid limit (Komati Joint Ventures, 2000), which was in close agreement with the above-mentioned Casagrande method result.

Referring to the specifications, the British standards as well as the ASTM specifications (ASTM, 1982) regard the cone penetrometer as the standard preferred method of attaining the liquid limit. The Casagrande method of liquid limit analysis is now regarded as a subsidiary method because the results appear not to be consistent and prone to experimental errors. The cone penetrometer result was ignored, as it was felt that in the above-referenced work too many discrepancies with regards to the method had occurred.

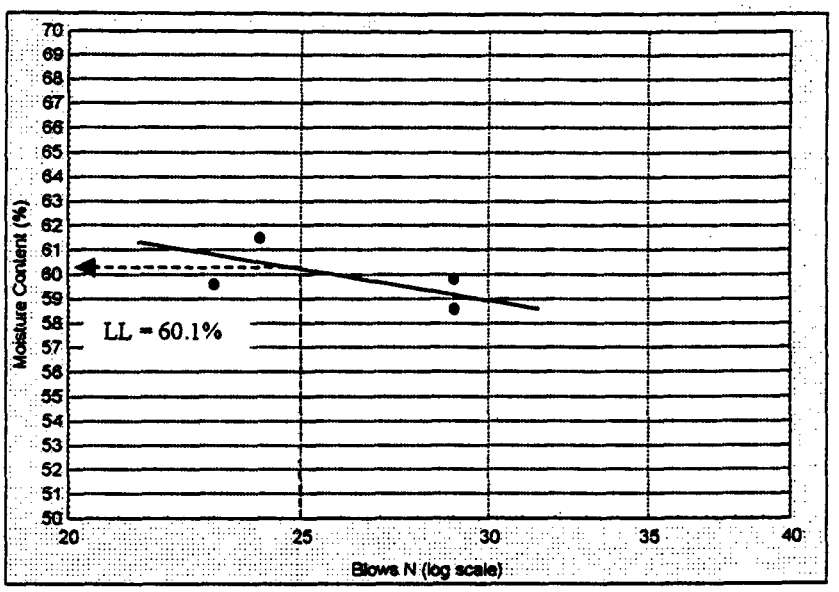

Atterberg Limit Analysis

Liquid Limit	Plastic Limit	Plasticity Index
%	%	
60.1	36.9	23.2

Figure 3.2 Atterberg limits for Maguga clay

The Atterberg limits identified the Maguga clay as clay of high plasticity with reference to the plasticity chart. The researchers (Fell et al, 1992) specified an allowable range of liquid limit and plasticity index by relating to the 'A' line on the plasticity chart for earth embankment material. This relationship is shown in Figure 3.3.

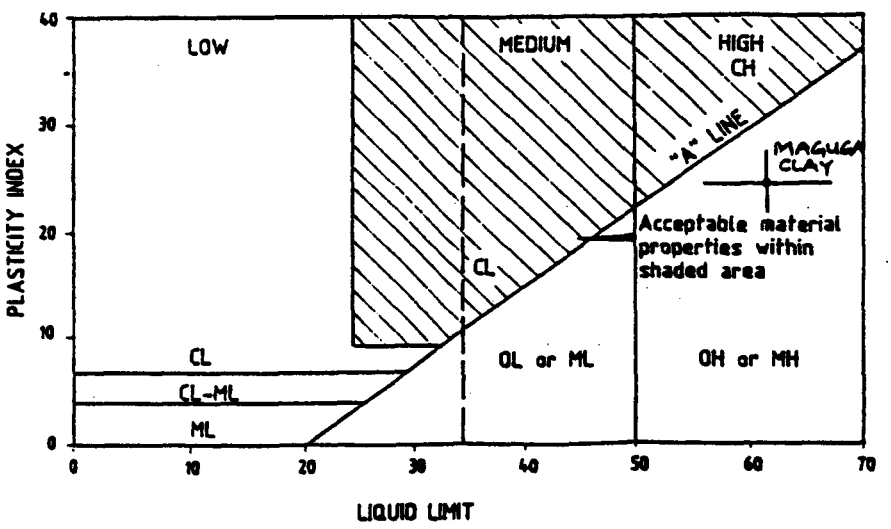

Figure 3.3 Suitable Atterberg limits for embankments in terms of plasticity chart (Fell et al, 1992)

The shaded area in Figure 3.3 represents the acceptable material properties for earth embankments in terms of the Atterberg limits. The Maguga clay result falls in the high plasticity range, however just outside the recommended shaded area. In fact the Maguga test material should be addressed as a silt of high plasticity, but will remain classified as Maguga clay for the remainder of the research work.

Specifications given by Australian authorities such as the Public Works Department of Western Australia (PWD) (Fell et al, 1992) allow for a plasticity index value greater that 15, which in the case of Maguga clay is satisfied by the plasticity index value of 23.2. All specifications tend to specify a minimum plasticity index and an upper bound for the liquid limit, so that clays of high plasticity, which may be difficult to compact, are identified in the borrow area.

3.3.3 Proctor Compaction

The specifications for the standard Proctor compaction method is BS1377:1975, Test 12. The procedures, for the compaction test are shown in Appendix B-3. The Proctor compaction relationship of Maguga clay is shown in Figure 3.4.

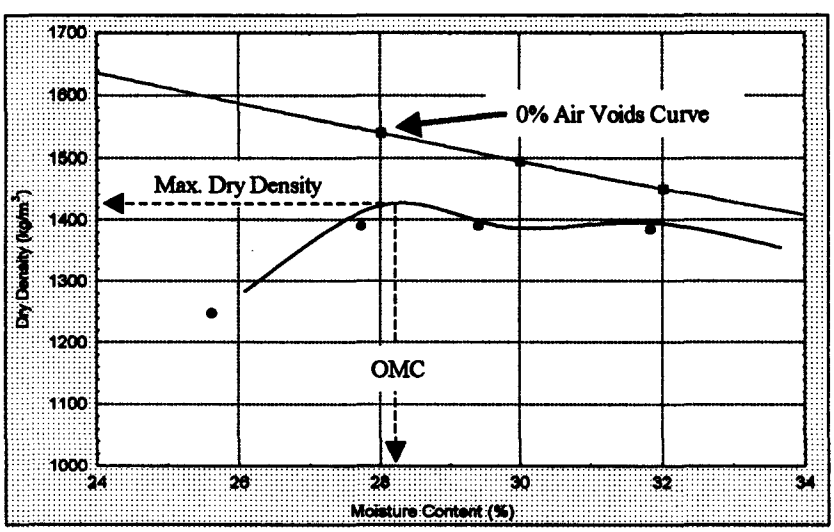

Max. Dry Density (kg/m^3)	Optimum Moisture Content (%)
1430	28.1

Figure 3.4 Proctor compaction relationship for Maguga clay

The Proctor compaction curve consisted of a flat, double-peak curve (the second peak defined by moisture content of approximately 32%). Referring to Figure 3.4, maximum dry density-optimum water content test results were 1430 kg/m^3 and 28.1%, respectively. The main objective of core material compaction within an embankment is to provide a stable, impermeable soil structure. The engineering properties of clay can be manipulated by means of the density so that desired improvements to the clay behaviour are achieved. At this stage it appeared that the density of Maguga clay was improved due to its firm, waxy and low compressible soil structure (this impression will be confirmed in the triaxial tests of Maguga clay to be discussed in *Chapter 5*).

The requirement for the maximum dry density ratio of ≥ 98% is reasonable and attainable with the moisture content range shown in Figure 3.4. For dams to be constructed in wet climates (annual rainfall greater than 800 mm), such as Swaziland, it would not be unreasonable to lower the density ratio to 95%, provided compaction was carried out above the optimum water content (Fell et al, 1992). Lowering the required maximum dry density and compacting the clay at wetter moisture contents would alleviate compaction difficulties with regards to stiff, low compressible clays such as Maguga clay. Compaction consistency was difficult to attain during the compaction test as well as in the sample preparation for the triaxial tests. The double-peaked compaction curve confirms that such a lower density condition could be applied. It should also be noted that if the 95% density ratio is used and the water content is under the optimum water content, this would not be acceptable because the soil structure would be permeable.

In an earth dam, proper compaction improves the shear strength of the soil; thereby further enhancing stability of the structure. The ingress of water within the core of an earth dam is reduced with correct compaction methods. A soil with low permeability is less likely to absorb water, as the water ingress will be retarded by the stiff, waxy soil structure.

The dry density-moisture relationship that is established by the standard Proctor compaction test provides necessary data for the simulation of conditions that are likely to

be achieved in the field. The compaction characteristics attained in the laboratory are also applied in other test methods to determine engineering properties such as the shear strength and compressibility.

3.3.4 Consolidation

The specification for the consolidation analysis, used for this research work, is ASTM: D 2435-80. The procedures for the consolidation test undertaken for this research work are shown in Appendix C-3.

In Table 3.1, the summarised consolidation test results of the Maguga clay are shown. The pressures of the various load steps are 50 kPa, 250 kPa, 500 kPa and 1200 kPa, while the unloading pressures are 500 kPa, 250 kPa and 50 kPa respectively. The zero kPa-unloading step is not shown, as a discrepancy in the final amount of settlement was observed. The coefficient of consolidation (c_v) results are determined as 0.85 to 1.49 m^2/year and the derived coefficient of permeability (k) results are between 7.81×10^{-9} m/s and 4.13×10^{-8} m/s.

Pressure (kPa)	Settlement (mm)	Voids Ratio	m_v (m^2/MN)	E_s (MN/m^2)	t_{90} (min)	c_v (m^2/year)	Coefficient of Permeability (m/s)
0	0.000	0.878	0	0	0	0	0
50	0.084	0.870	0.09	11.11	27.04	1.49	4.13E-08
250	0.445	0.825	0.12	8.33	36.00	1.09	3.32E-08
500	0.619	0.764	0.14	7.14	37.21	1.03	1.21E-08
1200	0.989	0.666	0.08	12.50	43.56	0.85	7.81E-09
500	-0.130	0.679	*		*	*	*
250	-0.096	0.688	*		*	*	*
50	-0.259	0.691	*		*	*	*

Table 3.1 Summary of consolidation test results for Maguga clay

The clay displayed the characteristics that were expected from the previous soil mechanical tests. The range of coefficient values (m_v and c_v) described the Maguga clay as a material of low compressibility and high plasticity (Head, 1980).

The derived coefficient of permeability for the one-dimensional consolidation test showed that the Maguga clay has a low permeability. The permeability of Maguga clay could be seen to decrease as the loading was incrementally increased. The permeability results highlight the attributes of Maguga clay as suitable material for embankment structures.

3.4 Summary

The geological and geotechnical characterisation of the Maguga clay highlights the suitability of the red, slightly silty-sandy, low permeable clay to be used as material in an embankment. The main characteristic that is of concern is with regards to the potential low compressibility of the Maguga clay. The compaction effort with respect to achieving the maximum dry density was difficult to attain at optimum moisture content of 28.1%. It is suggested that placement of potentially low compressible clay in the field may be difficult with regards to attaining optimum compaction density. This problem is overcome in the field by compacting the clay on the wet side (optimum water content +4%) at 95% density ratio (as mentioned before) to facilitate easier installation of the material and also on the choice of compaction machinery to be used.

Consolidation tests are also conducted with the objective that all consolidation characteristics of Maguga clay are attained and the results applied to the formulation of critical state parameters in *Chapter 6*.

A summary of the soil properties of Maguga clay, as obtained from the laboratory experiments, is presented in Table 3.2.

Soil Property	Unit	
Particle Range	mm	0.002 to 3
Plasticity Index	–	23.2
Specific Gravity	–	2.71
Optimum Moisture Content	%	28.1
Maximum Dry Density	kg/m^3	1430
Compressibility	–	Low
Permeability	m/s	4.10^{-8} to 8.10^{-9}

Table 3.2 Soil properties of Maguga clay

CHAPTER 4

TRIAXIAL TEST PROCEDURES AND TEST PROGRAM

4.1 Introduction

The investigation of the undrained triaxial test procedures and test program of Maguga clay is presented in *Chapter 4*. The clay samples are subjected to triaxial compression tests in a specialised triaxial test system, starting at selected effective mean pressures.

The investigation in the triaxial device involved testing procedures that consisted of following conventional and non-conventional stress paths. Conventional stress path testing is conducted on both, remoulded and undisturbed clay specimens, while remoulded samples are used for the non-conventional tests. Conventional triaxial tests are initiated from selected isotropic stress points defined on the effective mean stress axis, namely 75 kPa, 200 kPa and 500 kPa. The test results of the conventional triaxial testing are discussed in the first section of *Chapter 5*, followed by the non-conventional test responses.

The non-conventional stress path tests are conducted in a sequence of common stress path types as described in *Chapter 2*. Non-conventional stress paths are initiated from anisotropically defined stress points of effective mean stress of 125 kPa, 250 kPa and 350 kPa. These stress points were positioned on the K_o line (with $K_o = 0.50$).

Many common stress paths can be simulated in the laboratory, however, the prerequisites for efficient and competent stress path testing is a sound understanding of stress path theory. Additionally, the experimenter must be well familiar with the specifications and the control philosophy of the stress path device. The specifications and control philosophy is the subject of this chapter.

Conventional triaxial testing is conducted in accordance with the ASTM specifications (ASTM: D 2850-82). Currently, there are no specifications available for non-conventional stress path testing in specialised triaxial testing devices.

The test samples are of the dimensions of 38mm in diameter and approximately 77mm in height. The samples are prepared at the optimum moisture content of 28.1% at a target maximum dry density of 1460kg/m^3. All samples are prepared within 1% of the abovementioned specimen parameters so that sample consistency is maintained.

4.2 Triaxial Test Program

In total, twenty-one triaxial tests were undertaken at various effective mean stresses in terms of either isotropic or anisotropic loading conditions. Six conventional tests were undertaken with remoulded and undisturbed clay samples. The following fifteen tests were non-conventional stress path tests comprising of remoulded samples only. The complete test program with a short description of the stress path acronyms is listed in Table 4.1.

Test Description	Drainage	Sample	Effective Mean Stress kPa	Initial Dry Density kg/m^3
CONVENTIONAL STRESS PATHS				
Isotropic consolidation, compression (CTC)	undrained	remoulded	75	1454
	undrained	remoulded	200	1451
	undrained	remoulded	500	1466
Isotropic consolidation, compression (CTC)	undrained	undisturbed	75	1470
	undrained	undisturbed	200	1419
	undrained	undisturbed	500	1473
NON-CONVENTIONAL STRESS PATHS				
Anisotropic consolidation, compression (PL-CTC)	undrained	remoulded	125 *	1459
	undrained	remoulded	250 *	1468
K_o = 0.50	undrained	remoulded	350 *	1471
Anisotropic consolidation, constant q path (PL-RTC)	undrained	remoulded	125 *	1461
	undrained	remoulded	250 *	1466
K_o = 0.50	undrained	remoulded	350 *	1464
Constant p' path, anisotropic consolidation, compression	undrained	remoulded	75	1471
	undrained	remoulded	200	1462
(HC-TC-PL-CTC) K_o = 0.50	undrained	remoulded	300	1460
Constant p' path, anisotropic consolidation, Constant q path	undrained	remoulded	75	1462
	undrained	remoulded	200	1454
(HC-TC-PL-RTC) K_o = 0.50	undrained	remoulded	300	1466
Constant p' path, anisotropic consolidation, compression	undrained	remoulded	75	1462
	undrained	remoulded	200	1454
(HC-TC-PL-CTC) K_o = 0.75	undrained	remoulded	300	1466

Note: * effective mean stress on K_o line

Table 4.1 Summary of triaxial test program

The sensitivity in controling the non-conventional stress path tests was always problematic. A loss of control at high pressures (i.e. pressures greater than 450 kPa) resulted in rapid failure of the test sample. If manual intervention was at the precise time that control was lost test the test sample could be salvaged. Due to these reasons, it was decided to reduce the effective mean stress of 500 kPa to 300 kPa or 350 kPa for the non-conventional stress path tests.

The following subsections describe the stress path triaxial test system, the software for control and an example of the 'command' stages, which were followed during the HC-TC-PL-CTC stress path test.

4.3 The Computer-controlled Stress Path Triaxial Device

The computer-controlled stress path device consists of a Bishop and Wesley triaxial cell and a computer control package (TRIAX). The triaxial cell and the software TRIAX are discussed in the following sub-sections and form an essential component with regard to the control philosophy of the stress path device.

4.3.1 Bishop-Wesley Triaxial System

The Bishop-Wesley triaxial system is a hydraulically loaded triaxial cell. The system is basically divided into two parts. The upper part consisting of the cell top with the perspex cell wall and a lower section comprising of the hydraulic ram.

The upper section of the triaxial system (cell top with perspex cell wall) consists of the load plunder and the vertical displacement transducers. The test sample is placed into position on the pedestal, the cell top system secured and the cell filled with de-aired water. The load plunger is screwed down into position and the displacement transducer is set at the initial starting position. The whole top assembly with the specimen moves relative to the lower section on the application of strain- or stress-controlled loading. Vertical displacement is measured by means of vertical extension rods pushing against the displacement transducer attached to the lower ram section. The measurement of applied load is taken from a submersible load cell that is positioned in the plunger.

The lower ram section is connected to the sample pedestal. The pedestal base has a number of drainage taps, which lead to high accuracy pressure transducers that measure cell-, back- and pore-water pressures. The converted analogue to digital readings from these pressure transducers is recorded by the data acquisition system. The lower section (the ram chamber) contains the pressurising chamber of the triaxial device. The lower ram assembly moves vertically when the lower chamber is pressurised. Two bellofram seals secure the pressurised water in the lower chamber. The region between the bellofram seals, including the linear bearings, is open to the atmosphere. In Figure 4.1 a schematic of the Bishop-Wesley cell is shown.

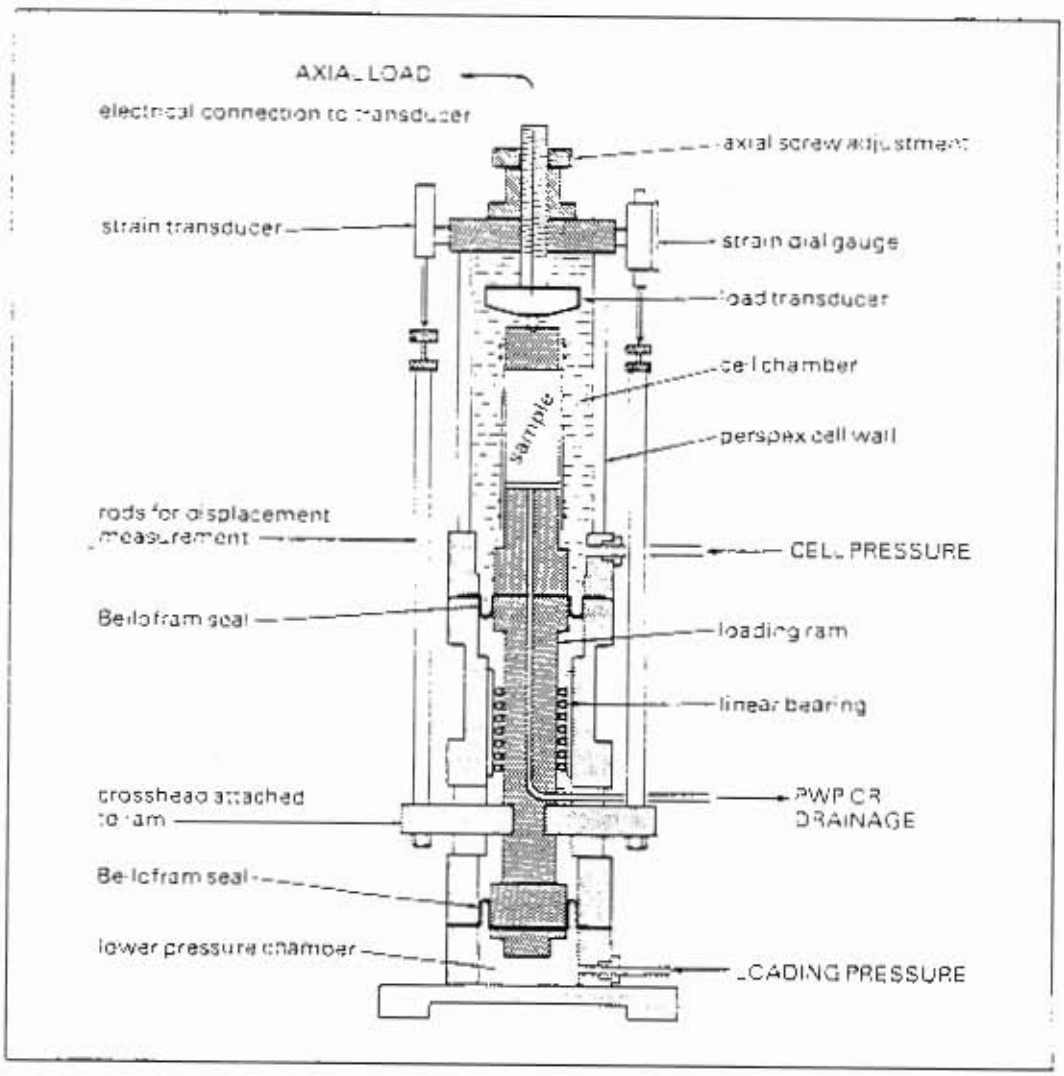

Figure 4.1 Schematic diagram of the Bishop-Wesley triaxial cell (Head, 1986)

4.3.2 Triaxial Software Package (TRIAX) and Control Philosophy

In 1982, the Imperial College in London developed a computerised triaxial system, which allowed the propagation of conventional and non-conventional stress paths to be undertaken in a controlled manner, so that *in-situ* conditions could be simulated accurately. This system is the first version of the triaxial testing system (TRIAX) with the addition of the Bishop-Wesley cell. The computer-controlled stress path device enabled triaxial testing to be taken to the utmost of its dimensional stress space capabilities.

In order to demonstrate the flexible control philosophy associated with the computer-controlled stress path device, the understanding of the capabilities of TRIAX is necessary. The control philosophy is complex and is best explained in terms of the stage procedures associated with a non-conventional stress path test. The hydrostatic compression (HC), triaxial compression (TC), proportional loading (PL) and conventional triaxial compression (CTC) stress path operation is discussed.

Control is undertaken in a number of stages. Each stage consists of four pressure boxes, namely, the back pressure, cell pressure, ram pressure and constant rate of strain. All boxes consist of respective control parameters and various rates of pressure application, which are decided upon by the experimenter. The control parameters or rates contained in the boxes can be changed at any stage of the testing period at the experimenter's discretion.

The stages can be manipulated either manually or automatically. Once the TRIAX software package is familiar to the experimenter, automatic control can be adopted, although certain valves still need to be opened and closed between certain test phases. Automatic changeover from one stage to the next is governed by predetermined alarms, which trigger stages that are to follow or stop the test stage if control in one of the boxes is lost. If the test is left to run overnight, then a multitude of alarms can be specified that apply to different conditions.

The flexibility of automatic control is at the user's discretion. Figure 4.2 is a copy of the screen displays comprising of the stage set-up and control parameters necessary to conduct the HC-TC-PL-CTC stress path test is shown.

4.3.2(a) Saturation

The control equation for backpressure (BOX 1) is simply given by the variable 'back' (see Figure 4.2). A *hold value* of 300 kPa (back>=300) is stipulated for the backpressure and is incremented at 15 pulses. Electronic pulses are generated from stepper motors that are housed in external electronic units. One pulse is equivalent to approximately 0.7 kPa, so 15 pulses would represent a pressure of 10.5 kPa. Incrementation adjusts the hold value with respect to time by linear manipulation. An increment value of 15 would mean that there is a pressure incrementation of 10.5 per minute, until the pressure reaches the specified *hold value* (300 kPa). A tolerance value of 0,5 kPa keeps the hold value between certain limits. If the actual pressure falls outside the tolerance value, the system automatically increases or decreases the pressures by manipulating the pulse rate until the desired hold value is reached.

By maintaining a low pulse for the back pressure (BOX 1) and the cell pressure (BOX 2) two important considerations are met. Firstly, a slow rate means that the saturation stage is controlled over a longer time period, which is essential to achieve 100% saturation. The air locked in the sample is given a longer time in which to dissolve into the water. Secondly, by controlling the pulse rate or increment rate of the back pressure box, the pulse rate of the cell pressure box is indirectly controlled and allows for adjustment at manageable levels. The second consideration is an important control mechanism when targeting the projected pressures for non-conventional stress paths, requiring the simultaneous operation of the three pressure boxes.

The control equation for BOX 2 (cell pressure) is given as 'cell' in effective terms and set to an effective cell stress of 10 kPa. Maintaining the cell pressure at 10 kPa higher than the back pressure ensured that sample stability was sustained. An increment value of 0 would mean that there is no pressure incrementation and the pressure is maintained at the

specified *hold value* (300 kPa + 10 kPa) within the tolerance range. Ram pressure (BOX 3) and strain rate pump (BOX 4) were not needed; therefore their status was off (not activated).

The saturation stage is made up by fourteen stages, each stage with its own control parameters, rate settings and alarms. The alarms between the sub sections triggered the following sub stage in the saturation stage. The alarm, as depicted in Figure 4.2, is activated once the condition (back>=300) is met. A WAIT command is initiated for the experimenter to control the condition. The WAIT action allows for a delay period before continuing with the next stage and maintains the *status quo* until the experimenter is satisfied with the general performance, the data acquisition, etc. and thereafter intervenes to initiate the next sub stage of the saturation stage.

Figure 4.2 Stage set-ups for HC-TC-PL-CTC stress path tests

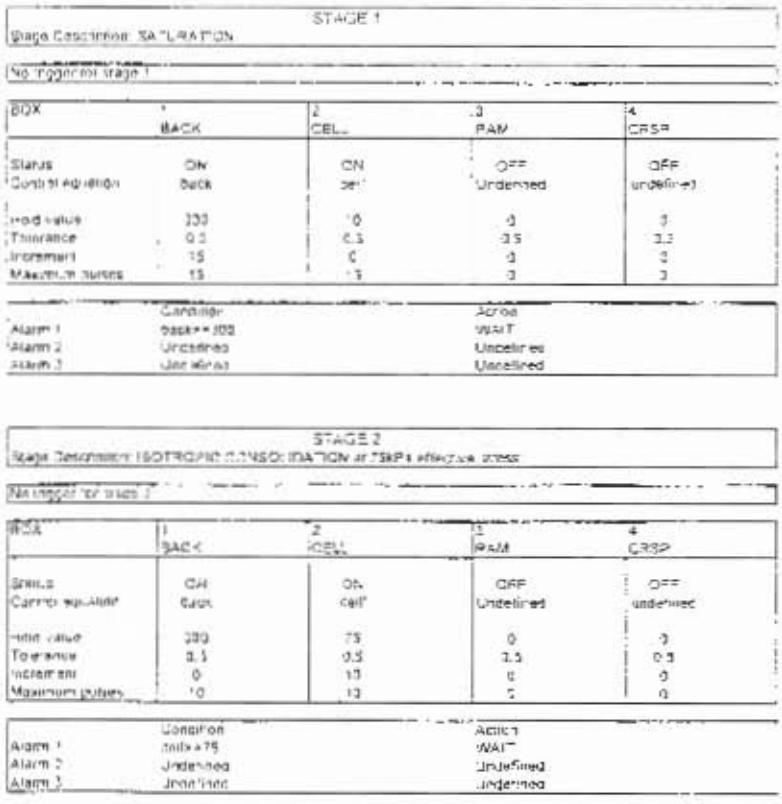

Figure 4.2 continued....

STAGE 3

Stage Description: CONSTANT MEAN STRESS at p = 75 kPa

No triggers for stage 3

BOX	1 BACK	2 CELL	3 RAM	4 CRSP
Status	ON	ON	ON	OFF
Control equation	back	cell	q	undefined
Hold value	300	75	current	0
Tolerance	0.5	0.5	0.5	0.5
Increment	15	0	10	0
Maximum pulses	15	10	10	0

	Condition	Action
Alarm 1	(sig3'/(sig1')=0.60	WAIT
Alarm 2	Undefined	Undefined
Alarm 3	Undefined	Undefined

STAGE 4

Stage Description: ANISOTROPIC CONSOLIDATION along K_o line where K_o = 0.60

No triggers for stage 4

BOX	1 BACK	2 CELL	3 RAM	4 CRSP
Status	ON	ON	ON	OFF
Control equation	back	(sig3'-0.60*(sig1'	q	undefined
Hold value	300	75	current	0
Tolerance	0.5	0.5	0.5	0.5
Increment	10	0	0	0
Maximum pulses	10	7	7	0

	Condition	Action
Alarm 1	p>=125	WAIT
Alarm 2	Undefined	Undefined
Alarm 3	Undefined	Undefined

STAGE 5

Stage Description: UNDRAINED APPLICATION OF LOAD (strain-controlled)

No triggers for stage 5

BOX	1 BACK	2 CELL	3 RAM	4 CRSP
Status	OFF	ON	OFF	ON
Control equation	undefined	cell	undefined	q
Hold value	0	current	0	1
Tolerance	0.5	0.5	0.5	0.5
Increment	0	0	0	7
Maximum pulses	0	7	0	7

	Condition	Action
Alarm 1	%strain>=12%	STOP
Alarm 2	Undefined	Undefined
Alarm 3	Undefined	Undefined

4.3.2(b) Isotropic Consolidation (HC stress path)

Isotropic consolidation comprises of stage 2 of the stress path testing, which is set at selected effective stresses (75 kPa, 200 kPa and 300 kPa for the shown test). The back pressure is adjusted manually to 300 kPa from an external back pressure system with the

valve in a closed position. The back pressure is adjusted to 300 kPa because the saturation stage resulted in high back pressures (500 kPa to 700 kPa), which had to be lowered so that the selected effective mean stress could be achieved. The cell pressure is incrementally increased to the required effective cell stress (cell'). When the required effective cell stress was reached (75 kPa) the alarm is triggered and a WAIT command is initiated. Once the back pressure valve is opened the isotropic consolidation stage is initiated. Volume changes as well as initial and final pore water pressure measurements are recorded at the relevant time intervals during the isotropic consolidation stage. The isotropic consolidation stage is completed once the pore water pressure stabilises and there are no longer any volume changes.

4.3.2(c) Constant Mean Stress p' (TC stress path)

The hold values for BOX 1 and BOX 2 is predetermined (see consolidation stage) and controlled within the tolerance values while an increase of deviator stress (BOX 3) took place. BOX 1 (back pressure) is kept at a higher pulse rate in comparison to the other boxes. By ensuring that the back pressure box remains the 'dominant' pressure, the test stage is managed such that the back pressure box will always maintain its target pressure. The ram pressure (BOX 3) is given a pulse rate of 10 kPa per hour, which is equivalent to a slow rate of strain.

The alarm is initiated once the K_o-line corresponding to sig3'/sig1' =0.50 is reached. The action to be taken is represented by a WAIT command. As the tester became more competent with the test procedure this was changed to a WAIT-TRIGGER command.

4.3.2(d) Anisotropic Consolidation (PL stress path)

When the K_o-line had been attained, the test sample could now be considered to be under *in-situ* stress conditions. Anisotropic consolidation within the triaxial device enables the pore water pressure to be dissipated under load application in conjunction with conditions of lateral restraint.

Anisotropic consolidation (under stress-controlled conditions) comprise of stage 4 in the test. Basically, there are only two ways of following the PL stress path (anisotropic consolidation). The first method involves adopting a procedure for controlling the radial strain using ram pressure (BOX 3). As the UCT stress path triaxial device has no radial strain gauge, this method is ignored. The second method was adopted and consisted of setting the control parameter for BOX 3 to 'q' and incrementing it at a certain pulse rate.

The lateral restraint of the test sample is managed by way of keeping the cell pressure (BOX 2) constant. Since the cell pressure σ'_3 or sig3' is the variable, which directly influences changes in the requirement of K_o (σ'_3/σ'_1 =0.50), a rearrangement of the equation is needed. The equation is rearranged so that σ'_3 is the dominant variable in the equation and is independent of all other variables. The new equation is (sig3') – 0.50*(sig1') = 0. To satisfy this equation the hold value of BOX 2 is set to 75 kPa, so that the control system could adjust BOX 2 as the test progresses along the K_o line. When an effective mean stress (p') value of 125 kPa is reached, the alarm set in stage 4 is stipulated and a WAIT action is followed.

4.3.2(e) Undrained Application of Load (strain-controlled CTC stress path)

The final stage of the non-conventional stress path test (stage 5) involves the shearing of the sample under strain-controlled conditions. The designated rate of load application is an important consideration in triaxial testing. The incrementation for constant strain pressure (BOX 4) is set at 7N/hr at a pulse rate of 7 units. BOX 2 (cell pressure) is set at the hold value, which is attained at the end of the PL stress path (stage 4). The alarm that is assigned to stage 5 is a STOP command, which is initiated when the axial strain is greater than 12% (strain>=12).

With a thorough understanding of the control philosophy, the simulation of, in principle, any triaxial stress path can be conducted in the laboratory. It should be noted that a few of the triaxial tests were difficult to control, but as the experimenter became more aware of the fundamentals involved in stress path propagation, the control method improved.

Although many textbooks discuss the control of triaxial tests in terms of theory and methods, it was felt that there was a lack of or very little information is provided regarding the specific rates to apply to a particular stress path. The specific rates that are applied are those, which in general practice, consist of conventional triaxial compression testing. Conventional rates of strain that are suggested by Toll (1993) by means of various relationships did not fulfill the requirements for sensitive, sophisticated testing. A great amount of experimenter discretion and patience is needed.

The non-conventional stress paths are followed by means of coordinated pressure increments that are experimentally changed at particular effective mean stress points in the test. By means of pressure manipulation, a correct rate of strain was found experimentally and the remaining stress path tests were then completed at this new rate.

4.4 Preparation and Installation of Test Specimen

The undisturbed specimens of Maguga clay were extracted from a 38mm diameter cutting tube that was pressed into an undisturbed block of clay. The cutting tube was pressed 100mm deep into the block at a rate of 2mm per minute by means of a Zwick universal testing machine. The slow rate ensured that any disturbance of the specimen due to the cutting process was kept at a minimum. The extracted samples were trimmed to approximately 77mm in accordance with the height-diameter ratio 2:1 as specified by ASTM D2850-82.

All remoulded test samples were prepared by the method of moist tamping. Moist tamping is a convenient and practical procedure to remould test samples. A sufficient amount of Maguga clay was air-dried. The dry material was then mixed with a small amount of water to the optimum moisture content (28% ± 0.2%) and left to hydrate for about 48 hours before tamping commenced. The amount of moist material was weighed so that the desired moist density corresponding to a prearranged volume (8.73×10^{-4} m^3) could be achieved. The Maguga clay samples were tamped into the equipment mould in three equal-mass layers. The lower layers were slightly under-compacted such that the compaction from successive layers would produce a sample of uniform density when

preparation was completed. Layers that were not compacted properly produced areas of weakness in the sample. The test samples displaying inconsistent compaction were rejected from the research work.

The dimensions and mass of the prepared samples were carefully measured. Samples that were not scheduled for testing were placed in an airtight bag and placed in a storage fridge. No loss (or addition) to the samples' mass occurred when the relevant test sample was removed from the fridge. The appropriate test sample was mounted on the pedestal in the triaxial cell and a spiral filter paper side-drain was carefully placed around the sample. The spiral side-drain was slightly wetted to enhance the drainage efficiency of the sample. A double latex membrane and o-rings were placed in position and the cell was filled with de-aired water. In Figure 4.3 a fully prepared sample in the triaxial cell is shown.

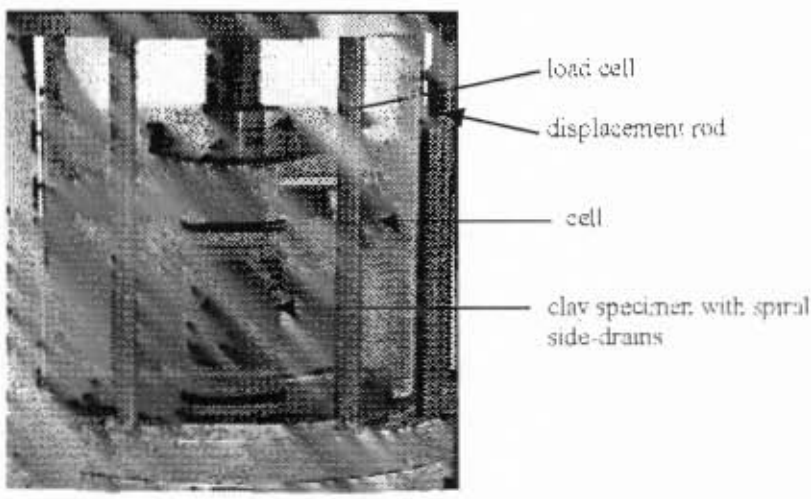

Figure 4.3 Prepared sample in the triaxial cell

4.5 Triaxial Stage Discussions

4.5.1 Saturation

The Maguga clay initially required 18 to 24 hours for 98% saturation to be achieved. This was not satisfactory and the prolonged period of saturation produced a phenomenon

that is termed 'undrained creep' (Head, 1986). This type of creep only occurs when the sample is kept under pressure with the drainage valve closed for a long period (such as overnight for instance). In this period the 'locked-in' pore water pressure increases gradually resulting in an increase of the coefficient B. The saturation period was improved by the placement of spiral filter side-drains around the sample. Side-drains are particularly effective if the test material permeability is less than about 10^{-8} m/s. The drains facilitate a more rapid equalisation of pore pressure by providing a shorter radial drainage path. The saturation target of 98% was now reached in approximately 12 hours.

The saturation of the Maguga clay was attained by increasing the back pressure in constant increments. The cell pressure was increased incrementally to ascertain the pore water pressure response of the clay (back pressure was closed). From these incremental stages of pressure increases a pore water coefficient B was ascertained using the equation:

$$B = \Delta u/\Delta\sigma_3 \qquad (4.1)$$

The major advantage in using the incremental increase of back pressure is that air that is trapped in the voids, between the membrane and the sample, in the cell and in the drainage lines is forced into solution (at about 300 kPa) under applied pressure. In the case of an undrained test, air is removed from the sample, which improves the response time of the pore pressure readings. Once the 98% saturation mark ($B \cong 1.0$) was reached the triaxial cell was closed in readiness for the next stage – consolidation.

4.5.2 Consolidation

Isotropic Consolidation

The consolidation stage is the phase of triaxial testing whereby excess pore pressure, present in the sample, is dissipated with time. In this research series the rate of consolidation was improved by placing spiral filter side-drains around the sample. The

side-drains shortened the dissipation of the excess pore pressure with respect to time by providing drainage in the radial direction (i.e. shortening of the drainage path).

In Figure 4.4 the drainage conditions that occurred in the vertical and radial directions during the consolidation stage is schematically shown.

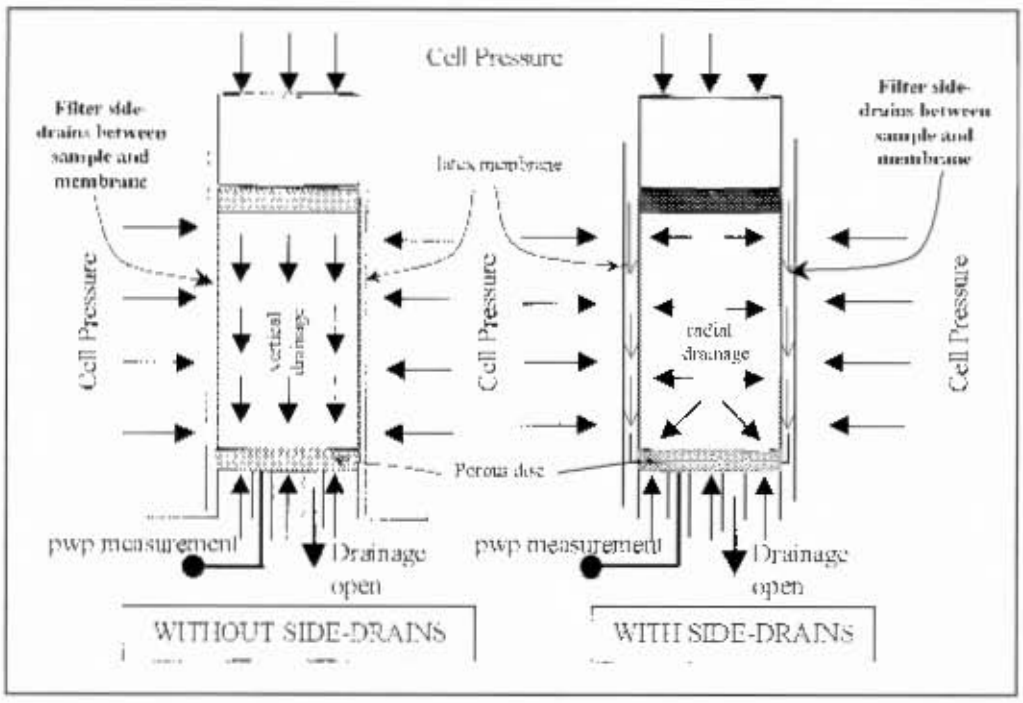

Figure 4.4 Drainage conditions during isotropic consolidation

The consolidation stage is initiated by setting the back pressure to a hold value of 300kPa in the stage editor. The back pressure valve still remained closed up to this point in the test. The cell pressure is then incrementally adjusted (either decreased or increased) to accommodate the desired effective stress. The back pressure valve is opened and consolidation is allowed to continue until at least 90% of the excess pore pressure is dissipated. The consolidation phase is deemed to be complete when there were no further back pressure volume changes and the pore pressure remained constant at 300kPa.

Anisotropic Consolidation

The anisotropic consolidation phase consists of applying an axial load (in increments) to the sample during consolidation. In this type of consolidation stage the load and cell pressure are applied in order to maintain a constant ratio of the horizontal and vertical principal effective stresses (σ'_h/σ'_v) equal to K_o, the coefficient of earth pressure at rest. The K_o condition applies to the consolidation in-situ of a wide stratum of soil, such as an earth embankment under its own weight. The K_o condition represents a state of no lateral movement by the soil in the centre of an embankment (as discussed in Section 2.3.2). In Figure 4.5 the initial stress condition after saturation and the drainage induced during an anisotropic consolidation phase is schematically shown.

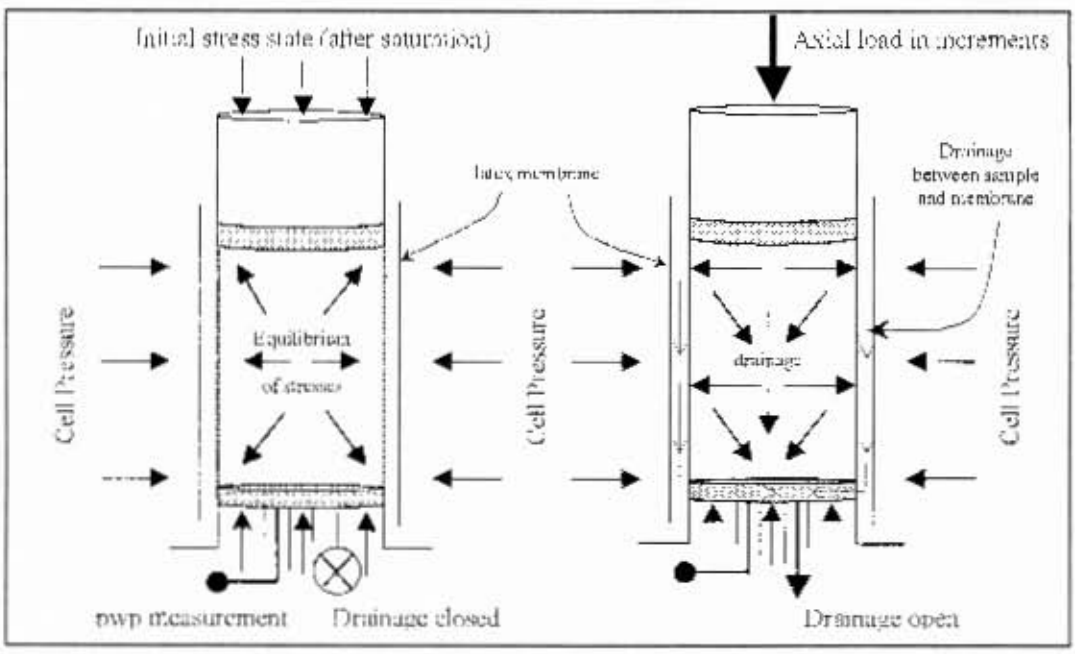

Figure 4.5 Initial stress state and drainage during anisotropic consolidation

4.5.3 Application of Load

Only undrained triaxial tests were conducted in the laboratory. Undrained tests allow no movement of water through the sample (i.e. no volumetric changes). The shearing phase of the triaxial test can be either stress-controlled or strain-controlled. Stress-control,

which is generally not available in standard triaxial testing, was used for the stress preconditioning stages such as the proportional loading (PL) and the constant effective mean stress p' (TC) stress paths. The flexibility of stress-control allowed the experimenter a certain degree of experimental control, which was not the case in strain-control. Stress-controlled operation was undertaken for the TC and PL stress path tests, while strain-control was implemented in the CTC and RTC stress path tests.

Undrained application of load

It was decided that since the sample was the minimum size specified in ASTM specifications, the rate should be decided upon according to the soil material characteristics and the judgment of the experimenter. Rates that were specified from various relationships by Toll (1993) were initially found to be too fast for the clayey test material. The rate was found experimentally and accepted at 0.00668 mm/min (strain-controlled). At this rate the samples reached ultimate shear failure in approximately 8 hours. The attributes of the spiral filter side-drains were again emphasised by the fact that they provided no additional support to the failing sample, hence no correction factor was needed

In Figure 4.6 a typical Maguga clay specimen at failure in undrained compression is shown.

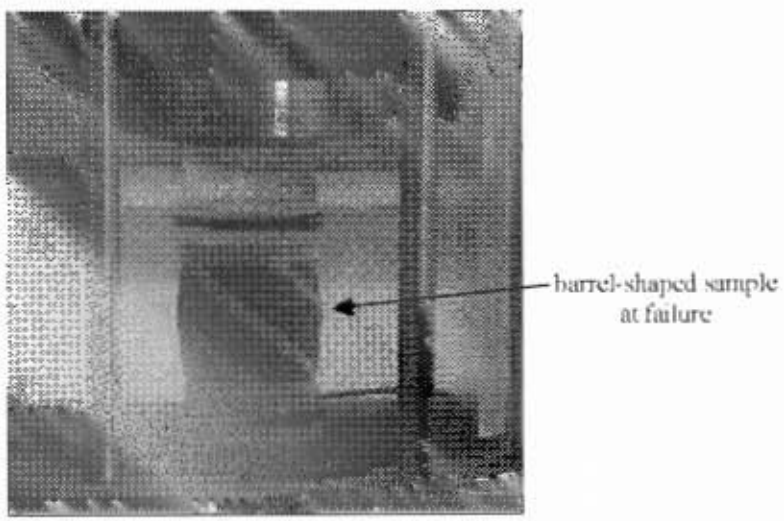

Figure 4.6 Typical representation of undrained compression

4.6 Initiation of Test Stages

The initiation of the test stages commenced when a step-by-step procedure had been followed. This procedure consisted of experimental checks and command checks of the TRIAX software. The testing started once certain criteria had been satisfied. The criteria were as follows:

STEP 1: Placement of sample in the triaxial cell and the filling of the cell with de-aired water. Ensure that most air bubbles are removed from inside the cell by carefully guiding the bubbles through the bleeding plugs. Check to see that there are no leakages and that the pressure supply holds at a constant level.

STEP 2: The function keys on the keyboard control all commands of TRIAX. The first command to be pressed is SHIFT F8 (*Triaxial Initialise*). This command asks the user if he/she is satisfied with the calculated tables and provides an option to delete or add any calculation variables. Check to see that the right variables are displayed.

STEP 3: Initiate F2 (*Disk On/Off*) and F4 (*Scan On/Off*). These commands enable the user to make automatic or manual readings at specific time intervals and records them in a file that is specified and named by the user. Check to see if they are on by pressing CONTROL F5 (*Device List*). By no means should the scan and disc commands be switched off at any time in the testing period. If one of these commands is off then step 2 must be repeated.

STEP 4: Reset the current cell, back, displacement and load measurements by pressing F7 (*Reset*) so that a reference point of measurement is established. Check that the user has recorded the necessary datum measurements.

STEP 5: Check that the correct control equations, hold values, pulse rates and alarms are in the correct control boxes by pressing SHIFT F7 (*Stage Set*). The stage editor

will automatically check to see that the correct variables have been entered once the user is satisfied with a particular stage editor.

STEP 6. Switch the printer on by pressing F1 (*Printer On/Off*) and start the test F9 (*Control On/Off*). Check that initial measurements have been recorded. The plotting of graphs F6 (*Plot On/Off*) can be switched on at any time of the testing.

STEP 7. On completion of testing, the results can be converted to a compatible format by pressing CONTROL F9 (*Tabulate Calculations*). The computer then follows a sequence whereby the sample properties (height, length, diameter, dry density and specific gravity) are asked for. On completion of the sample properties, the TRIAX program will inform the user to save the data in a recognisable format.

CHAPTER 5

TRIAXIAL RESULTS, ANALYSES AND DISCUSSIONS

5.1 Introduction

All conventional and non-conventional triaxial stress path results are presented in *Chapter 5*. Conventional (CTC) tests were conducted on 'undisturbed' and remoulded Maguga clay under undrained conditions, while only remoulded test samples were used in the non-conventional tests. The non-conventional triaxial stress path tests consist of both drained and undrained conditions. The drained application is undertaken to facilitate the application of a stress 'history'.

A comparison is made between 'undisturbed' and remoulded conventional triaxial compression tests. The objective is to compare the undrained stress-strain-strength behaviour of 'undisturbed' and remoulded samples. The results of the conventional triaxial compression tests will later (in *Chapter* 6) be implemented in the evaluation of the critical state model parameters.

Further, non-conventional triaxial test results were assessed to investigate the soil behaviour due to a combination of common stress paths that could be experienced in the field. The combination of simulated stress paths were composed of loading and unloading paths to demonstrate that remoulded samples for laboratory testing are influenced by the stress 'history' that the soil structure is subjected to. The analysis of the stability of dam embankments (as well as other geotechnical applications) does not take account of stress paths in a non-conventional context.

The aim of *Chapter 5* is to highlight the stress-strain-strength characteristics of the triaxial test results and emphasise their diversity as a result of the induced stress path. The results and the observations are concluded in a summary at the end of *Chapter 5*. The results, observations and comparisons are presented in terms of the Mohr-Coulomb shear strength parameters and stress-strain relationships.

5.2 Remoulded and Undisturbed Shear Response and Discussion

5.2.1 CTC Undrained Stress Path (remoulded)

In Figure 5.1, the conventional (CTC) stress path results of remoulded Maguga clay specimens are shown in terms of deviator stress (q)-effective mean stress (p'), deviator stress (q)-axial strain (ε_{axial}) and pore water pressure (u)-axial strain (ε_{axial}) diagrams, tested at effective stresses of 75 kPa, 200 kPa and 500 kPa. The Mohr-Coulomb shear strength parameters, derived from the failure surface (as shown) are calculated using the conversion equations (2.3) in *Chapter 2*.

Referring to Figure 5.1(a), from the stress path response of the conventional triaxial test the shear strength parameters $\phi' = 27.9°$ and $c' = 10.0$ kPa are calculated. The q-p' relationships demonstrate normally consolidated behaviour, except for the test results at an effective stress of 75 kPa.

The q-p' response of the test consolidated at 75 kPa is attributed to either a local failure within the soil structure or simply demonstrates an interesting property associated with the Cambridge Stress Plot method. The 'roughly' constant p' path attained in the 75 kPa result (shown in Figure 5.1(a)) is by definition of the Cambridge method characterised by a soil with elastic properties (Head, 1986). Normally consolidated, elastic soil behaviour is associated with a constant p' stress path in the q-p' diagram. The conventional (CTC) triaxial results provide an insight with regards to Maguga clay behaviour in low-pressure ranges (the 75 kPa consolidated test was not repeated due to program constraints).

The importance of soil structure consistency (i.e. compaction effort) is primarily the reason for the behavioural characteristics that are attained in remoulded soil tests. The compaction efficiency is in turn affected by the method of compaction that is used to produce the test samples (Hoeg et al. 2000). The response conducted on remoulded Maguga clay with the lowest initial effective mean stress (75 kPa) is not expected and could also be attributed to inconsistent compaction efficiency of the soil structure during the preparation of the sample.

In Figure 5.1(b), the tests with an effective mean stress of 200 kPa and 500 kPa gave similar and consistent stress-strain responses showing typical ductile behaviour associated with soil material of high plasticity. The test consolidated at 75 kPa displayed a clearly defined peak at a deviatoric stress of 80 kPa at approximately 0.4% axial strain. An insignificant weakening of deviator stress then followed the peak strength, which, in turn, was followed by a slight increase towards a residual strength of 75 kPa. Again, this response could be attributed to a local weakness, within the soil structure.

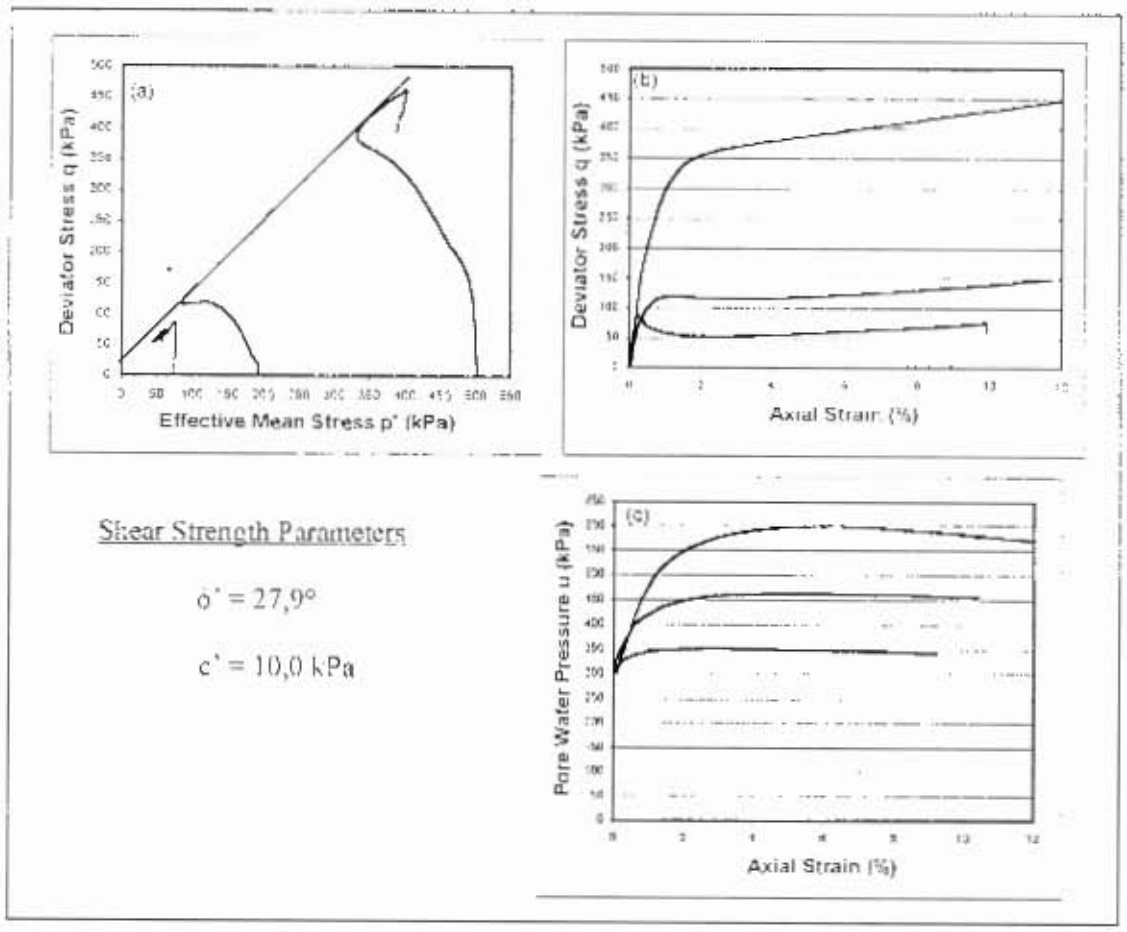

Figure 5.1 CTC stress path results of remoulded Maguga clay

Pore pressure using effective stress methods is a critical issue of stability analysis for dam embankments. It is relatively easy to monitor pore pressures in an embankment and compare these pressures to those attained in conventional triaxial tests. In Figure 5.1(c), the pore water pressure-axial strain relationship for the 75 kPa, 200 kPa and 500 kPa

effective mean stresses are shown. All three tests displayed an asymptotical approach to an 'undefined' peak with a slight decrease thereafter.

5.2.2 CTC Undrained Stress Path (undisturbed)

In Figure 5.2 the conventional (CTC) stress path results of undisturbed Maguga clay specimens are shown in terms of deviator stress (q)-effective mean stress (p'), deviator stress (q)-axial strain (ε_{axial}) and pore water pressure (u)-axial strain (ε_{axial}) diagrams, tested at effective stresses 75 kPa, 200 kPa and 500 kPa. The Mohr-Coulomb shear strength parameters are also shown.

In Figure 5.2(a) the q-p' relationships again demonstrate a normally consolidated behaviour of the undisturbed clay.

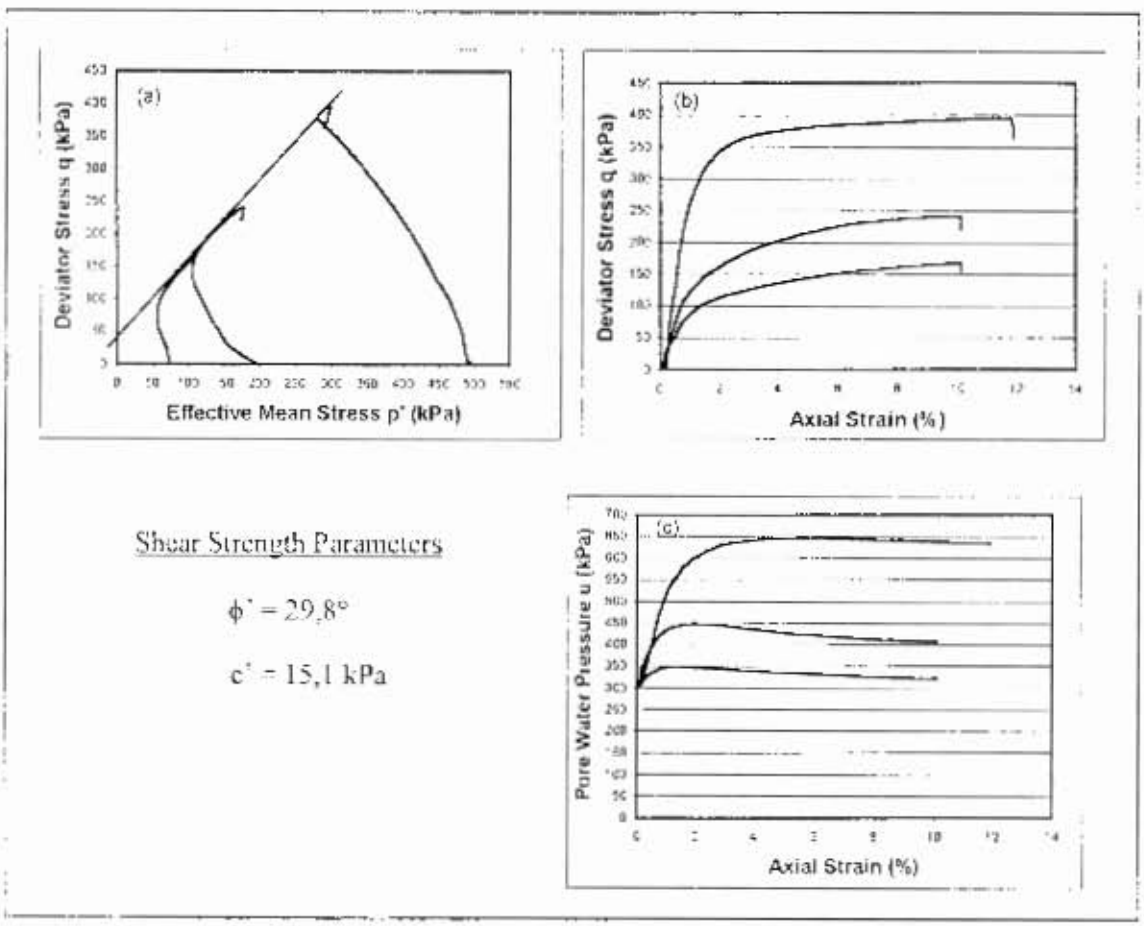

Figure 5.2 CTC stress path results of undisturbed Maguga clay

The tests were stopped at 10% and 12% axial strain, respectively (assuming that failure was achieved). The shear strength parameters (using equation 2.3), resulted in shear parameters of $\phi' = 29.8°$ and $c' = 15.1$ kPa for the undisturbed clay material.

Referring to Figure 5.2(b), the response of all the tests is very consistent. The deviator stress-axial strain relationships approach a peak deviator stress (which decrease abruptly once the control function of the stress path device is switched off).

The pore water pressure-axial strain relationship is shown in Figure 5.2(c). The pore water pressure for the undisturbed (CTC) tests peak at relatively low strain levels and then decreases once peak failure conditions are satisfied.

In Table 5.1, the initial and final properties of the remoulded and undisturbed samples for the conventional triaxial tests are listed.

		Initial Properties			Final Properties		
Test Description	Effective Mean Stress (kPa)	Moisture content (%)	Dry density (kN/m^3)	Void ratio	Moisture content (%)	Dry density (kN/m^3)	Void ratio
CTC (remoulded)	75	27.9	1454	0,87	33.8	1461	0,85
	200	28.1	1451	0,87	33.1	1459	0,85
	500	28.0	1466	0,85	30.9	1473	0,84
CTC (undisturbed	75	33.8	1370	0,98	37.6	1455	0,91
	200	33.8	1419	0,90	33.6	1434	0,89
	500	33.8	1374	0,97	35.4	1466	0,85

Table 5.1 CTC stress path: Initial and final properties of remoulded and undisturbed samples

The initial water contents of the remoulded test samples were prepared at optimum moisture content (OMC = 28.1%), while the undisturbed test samples had an initial water content of 33.8% (OMC + 6%). The initial dry densities of the remoulded samples are prepared within 1% of the target maximum dry density of 1460 kg/m^3. The initial dry densities of the undisturbed samples are all lower than those of the remoulded maximum dry densities. The final dry densities of all remoulded samples subjected to conventional and non-conventional triaxial tests (see Tables 5.1 to 5.3) demonstrate a tendency to approach densities at failure characterised by a void ratio of approximately 0.85.

It is this void ratio that will be used in the normalisation process of the triaxial test results in the critical state analysis of *Chapter 6*.

5.2.3 CTC Stress path: Discussions and comparisons of remoulded and undisturbed Maguga clay

The analysis of the long-term stability of dam embankments is undertaken using effective stress methods to determine ϕ' and c'. The reasoning behind using effective stress methods is based on the fact that strength parameters can be estimated with some degree of confidence (provided triaxial tests are carried out correctly), and the pore pressures can be estimated reasonably accurately. The effective stress method allows a confident assessment of the stability of the embankment (with regards to the factor of safety).

The initial moisture content of the undisturbed samples is 6% higher than those of the remoulded samples. The undrained strength of compacted clay is dependent on the compaction density and the moisture (water) content. As can be seen from Figure 5.3, clay with water content lower than the optimum water content shows a stiffer soil structure response, which causes the soil to peak at an early strain (see Sample No. 1 and 2 in Figure 5.3). As the water content is raised above the optimum water content, the soil structure becomes more plastic (Sample No. 4 to 6).

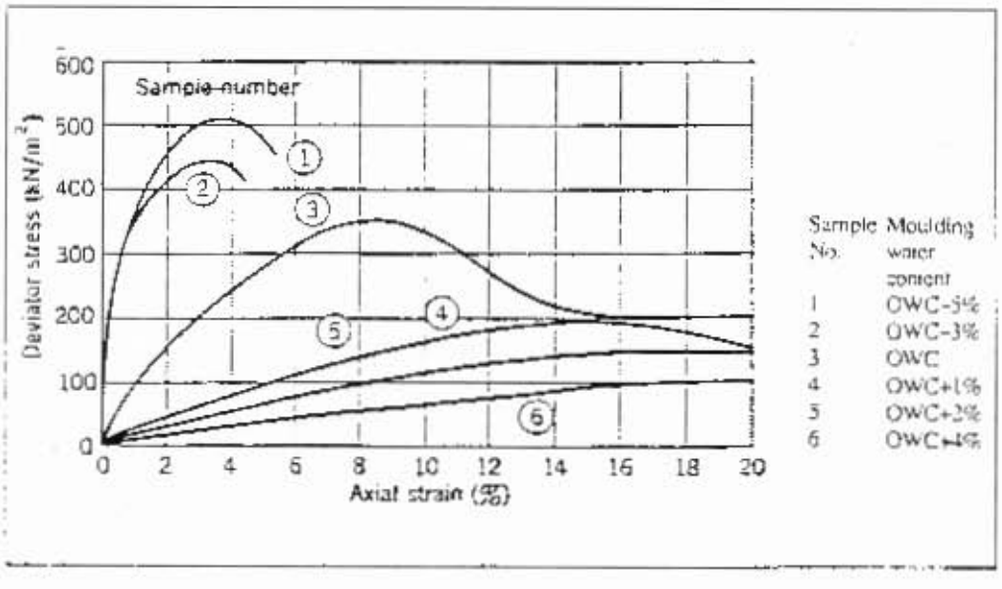

Figure 5.3 Dependence of undrained strength of compacted clay on compaction density and water content (Lambe and Whitman, 1979)

The q-ε_{axial} test results on remoulded material peaked at an early strain and then progressed in the vicinity of stress-strain curve of Sample No. 3 (representing optimum water content conditions). The stress-strain curves of the remoulded test samples were too poor to make any conclusions relative to the optimum moisture content (see Figure 5.1). However, the undisturbed q-ε_{axial} test results show a clear tendency to peak at a greater strain (approximately 10% to 12%). The undisturbed test results are suitably represented by the stress-strain curve of Sample No. 4 (OMC + 1%). The difference (OMC - 5%) between the initial water content of the undisturbed samples (33.8% = OMC - 6%) and that, which is shown in Figure 5.3 (OMC + 1%), reinforces the possibility of another 'peak' on the compaction curve (refer to *Chapter 3*).

The shear strength parameters of the undisturbed clay material are 2° and about 5 kPa higher than those attained in the remoulded CTC test results. The response of the undisturbed clay could be attributed to the stiff soil structure of the material (properties that are discussed in *Chapter 3*). The internal soil structure of the clay thus clearly plays an important part in the behavioural response of the clay. The void ratio changes and changes in water content that occur during the various triaxial stages (i.e. saturation and isotropic consolidation) represent different soil structure deformations at a particulate level.

The peak deviator stress results of the undisturbed clay are higher than those of the remoulded tests. The difference is considerable in the 75 kPa and 200 kPa effective mean stress tests. The peak deviator stress of the undisturbed clay is up to 50% higher than those in the remoulded tests. The difference in deviatoric stress influences the magnitude of the Mohr-Coulomb shear strength parameters ϕ' and c' and therefore the factor of safety (FS) for the embankment.

The factor of safety for an embankment (in terms of deviator stress) is based upon the deviator stress attained in the triaxial tests over the calculated working deviator stress of the embankment (Factor of Safety (FS) = $q_{ultimate}/q_d$). The factor of safety would then be incorporated into formulations, which are based on the parameters ϕ' and c' (i.e. $\tan \phi_d = \tan(\phi'/FS)$ and $c_d = c'/FS$).

The pore water pressure results from both conventional triaxial compression (CTC) series are similar. The only difference that could be noted is the fact that the peak pore pressure condition is reached at a higher strain in the remoulded test samples because of the less stiff nature of the soil structure. The application of loading onto the remoulded sample probably resulted in a redistribution of the load within the soil structure itself. The initial void ratio is higher in the remoulded soil structure; hence a build-up of excess pore pressure could be readily 'dissipated' through the sample. The stiff, undisturbed clay (with a higher initial water content and lower void ratio) could not redistribute the pore pressure about the same peak pore water pressure, hence the build-up of pore water pressure was observed at a low strain.

5.3 Non-conventional Stress Path Results and Discussions

Since all non-conventional stress path triaxial tests followed or joined up with the K_o state of stress, the knowledge of the coefficient at rest is a prerequisite of these tests (as discussed in Section 2.3.1).

The appropriate choice of the value for the K_o coefficient for the remoulded Maguga clay in an envisaged embankment was a difficult one. According to Head (1986), a value of 0.8 to 1.2 for a lightly, overconsolidated clay and 0.7 for remoulded clay is suggested. Wood (1990) stated that a soil that is composed of rigid, interlocked particles that could support its own weight without pushing sideways and thus preventing lateral movement, such a soil would be expected to have a low value of K_o. Using Jaky's (1944) expression (see equation 2.5 in *Chapter 2*) and the angle of internal friction (ϕ') of 27.9° attained from the remoulded, conventional triaxial test (CTC) gave a K_o coefficient of approximately 0.50. It is felt this to be a more representative value than the one suggested by Head (1986).

5.3.1 HC-TC-PL-RTC Stress Path

In Figure 5.4 the hydrostatic compression (HC), triaxial compression (TC), proportional loading (PL) and reduced triaxial compression (RTC) stress path results of remoulded

specimens are shown in terms of deviator stress (q)-effective mean stress (p'), deviator stress (q)-axial strain (ε_{axial}) and pore water pressure (u)-axial strain (ε_{axial}) diagrams, tested at effective stresses 75 kPa, 200 kPa and 300 kPa. The Mohr-Coulomb shear strength parameters (from conversion equation (2.3) in *Chapter 2*), are also shown.

The deviator stress-effective mean stress relationship for the non-conventional HC-TC-PL-RTC stress path is shown in Figure 5.4(a). The reduced triaxial compression (RTC) stress paths are initiated at effective mean stresses 125 kPa, 250 kPa and 350 kPa located on the K_o = 0,50 line. The converted shear strength parameters gave ϕ' = 29,8° and c' = 13,5 kPa for the HC-TC-PL-RTC stress path test of the remoulded material.

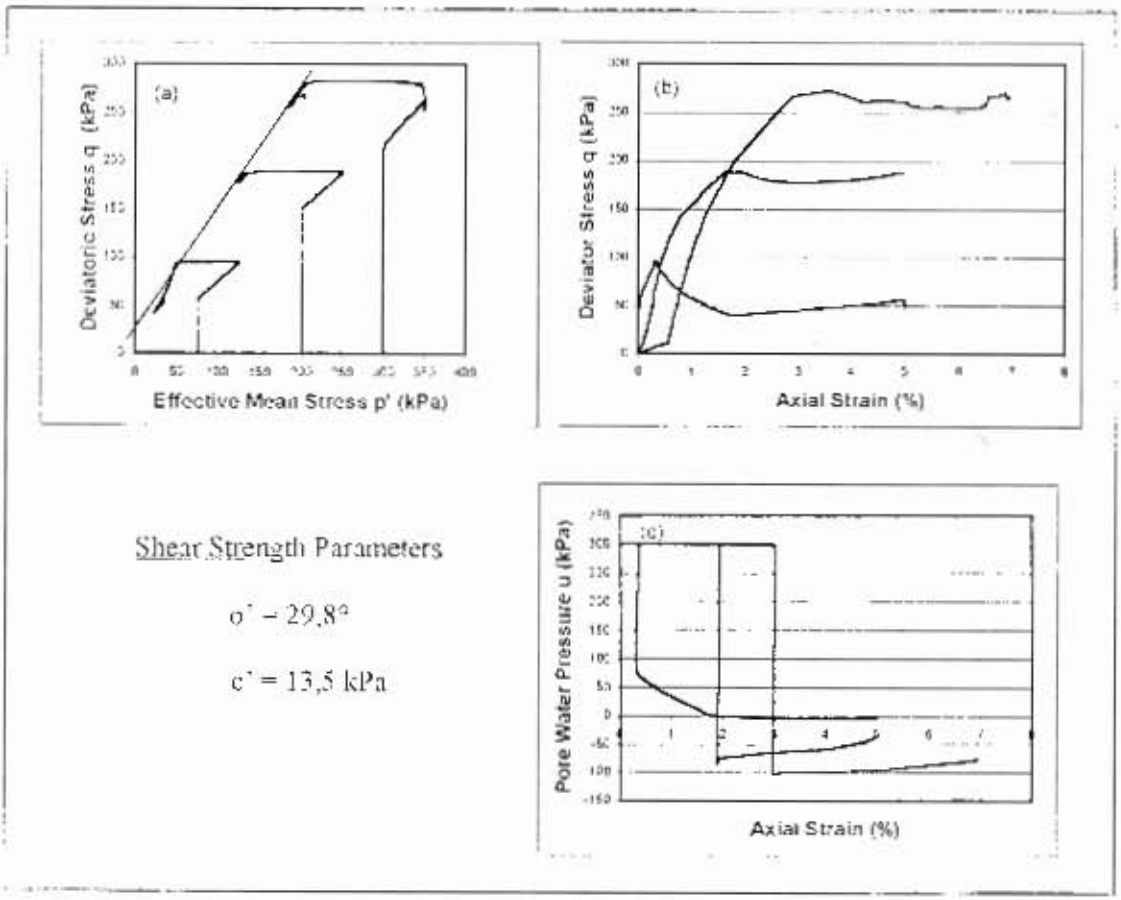

Figure 5.4 HC-TC-PL-RTC stress path results of remoulded Maguga clay

In Figure 5.4(b) the deviator stress-axial strain relationship is shown. This non-conventional stress path test reached failure conditions rapidly once the reduced triaxial

compression (RTC) stress path was initiated and never reached the set 'cut-off' axial strain mark of 10%.

As can be seen in Figure 5.4(b), the stress-strain relationships peaked at a low axial strain, which is followed by an insignificant weakening of deviator stress. The remoulded stress-strain relationship reflected the behaviour of a stiff material.

Referring to Figure 5.4(c), the pore water pressure-axial strain relationship is shown. The smooth pore water pressure curves from previous conventional tests cannot be observed in this non-conventional stress path test. The pore water pressure is forced to stay constant while σ_1 and σ_3 are manipulated following the triaxial compression (TC) and proportional loading (PL) stress path application, hence the respective pore water response as shown. A rapid drop in pore water pressure is observed as soon as the RTC path is initiated. This sudden drop was to be expected by definition of the RTC path and preceded into the negative pore pressure region. The pore water pressure then increased insignificantly when the test samples approached failure.

5.3.2 HC-TC-PL-RTC Stress path: Discussion and comparison with previous test results

The hydrostatic compression (HC) stress path is discussed in this section of the research work (and neglected in the conventional section) as it forms a necessary part of the 'preconditioning' phase of non-conventional stress path tests.

The non-conventional HC-TC-PL-RTC stress path test resulted in shear strength parameters, which are very similar to the shear parameters that were attained in the CTC stress path test of undisturbed clay material. The shear strength similarity may be attributed to the stress preconditioning (i.e the controlled 'drained' HC-TC-PL stress applications), which was applied to the remoulded test samples. The application of the HC-TC-PL stress paths clearly changed the soil structure of the remoulded clay to a structure of a 'stiffer' nature.

The deviator stress-axial strain relationships of Figure 5.4(b) show the peak deviator stress characteristics, which is generally associated with stiff material behaviour. The gradient of the deviator stress-axial strain relationships show for all three tests, the same change in gradient. The gradient of the q-ε_{axial} curves are steep during the TC stress path application and decrease slightly once the PL stress path is initiated. This is an indication of the remoulded material changing from a stiff soil structure to a more plastic structure (i.e. a change in the stiffness of the test sample). The change in stiffness is not only attributed to structural differences, but also affected by the drainage conditions (i.e. controlled 'drained' or undrained conditions) as well as the combination of applied stress. The fact that the RTC and CTC pressure systems differ in many aspects (such as stress path direction and the rate of loading/unloading application) also has an effect on the stiffness of the test samples. The changes in stiffness resulted in the peak deviator stress response of all three HC-TC-PL-RTC tests to be approximately 30% lower than that, which was attained in the conventional (CTC) stress paths of undisturbed samples.

The failure of the samples occurred rapidly with the RTC stress path initiation from the selected stress points on the K_o line. The rapid failure of the sample is also accompanied by a rapid decrease in pore water pressure (see Figure 5.4(c)). The pore water response decreased considerably until negative pore pressures were observed. The pore water pressure scenario is best described by a schematic in Figure 5.5, to demonstrate what is happening to the pore water pressure in terms of soil structure stability.

Referring to Figure 5.5, the stress conditions before the initiation of the reduced triaxial compression (RTC) stress path are such that the pore water pressure is at equilibrium with the stress applications and the current application of loading on the PL stress path.

The 'before' stress condition is such that:

$$q = (\sigma'_1 + \Delta\sigma'_1) - (\sigma'_3 + \Delta\sigma'_3)$$

and

$$p' = (\sigma'_1 - \Delta\sigma'_1) - 2(\sigma'_3 + \Delta\sigma'_3)/3$$

with $K_o - \Delta\sigma'_3 / \Delta\sigma'_1 = 0.50$, therefore $\Delta\sigma'_1 = 2 \times \Delta\sigma'_3$, which means that σ'_1 is increased by $\Delta\sigma'_3$ and σ'_3 is increased by $\Delta\sigma'_3$ while the pore water pressure (u) remains constant according to TRIAX control (as shown in Figure 5.4(b)).

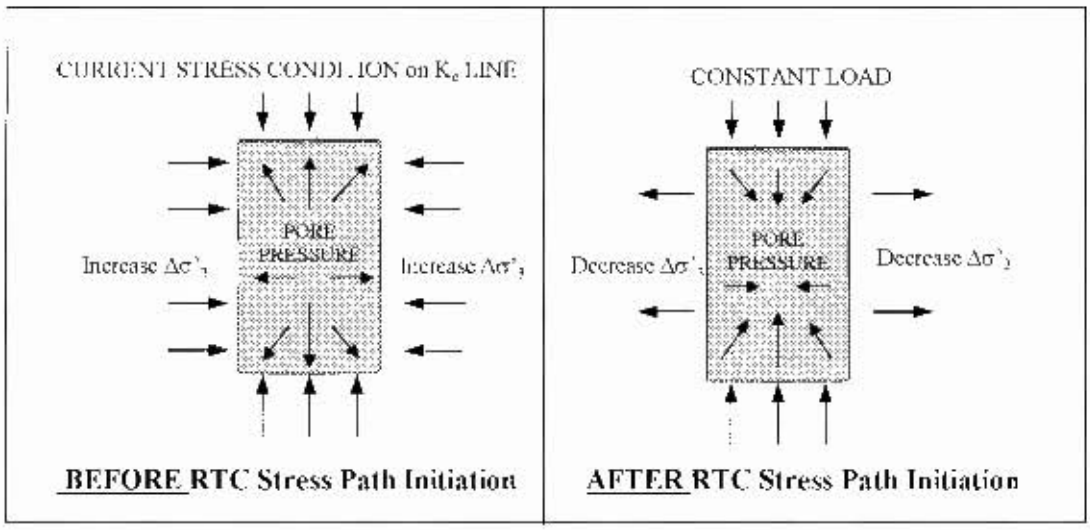

Figure 5.5 Schematic representation of pore water pressure before and after initiation of RTC stress path

After the initiation of the reduced triaxial compression (RTC) stress path, the confining pressure σ'_3 is decreased incrementally, while the deviator stress is kept constant. The stress condition after initiation is such that:

$q - \sigma'_3$ with $\Delta\sigma'_1 = 0$, while σ'_3 is decreased by $\Delta\sigma'_3$ and there is a rapid drop in pore water pressure, $\Delta u \neq 0$ (see Figure 5.4(c)).

The soil structure counteracts the decrease in confining pressure (σ'_3) by constricting the sample (the sample tries to 'pull or keep itself together'). The pore water pressure within the soil structure counteracts the imbalance of stress and tries to reach a new equilibrium with regards to the new stress conditions, while the loading application is kept constant. The rapid drop of the pore water pressure at the onset of the RTC stress path also has an effect on the stiffness of the test samples.

In reality, the lower embankment layers during initial construction consist of soil that is usually heavily over-consolidated and has negative pore water pressure. As additional

layers are placed, the loading on lower embankment layers will produce an increase in pore water pressure, resulting in positive pore pressures.

5.3.3 HC-TC-PL-CTC Stress Path

In Figure 5.6 the hydrostatic compression (HC), triaxial compression (TC), proportional loading (PL) and conventional triaxial compression (CTC) stress path results of remoulded Maguga clay are shown in terms of deviator stress (q)-effective mean stress (p'), deviator stress (q)-axial strain (ε_{axial}) and pore water pressure (u)-axial strain (ε_{axial}) diagrams, tested at effective mean stresses of 75 kPa, 200 kPa and 300 kPa. The Mohr-Coulomb shear strength parameters are also given.

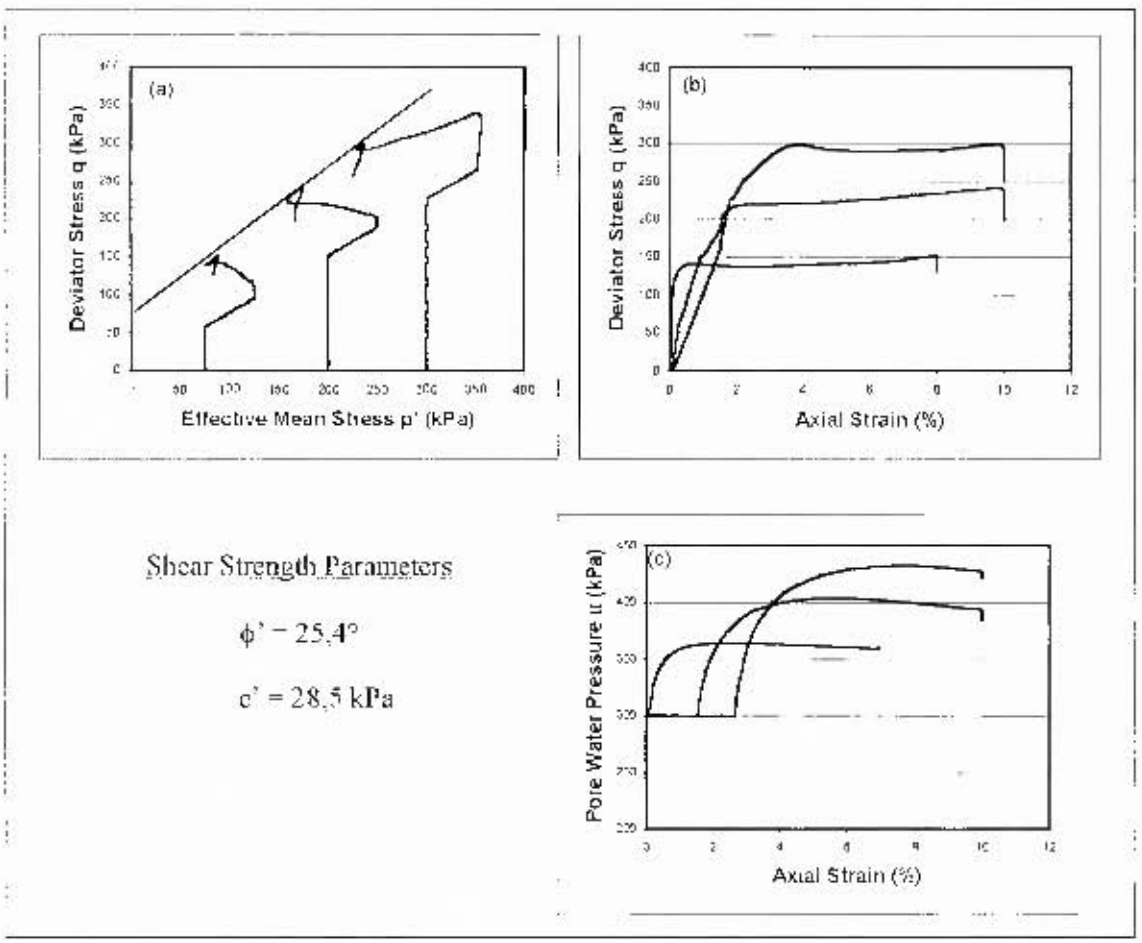

Figure 5.6 HC-TC-PL-CTC stress path results of remoulded Maguga clay

The hydrostatic compression (HC) stress path (isotropic compression) again formed the focal point for this stress path investigation. The Maguga clay is subjected to the same controlled 'drained' HC-TC-PL stress path that was followed in the preceding non-conventional stress path test. Anisotropic consolidation along the $K_o = 0.50$ line (PL stress path) was followed by a conventional (CTC) stress path that was taken to failure in undrained condition.

In Figure 5.6(a), the deviator stress-effective mean stress relationship is shown. As mentioned before, the conventional (CTC) stress paths were initiated at effective mean stresses on the K_o line, namely 125 kPa, 250 kPa and 350 kPa, respectively. The shear strength parameters are $\phi' = 25.4°$ and $c' = 28.5$ kPa for the non-conventional (HC-TC-PL-RTC) stress path tests on remoulded clay specimens.

Referring to Figure 5.6(b), the deviator stress-axial strain relationships are shown. The stress preconditioning by the various common stress paths, namely the controlled 'drained' HC-TC-PL stress paths produced a response characterised by stiff soil behaviour. This non-conventional test was taken to failure and stopped at the preset 10% axial strain mark. The decrease in deviatoric stress after failure was as a result of the stress path device being switched off and can be disregarded.

In Figure 5.6(c), the pore water pressure-axial strain relationships are shown. The pore water pressure curves are representative of failure conditions defined by peak deviatoric stresses. The undrained pore pressure response is typical for the remoulded test samples.

The initial and final soil properties of the non-conventional (HC-TC-PL-CTC) and (HC-TC-PL-RTC) stress paths are listed in Table 5.2.

Test Description	Initial Properties				Final Properties			
	Effective Mean Stress (kPa)	Moisture content (%)	Dry density (kN/m^3)	Void ratio	Moisture content (%)	Dry density (kN/m^3)	Void ratio	Volumetric (%)
HC-TC-PL-CTC (remoulded)	125	27.8	1471	0.84	33.0	1491	0.82	10.86
	250	27.8	1462	0.85	32.2	1471	0.84	7.79
	350	27.8	1460	0.86	31.8	1473	0.84	7.93
HC-TC-PL-RTC (remoulded)	125	27.9	1461	0.85	33.7	1469	0.84	8.95
	250	27.9	1453	0.87	31.6	1466	0.85	7.66
	350	27.9	1464	0.85	30.8	1478	0.83	4.87

Table 5.2 HC-TC-PL-CTC and HC-TC-PL-RTC stress path: Initial and final properties of remoulded samples

As in the previous test series, consistency of the remoulded, triaxial compression tests was maintained throughout the testing period by ensuring that the initial sample properties such as density, moisture content and compaction effort were within 1% of the required values. The target values being the maximum dry density of 1460 kg/m^3 at an optimum moisture content of 28.1% and a sample height of 77.0mm to maintain a consistent volume. Considerable care has been taken to ensure that no loss or gain of moisture content occurred prior to the testing period.

5.3.4 HC-TC-PL-CTC Stress path: Discussion and comparison with previous test results

The non-conventional (HC-TC-PL-CTC) stress path test consisted of stress preconditioning to firstly achieve the selected stress points on the K_o line (where $K_o = 0.50$) and to induce a stress 'history' onto the test sample soil structure itself. The response of the remoulded Maguga clay in this non-conventional test is similar to that, which was observed in the preceding non-conventional (HC-TC-PL-RTC) stress path test. The stiff stress-strain relationship can again be seen in Figure 5.6(b). The gradients of the TC-PL-CTC stress path applications are steeper than those that were observed in the HC-TC-PL-RTC stress path test and all have the a smooth, constant gradient.

The steeper gradients illustrate that these non-conventional test samples were stiffer in comparison to the previous non-conventional stress path test, hence the lower volumetric strains (compare Table 5.2). The stiff soil structure opposed the volumetric straining affects of the sample during the application of the stress states.

There is a 4.4° decrease in the friction angle (ϕ') and an overall increase of approximately 15.0 kPa in the cohesion (c') when compared with the shear parameters of the preceding HC-TC-PL-RTC stress path test. In comparison with the shear strength parameters of the conventional (CTC) tests of remoulded clay, the remoulded HC-TC-PL-CTC shear strength parameters ϕ' and c' were 2.5° lower and 18.5 kPa higher, respectively. This difference is attributed to the sequential stress 'history' that the soil is subjected to. The stress 'history' does affect the enhancement of the shear strength by particle rearrangements within the soil structure.

Bearing the fact in mind that the response from remoulded clay is influenced by the stress history that is simulated, another non-conventional (HC-TC-PL-CTC) stress path test was conducted to investigate the effect of a change in the K_o coefficient. The test was undertaken along the K_o line = 0.75. In Figure 5.7 the non-conventional (HC-TC-PL-CTC) stress paths tested at K_o = 0.50 and 0.75 are shown.

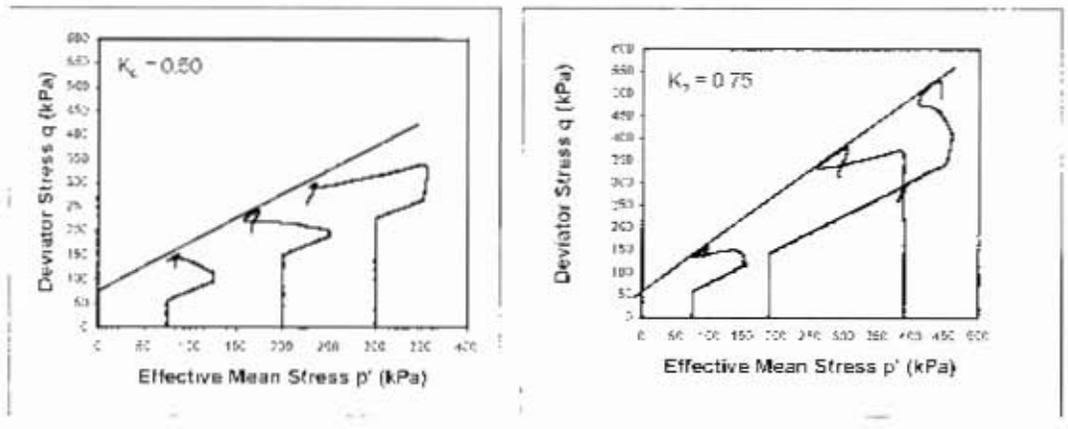

Figure 5.7 HC-TC-PL-CTC stress path results for K_o = 0.50 and 0.75

The Mohr-Coulomb shear strength parameters of the non-conventional (HC-TC-PL-CTC) stress path (with K_o = 0.75) are ϕ' = 27.1° and c' = 23.8 kPa, respectively. The

remoulded test samples are prepared at the same density and moisture contents as in previous stress path tests, so that experimental consistency is maintained.

The HC-TC-PL-CTC stress path results (with K_o = 0.75) indicate little change in the cohesion intercept, but there is a 1.7° increase in the angle of internal friction. The higher coefficient of lateral strain (at rest) resulted in higher deviator stress conditions at the failure surface. The remoulded soil samples could accommodate higher deviatoric stresses because the soil structure is stiffened due to the preconditioned stress state, hence the higher angle of internal friction.

5.3.5 PL-RTC Stress Path

In Figure 5.8, the proportional loading (PL) and reduced triaxial compression (RTC) stress path results are shown in terms of deviator stress (q)-effective mean stress (p'), deviator stress (q)-axial strain (ε_{axial}) and pore water pressure (u)-axial strain (ε_{axial}) diagrams. The Mohr-Coulomb shear strength parameters are also given

This stress path test investigates the stress-strain-strength relationship of a sample initially loaded following a controlled 'drained' PL stress path and then taken to the failure by way of a RTC stress path in undrained condition. The PL stress path is programmed to follow the K_o = 0.50 line by applying anisotropic compression to the test sample. The remoulded test samples are subjected to axial loading while lateral restraint is maintained.

In Figure 5.8(a) the deviator stress-effective mean stress relationships for the non-conventional (PL-RTC) stress paths are shown. The shear strength parameters are evaluated as, ϕ' = 26.6° and c' = 18.1 kPa for the non-conventional (PL-RTC) stress path tests of remoulded clay material. The reduced triaxial compression (RTC) stress path is again initiated at selected effective mean stresses, namely 125 kPa, 250 kPa and 350 kPa.

The deviator stress-axial strain relationship is shown in Figure 5.8(b). As was the case in the previous HC-TC-PL-RTC stress path test, the peak deviatoric stresses occurred at the

selected initiation stress points on the K_o line, at low axial strain. There was a significant decrease in deviator stress as the failure surface was approached.

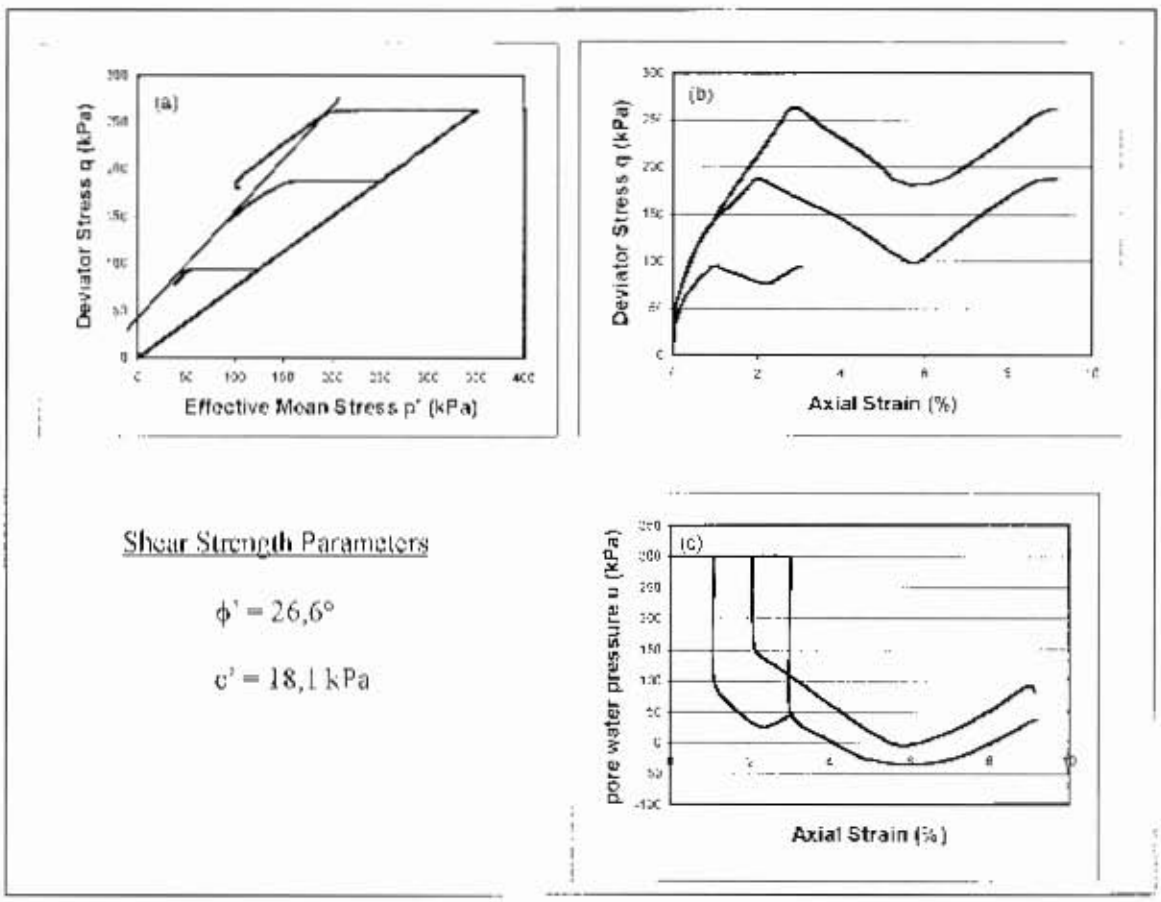

Figure 5.8 PL-RTC stress path results of remoulded Maguga clay

In this non-conventional stress path test the response of the remoulded test samples was surprising once the stress path device was switched off (at approximately 6% strain). There was a continued application of loading after the stress path device was switched off, which is attributed to the release of particular stresses that were locked within the soil structure during the controlled 'drained' PL stress path application.

Referring to Figure 5.8(c), the pore water pressure-axial strain relationship showed similar tendencies as were observed in the HC-TC-PL-RTC stress path test. The pore water pressure is constant until the initiation of the RTC path. Upon initiation, the pore water pressure of all tests dropped rapidly towards the zero pore water pressure line.

The increase in pore water pressure after the stress path device was switched off is again attributed to the release of locked-in preconditioning stress.

The initial and final properties of the non-conventional (PL-RTC) stress path tests are shown in Table 5.3

5.3.6 PL-RTC Stress path: Discussion and comparison with previous test results

This part of the investigation has focused on the initiation of the reduced triaxial compression (RTC) stress paths from two perspectives. In comparing the non-conventional (HC-TC-PL-RTC) and (PL-RTC) stress path test results, stress preconditioning of remoulded Maguga clay does affect the shear strength and pore water responses. The Mohr-Coulomb shear strength parameters for the PL-RTC test were $\Delta\phi' = 3.2°$ lower and $\Delta c' = 4.6$ kPa higher than those experienced in the HC-TC-PL-RTC stress path test. It seems that there is a greater affect on the stress-strain-strength behaviour of remoulded samples if the combinations of stress paths are increased. The more complex the preconditioned stress application (i.e. more combinations of stress paths), the stiffer the soil structure response.

The peak deviatoric stresses coincided with the effective mean stresses 125 kPa, 250 kPa and 350 kPa (i.e. the initiation points of the RTC stress path). The gradients of the deviator stress-axial strain diagram were identical to the gradients that were attained in the HC-TC-PL-RTC stress path tests, even though the stress 'history' is different.

5.3.7 PL-CTC Stress Path

In Figure 5.9 the proportional loading (PL) and conventional triaxial compression (CTC) stress path results are shown in terms of deviator stress (q)-effective mean stress (p'), deviator stress (q)-axial strain (ε_{axial}) and pore water pressure (u)-axial strain (ε_{axial}) diagrams. The Mohr-Coulomb shear strength parameters are also given.

In Figure 5.9(a) the deviator stress-effective mean stress relationships are shown. This non-conventional stress path test consisted of following a proportional loading (PL) stress

path along the K_o line (with $K_o = 0.50$). Conventional (CTC) tests were undertaken again at the same selected stress points on the K_o line with effective mean stress $p' = 125$ kPa, 250 kPa and 350 kPa. The shear strength parameters calculated from the conversion factors are $\phi' = 25{,}8°$ and $c' = 23{,}7$ kPa, respectively.

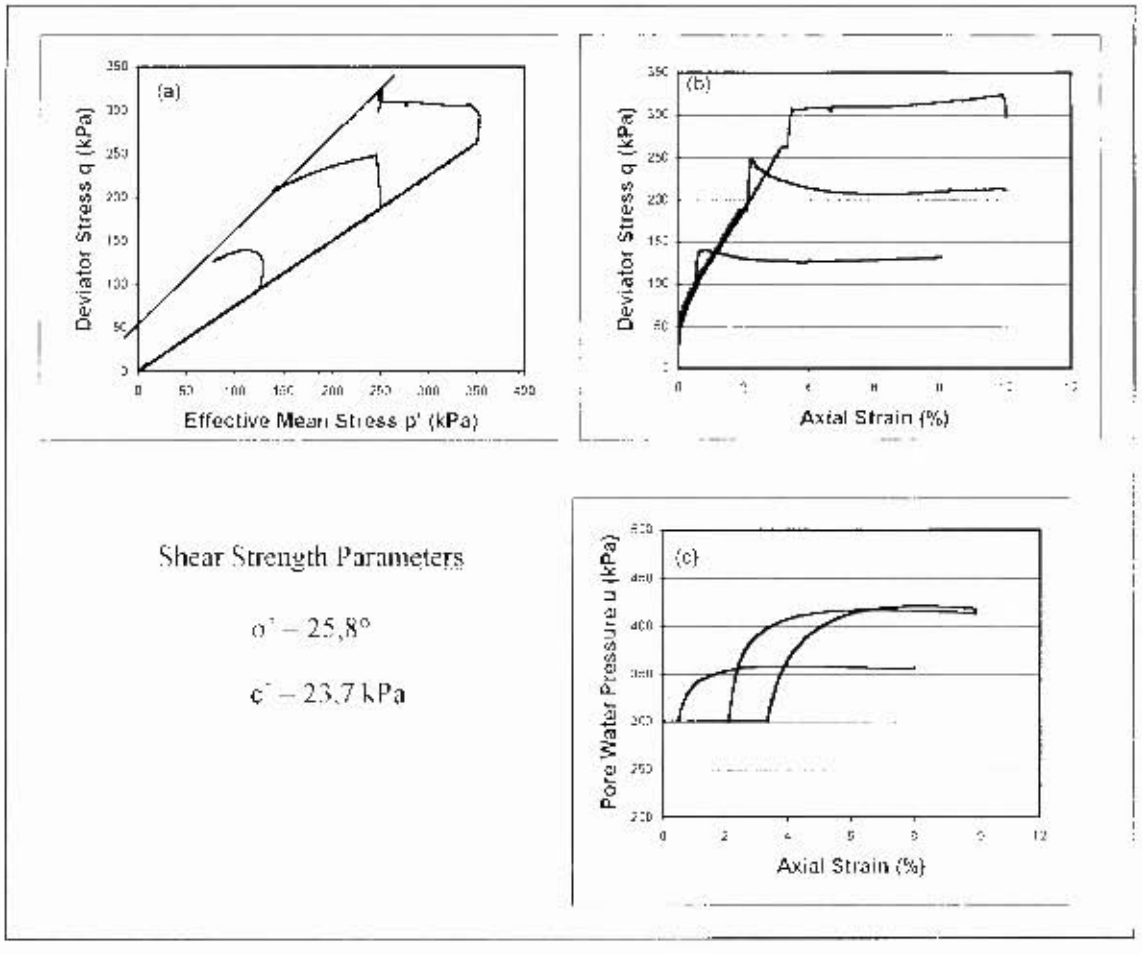

Figure 5.9 PL-CTC stress path results of remoulded Maguga clay

Referring to the deviator stress-axial strain relationship presented in Figure 5.9(b), the deviator stress responded in a completely different manner compared to the preceding PL-RTC test. There is a rapid increase in the deviatoric stress as the conventional (CTC) stress path is initiated up to pronounced peak points. Thereafter, a minor decrease of deviatoric stress was observed, which tapered off to a constant stress state condition.

The pore water pressure-axial strain response is shown in Figure 5.9(c). The pore pressure remained constant at 300 kPa, while the proportional loading path was followed.

On initiation of the conventional triaxial compression (CTC) stress paths, the typical undrained pore water pressure responses were observed.

The initial and final properties of the non-conventional (PL-RTC) and (PL-CTC) stress path tests of the remoulded samples are listed in Table 5.3 for comparative purposes.

	Initial Properties				Final Properties			
Test Description	Effective Mean Stress (kPa)	Moisture content (%)	Dry density (kN/m^3)	Void ratio	Moisture content (%)	Dry density (kN/m^3)	Void ratio	$\varepsilon_{volumetric}$ (%)
PL-RTC (remoulded)	125	27.8	1461	0.85	33.8	1468	0.85	8.84
	250	27.8	1464	0.85	33.4	1465	0.85	7.11
	350	27.8	1466	0.85	30.9	1477	0.84	4.48
PL-CTC (remoulded)	125	27.8	1459	0.86	33.8	1478	0.83	10.67
	250	27.8	1468	0.85	32.4	1478	0.83	6.31
	350	27.8	1471	0.84	31.4	1483	0.83	5.35

Table 5.3 Initial and final properties of PL-RTC stress path and PL-CTC stress path

5.3.8 PL-CTC Stress path: Discussion and comparison with previous test results

In a comparison of the PL-CTC test with the conventional (CTC) stress path tests of samples (be it undisturbed or remoulded), these tests displayed shear strength characteristics with a lower ϕ' (2° to 3° lower) and an increase in c' (9 kPa to 14 kPa increase).

The apparent vertical 'jump' of deviator stress, as shown in Figure 5.9(b), is attributed to a possible control error associated with initiation of the conventional triaxial compression (CTC) stress path.

In conclusion, it appears that the PL-RTC and PL-CTC stress path tests reinforce the hypothesis that the behaviour of Maguga clay is changed by stress application that is ultimately attributed to the 'preconditioning' of the remoulded soil structure.

5.4 Overview of stress path tests in terms of ϕ' and c'

Stress Path Nr.	Stress Path	Test Description	ϕ' (degrees)	c' (kPa)
1	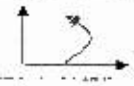	HC-CTC ®	27,9	10.0
2		HC-CTC (U)	29,8	15,1
3	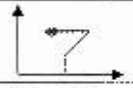	HC-TC-PL RTC ® (K_o = 0.50)	29,8	13,5
4	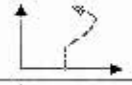	HC-TC-PL-CTC ® (K_o = 0.50)	25,4	28,5
5	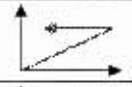	PL-RTC ® (K_o = 0.50)	26,6	18,1
6	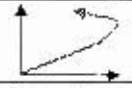	PL-CTC ® (K_o = 0.50)	25,8	23,7
7	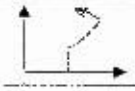	HC-TC-PL-CTC ® (K_o = 0.75)	27,1	23,8

® =Reconstituted (U) = Undisturbed

Table 5.4 Shear strength parameters of Maguga clay subjected to various stress path tests

CHAPTER 6

ANALYSIS OF RESULTS IN TERMS OF CRITICAL STATE MODEL

6.1 Brief Review of Critical State Model

In *Chapter 6* the critical state analysis of the Maguga clay is discussed. This chapter is assessed by building on the critical state concept with reference to particular Cam Clay concepts. The critical state model is a powerful theoretical concept, which enables a *qualitative* response of a soil (from an application of loading) to be expressed in terms of its specific volume and shear strength.

Cohesive soils reach critical state at steady effective stress and constant volume conditions. This region of constant stress-volume is generated in clays at shear strains greater than 10% (Atkinson, 1993). Atkinson (1993) proposed that soil bonds are held together by means of cohesive and frictional bonds; so cohesive and frictional bonds accommodate the shear stresses that determine soil strength. As the clay is loaded, cohesive and frictional bonds are broken and rearrangement of the particles within the soil structure takes place. Malangraki and Toll (2000) extended the analogy by suggesting that only certain cohesive bonds are broken depending on the current stress path that is followed. As the stress path direction is changed, different frictional bonds resist the shearing stress until an ultimate or critical state is reached. At this ultimate state, all frictional bonds within the soil structure are broken. Clays still exhibit some shear strength that is attributed to plastic straining of the soil structure.

The critical state concept is presented in two parts. The first part deals with analysing the undisturbed triaxial compression test results, together with the consolidation results, so that critical state parameters can be computed. An estimation of some of the critical state strength parameters can also be computed using the Atterberg limits, which is given

in this thesis only for comparative purposes. The critical state strength parameters, calculated from conventional triaxial results on undisturbed Maguga clay, will be used in the second part of this thesis to examine the application of the critical state model and predict the response of the clay under any given stress condition.

The critical state model facilitates a conceptual analysis and allows elementary numerical predictions of soil behaviour. The model provides a significant contribution in allowing the geotechnical engineer to achieve a better conceptual understanding of the nature of the problem and the modes of behaviour likely to occur.

The critical state concept is composed from observed responses consisting of simple relationships between the combinations of effective stresses and specific volumes at which critical states are attained. The critical state line (CSL) in the q-p' diagram and the specific volume (v)-effective mean stress (p') relationship obtained from the respective soil mechanical tests are shown in Figure 6.1.

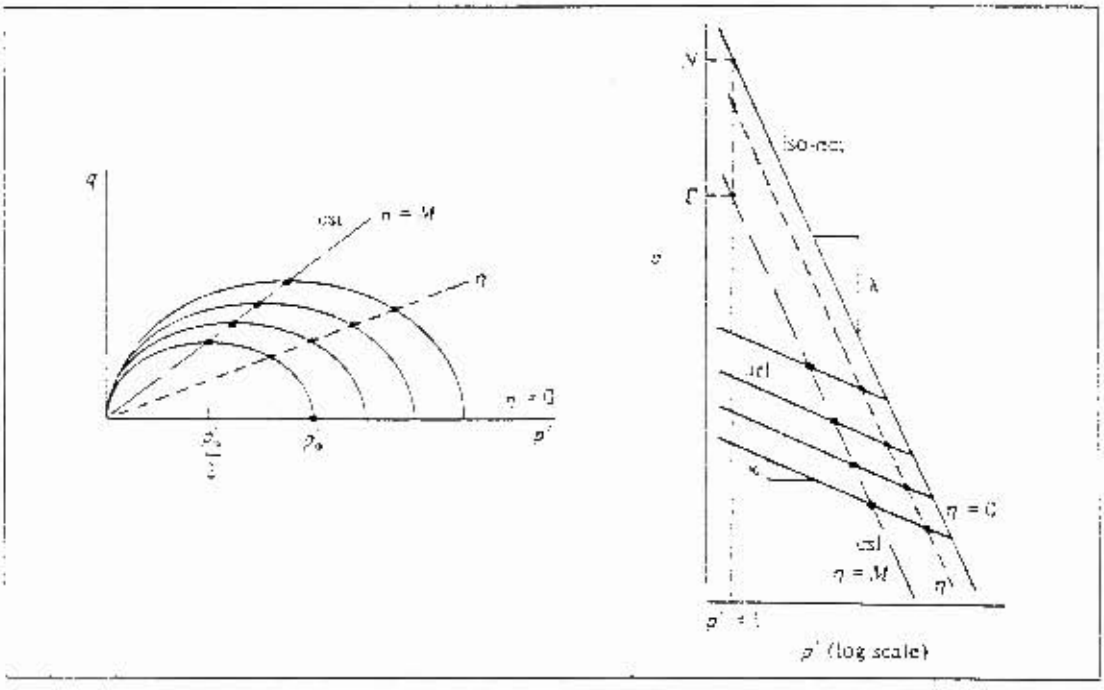

Figure 6.1 Critical state line and v-p' relationship for soil mechanical tests (after Wood, 1990)

The critical state characteristics (in Figure 6.1) are defined by the following equations:

$$q_f = M \times p'_f$$
$$v_f = \Gamma - \lambda \times \ln p'_f \qquad (6.1)$$

where p'_f = the effective mean normal stress at failure

q_f = the effective deviator stress at failure

M = the critical state ratio = $\Delta q_f / \Delta p'_f$ or gradient of CSL in q-p' diagram

v_f = the specific volume at failure

Γ = the specific volume of CSL at p' = 1.0 kPa

λ = the gradient of critical state line in v-p' diagram

The normal compression line (NCL) and unloading-reloading line (URL), obtained from the consolidation test results are also shown in Figure 6.1. The NCL and URL lines are defined by the following equations:

$$v = N - \lambda \times \ln p'$$
$$v = v_\kappa - \kappa \times \ln p' \qquad (6.2)$$

where N – the specific volume of NCL at p' = 1.0 kPa

λ = the gradient of normal compression line in v-p' diagram

κ = the gradient of unloading-reloading line in v-p' diagram

v_κ = the specific volume of URL at p' = 1.0 kPa

6.2 Evaluation of Critical State Parameters using Undisturbed (CTC) Triaxial and Consolidation Test Results

In this section of the thesis, the undisturbed (CTC) stress path results as well as the consolidation test results are analysed and the critical state parameters M, Γ, λ, N and κ are evaluated. In Table 6.1 all the results of the triaxial compression test (CTC) of undisturbed Maguga clay attained at axial strain of 10% (i.e. at failure) are summarised.

Effective Mean Stress (kPa)	p'_f (kPa)	q_f (kPa)	σ_{3f} (kPa)	u_f (kPa)	w_f (%)	e_f	v_f
75	110.8	167.4	376.0	321.0	37.6	0.91	1.91
200	177.5	240.3	502.5	405.2	34.8	0.89	1.89
500	293.7	393.3	800.5	637.9	32.4	0.85	1.85

Table 6.1 Undrained CTC stress path test results of undisturbed Maguga clay at failure

6.2.1 Evaluation of critical stress ratio (M)

The failure values listed in Table 6.1 are plotted in the q-p' diagram and the critical stress ratio (M) of the critical state line (CSL) derived. In Figure 6.2 the undisturbed CTC failure surface and 'best fit' critical state line are shown. The critical state line is drawn through the origin because the critical state theory assumes that a particular soil exhibits no cohesive strength at axial strains greater than 10%.

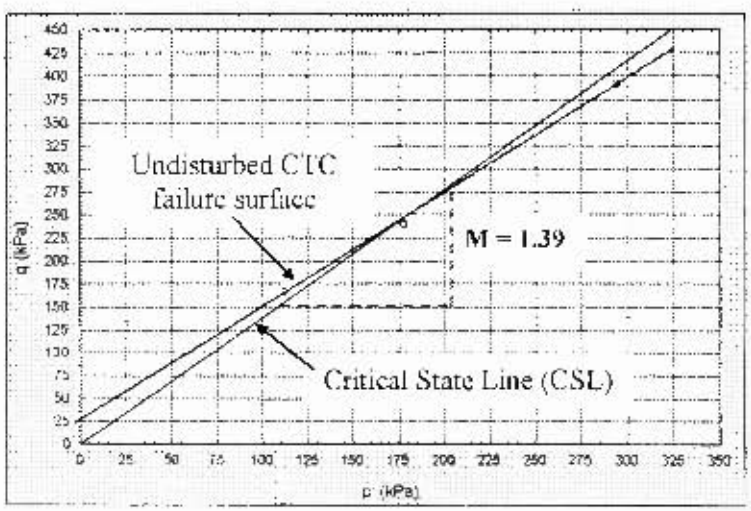

Figure 6.2 Critical state line and failure surface of CTC tests of undisturbed Maguga clay

The stress ratio M is equal to 1.39, which is equivalent to a critical angle of internal friction (ϕ'_c) equal to 34.4°. This represents a friction angle, which is close to 5° higher in comparison to the $\phi'_{undisturbed}$ determined in the Mohr-Coulomb diagram (see Section 5.2.2). The $\phi'_{remoulded}$ value is even lower, namely 27.9° (see Table 5.1).

6.2.2 Evaluation of λ, Γ, N and κ parameters

The evaluation of λ can be attained from either the triaxial compression test results or from the consolidation test results. Both methods of evaluation are undertaken in this sub-section.

Critical State Line

In Figure 6.3, the plot of specific volume versus ln p' with the conventional triaxial compression (CTC) results of undisturbed Maguga clay is shown. The line shown in Figure 6.3 represents the critical state line.

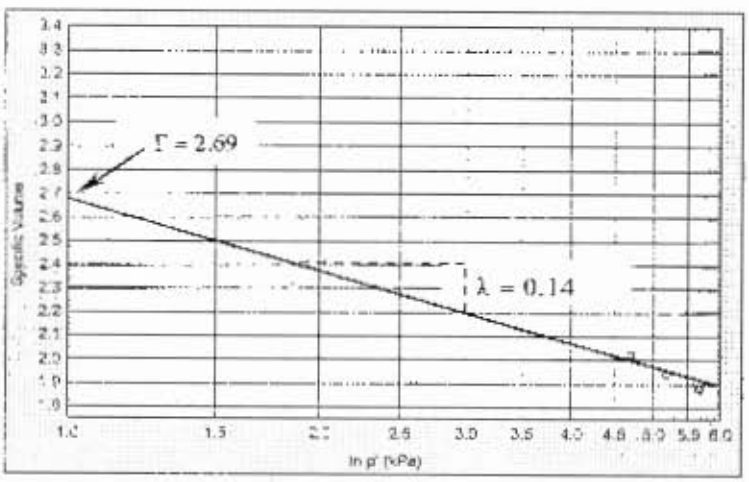

Figure 6.3 Critical state line derived from CTC triaxial test of undisturbed Maguga clay

The critical state parameter λ is calculated from the CTC triaxial test of undisturbed Maguga clay to be equal to 0.14, while the specific volume intercept Γ at p' = 1 kPa is equal to 2.69. According to the theory, the slope of this critical state line as well as the isotropic normal compression line is the same, i.e the slopes are equal to λ.

In comparison, there exists an empirical relationship between the critical state parameter λ and plastic index of clay; which takes cognizance that clays of different plasticities

have different values of compressibility λ. Atkinson (1993) proposed an approximate relationship for remoulded clay as follows:

$$\lambda_{Atterberg} = (\text{Plasticity Index} \times \text{Specific Gravity})/460 \qquad (6.3)$$

With a plastic index (PI) equal to 23.2 and the specific gravity (G_s) of Maguga clay equal to 2.71 (see *Chapter 3*), a $\lambda_{Atterberg}$ value of 0.14 can be evaluated. The plastic index is an important material classification parameter, which will be implemented in the back-prediction of the conventional triaxial compression test (see Section 6.4) to estimate the angle of internal friction of the clay material.

Normal compression line

The specific volume-lnp' relationship for the consolidation test of the remoulded Maguga clay with loading and unloading curves is shown in Figure 6.4.

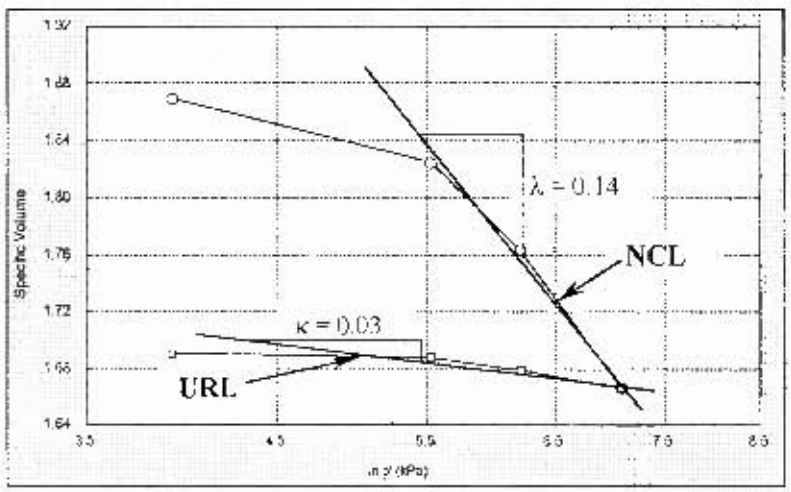

Figure 6.4 v-ln p' diagram with loading (NCL) and unloading-reloading (URL) curves of remoulded Maguga clay

The gradient of the loading curve (λ) and unloading curve (κ) are equal to 0.14 and 0.03, respectively.

The representation of the consolidation test results in terms of a v-lnp' diagram generates a line beneath the critical state line as shown in Figure 6.5. This linear relationship indicates an over-consolidated line (OCL). This line is not the isotropic normal compression line.

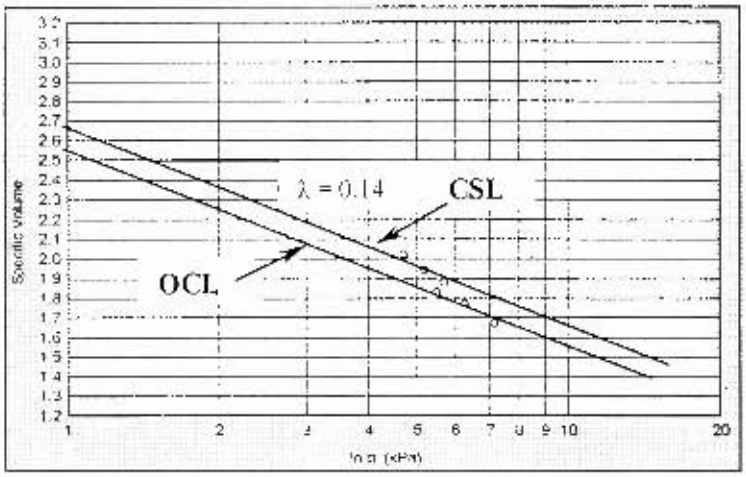

Figure 6.5 v-ln p' diagram with critical state line (CSL) and over-consolidated line (OCL) curves of remoulded Maguga clay

Isotropic Normal Compression Line

The critical state theory positions the isotropic normal compression line (NCL) above the critical state line. The vertical separation $\{(\lambda - \kappa) \times \ln 2\}$ between the isotropic normal compression line and the critical state line (as shown in Figure 6.6) can be mathematically expressed by combining the critical state line and the normal compression line in terms of the critical specific volume (v_{cs}). Wood (1990) stated that each critical state combination of q_{cs} and p'_{cs} is associated with a critical state combination of v_{cs} and p'_{cs} in the normal compression plane and can be written as:

$$v_{cs} = \Gamma - \lambda \times \ln p'_{cs}$$

where (6.4)

$$\Gamma = N - (\lambda - \kappa) \times \ln 2$$

In Figure 6.6 the isotropic normal compression line (NCL) and critical state line (CSL) in terms of a specific volume-lnp' diagram is shown

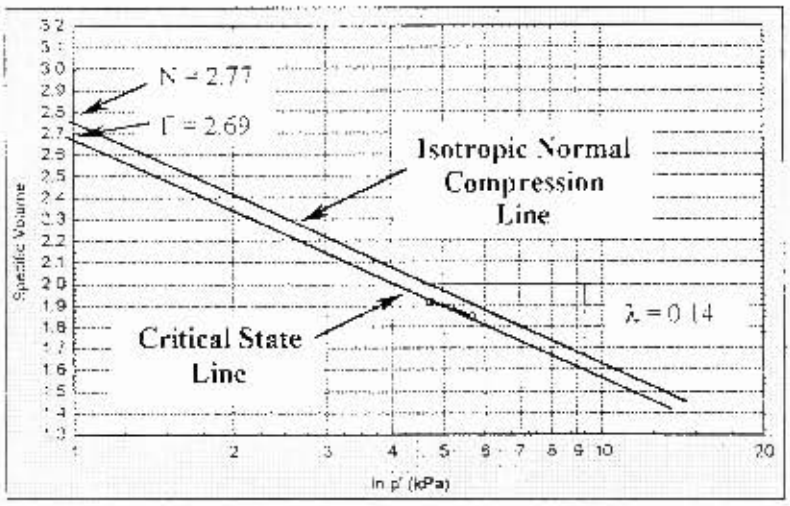

Figure 6.6 v-ln p' diagram with critical state line (CSL) and isotropic normal compression (NCL) curves of remoulded Maguga clay

As in equation 6.2, the isotropic normal compression line (NCL) is given by the $v = N - \lambda \times \ln p'$. The value of λ and N are 0.14 and 2.77, respectively. This is shown in Figure 6.6 using a different scale

A summary of the derived critical state parameters is shown in Table 6.2.

Critical State Parameter	
M	1.39
λ	0.14
Γ	2.69
N	2.77
κ	0.03

Table 6.2 Summary of critical state parameters

The following section consists of the implementation of the critical state parameters and introduces the concept of 'normalising' test results.

6.3 Normalising Triaxial Test Results

The triaxial test results are normalised so that a dimensionless representation incorporating all conventional and non-conventional triaxial compression tests of remoulded Maguga clay can be shown on a single unified diagram.

The q_f and p'_f values for the conventional and non-conventional triaxial compression tests of remoulded Maguga clay are shown in Figure 6.5. As shown, no matter what stress path combination was followed or stress preconditioning experienced, the failure points of all stress paths investigated tend to fall close to or near the critical state line given by the stress ratio M equal to 1.39.

It is believed, as Parry (1958) also observed while testing London clay, that the different stress states of Maguga clay were in fact still in the process of 'moving' towards their critical states when the tests were terminated. When triaxial compression tests ended to the right of the critical state line (i.e. normally consolidated clay material), then the pore pressures are observed to be increasing at the end of the test and hence the effective mean stress decreases, i.e. the effective mean stress state of the clay moves to the left towards the critical state line.

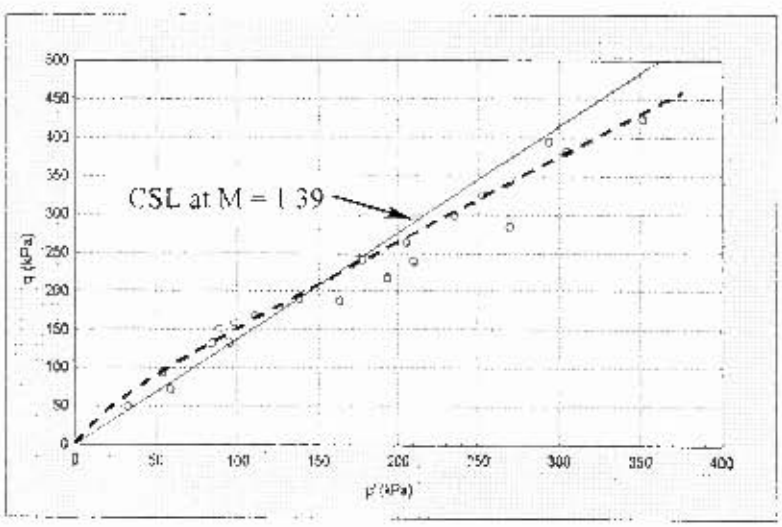

Figure 6.7 Failure points of all undrained triaxial tests of remoulded Maguga clay

Conversely, undrained tests that ended to the left of the critical state line (i.e. over-consolidated clay material), resulted in the decrease of pore pressure at the end of the test and hence the effective mean stress increased. The effective mean stress state of the clay moved to the right towards the critical state line. This typical response was observed and discussed in the conventional and non-conventional triaxial compression tests of remoulded Maguga clay (see *Chapter 5*).

The critical state theory assumes that there is no cohesive strength associated with clay at axial strains greater than 10%, but it was of the experimenters opinion that the critical state line would reflect the results more accurately if it were drawn as a curve (as shown by the dashed curve in Figure 6.7).

The following subsection discusses the normalisation of stresses that enables all stress states in terms of q and p' to be presented in non-dimensional q-p' stress space.

6.3.1 Undrained conventional and non-conventional triaxial compression test results of remoulded Maguga clay in non-dimensional stress space

The stresses at failure, namely q_f and p_f' can be normalised with respect to either the equivalent critical pressure (p'_e) or the equivalent consolidation pressure (p'_e). The equivalent critical pressure (p'_e) is generally attained from an overconsolidated compression line (OCL). Atkinson (1993) stated that the overconsolidation ratio is an important factor in determining soil behaviour, hence Atkinson normalised his test results in terms of the equivalent critical pressure (p'_e). However, this method was ignored and the p_e' approach was utilised, since this research work did not consider soil behaviour in terms of a overconsolidation ratio.

As shown in Figure 6.8, the equivalent consolidation pressure (p'_e) is a projection of a state of stress from the normal compression line onto the ln p' axis.

The equivalent consolidation pressure (p'_e) represents a specific volume on the isotropic normal compression line interpreted from the *final specific volume* of the conventional triaxial samples of remoulded Maguga clay.

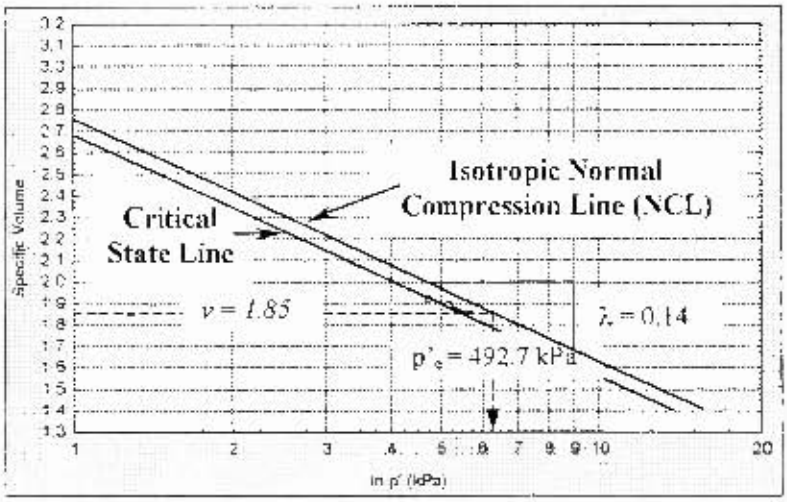

Figure 6.8 Evaluation of equivalent consolidation pressure (p'_e) from v-ln p' diagram

A final specific volume of approximately 1.85 was observed in the conventional triaxial compression (CTC) tests of remoulded Maguga clay (see *Chapter 5*). Thus, the value of p'_e at a specific volume of 1.85 is equal to 492.7 kPa, as shown in Figure 6.8.

The stress parameters q_f and p_f', representing different failure conditions for all the non-conventional triaxial tests of remoulded Maguga clay, are divided by the equivalent consolidation pressure (p'_e = 492.7 kPa) in order to normalise the stress parameters. The peak states of stress and other states before critical state are different (i.e. the stress states of different stress paths are not unique). Normalisation simplifies the representation of different states of stress by providing the same equivalent state after the normalisation process.

All the triaxial compression test results are now plotted in non-dimensional q-p' stress space as shown in Figure 6.9 (see Appendices for the tabulation of all triaxial compression test results). The boundaries, which are defined by points N and C, contain

all the stress state yield surfaces in dimensionless stress space and is represented by an elliptical curve (i.e. the shape was assumed from Cam clay assumptions). The development of the elliptical boundary surface for Maguga clay, containing the points N and C, is derived from the following (Wood, 1990):

$$\text{Point N } (1;\ 0) \text{ and Point C } (2^{-\Lambda};\ M\times 2^{-\Lambda})$$

where

$$\Lambda = (\lambda-\kappa)/\lambda = (0.14\text{-}0.03)/0.14 = 0.786;\ \text{and } M = 1.39$$

Point N (1;0) corresponds to normal consolidation compression and point C (0.58;0.81) corresponds to a point on the critical state line governed by M equal to 1.39. The point C is not at the apex of the curve because the effective stress path associated with a CTC triaxial test in undrained condition does not have a zero slope ($\delta q/\delta p' \neq 0$) at critical state, which is a consequence of the elastic volumetric strains that are assumed to occur in the critical state model. If there were no elastic volumetric strains, the gradient of theunloading curve (κ) would be equal to zero and the parameter Λ would be equal to 1 and the point C would then be at the summit of the elliptical curve.

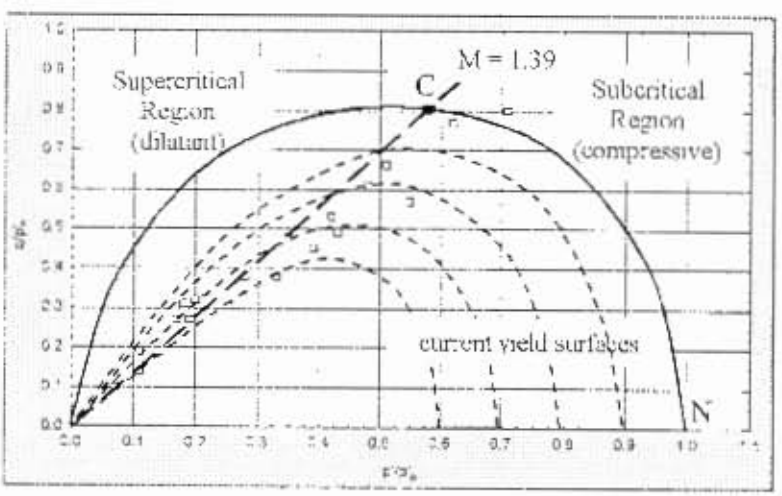

Figure 6.9 Undrained triaxial compression tests plotted in non-dimensional effective stress space

The distinction between the dilatant (dry) side and the compressive (wet) side of critical state determines the characteristics of the clay behaviour. Maguga clay is overconsolidated in the supercritical (dilatant) region and the clay particles must move apart during the application of loading. Maguga clay is normally consolidated in the subcritical (compressive) region. In normally consolidated conditions the clay particles are spaced apart and, on the application of loading move into the neighbouring void spaces.

The elliptical boundary surface (defined by points N and C in Figure 6.7) contains all possible states of stress of remoulded Maguga clay. It has been established from *Chapter 5* that the Maguga clay responded differently for each type of stress path test that was simulated, the behavioural differences being attributed to the applied stress conditions

The Maguga clay samples followed different yield (failure) surfaces, which did not reach the critical state as failure was reached at low axial strains and the loading was terminated. The position of the critical state points associated with the failure surfaces can be established, even though the loading was terminated before their critical states.

6.4 Qualitative back-prediction of stress-strain behaviour of Maguga clay

A reliable prediction of soil behaviour can be attained using a vast assortment of models, each with its own assumptions and theoretically defined parameters. Advanced models may be too sophisticated for the degree of application needed; hence this research work focussed on critical state theory and assumptions.

The acceptance of a common critical state line permits an assessment to be made of the expected soil response of any triaxial compression test on a soil with any consolidation history.

The steps involved in the back-prediction are as follows:

STEP 1) The position of the critical state line as governed by the stress ratio M is attained from the conventional triaxial test results where M is equal to 1.39. If no triaxial compression tests are available, then the stress ratio M can be assumed using the following equations assembled by Mitchell (1976) and adapted by Wood (1990). The internal angle of friction can be described by the equation:

$$\sin \phi' = 0.35 - 0.1 \times \ln(\text{plasticity index}) \qquad (6.6)$$

Taking the plastic index of 23.2 (see *Chapter 3*) and substituting into the above equation gives an approximate angle of friction equal to 29.7°. An estimated critical stress ratio M approximately equal to 1.19, which is in good agreement with the 'real' stress ratio M (with M = 1.39).

STEP 2) Compute the total stress paths starting from the preselected stress points 75 kPa, 200 kPa and 500 kPa, knowing that the total stress path has a gradient of 1:3 and must stop at the failure surface governed by M = 1.39.

Referring to Figure 6.10, the total mean stress points (p) are calculated from the intersections points of the total stress paths (TSP) and the linear stress ratio η (with $\eta = q/p$). As the stress ratio η is increased, total mean stress values are computed. By definition of the stress ratio η, the corresponding deviator stress values can be estimated ($q = \eta \times p$).

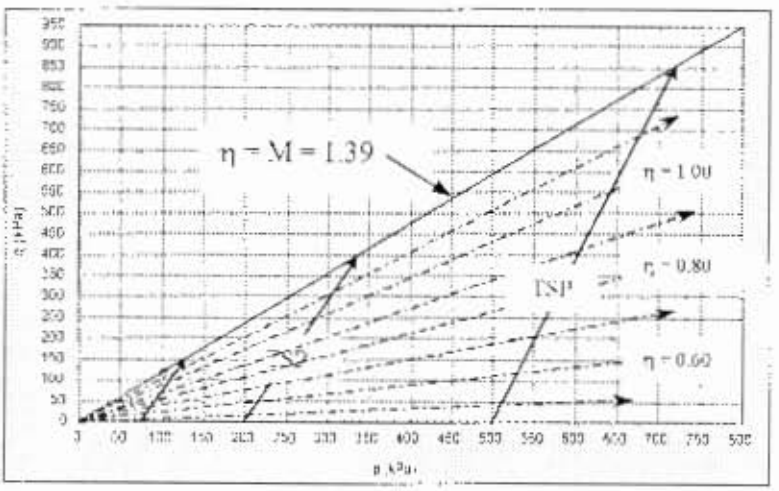

Figure 6.10 Predicted critical state line showing total stress path-stress ratio η intersection points

STEP 3) Compute the effective mean stress p' values from equation 6.8, which defines the shape of the effective stress path in terms of M, η and p'_o.

It was shown in Figure 6.9 that the current yield surfaces are elliptical in shape, an assumption developed in the Cam clay theory. The changes in size of these current yield surfaces are controlled by the initial effective stress (p'_o) as well as changes in mean effective stress p'. An equation developed by Wood (1990) specifies the shape of the undrained effective stress path in the q-p' plane, assuming that elastic and plastic volumetric strains are occurring. Obviously, there are no changes of volumetric strain in a conventional undrained stress path test, as the volume remains constant throughout the loading application. The equation specifying the Cam-clay yield curve is as follows:

$$p'_o/p' = \{ (M^2 + \eta^2)/(M^2 - \eta_o^2) \}^{\Lambda} \quad (6.8)$$

where

$$\Lambda = (\lambda - \kappa)/\lambda = 0.786$$

The parameters p'_o and η_o define an initial effective stress state (i.e. p'_o is equal to 75 kPa, 200 kPa and 500 kPa with η_o equal to zero). From Equation 6.8, we can obtain

the effective mean stress points (p') of the yield curve corresponding to deviator stresses, which are defined by $q = \eta \times p'$. The pore water pressure (u) can be derived by taking the total mean stress from STEP 2 and subtracting the corresponding effective mean stress, $u = p - p'$.

STEP 4) Derive the plastic volumetric strain ($\delta\varepsilon^p_v$) and plastic shear strains ($\delta\varepsilon^p_s$) increments using the following equations (Schofield et al, 1968):

$$\delta\varepsilon^p_v = \{ (\kappa \times \delta p') / (v_o \times p'_o) \}$$
$$\delta\varepsilon^p_s = \delta\varepsilon^p_v / M \qquad (6.9)$$

In Figure 6.11 a comparison between the conventional (CTC) stress path tests of remoulded Maguga clay and the back-prediction in terms of deviator stress (q)-effective mean stress (p') and deviator stress (q)-axial strain (ε_{axial}) is shown. The back-predicted test results (for only the triaxial test consolidated at 75 kPa) are shown in Appendix D-6.

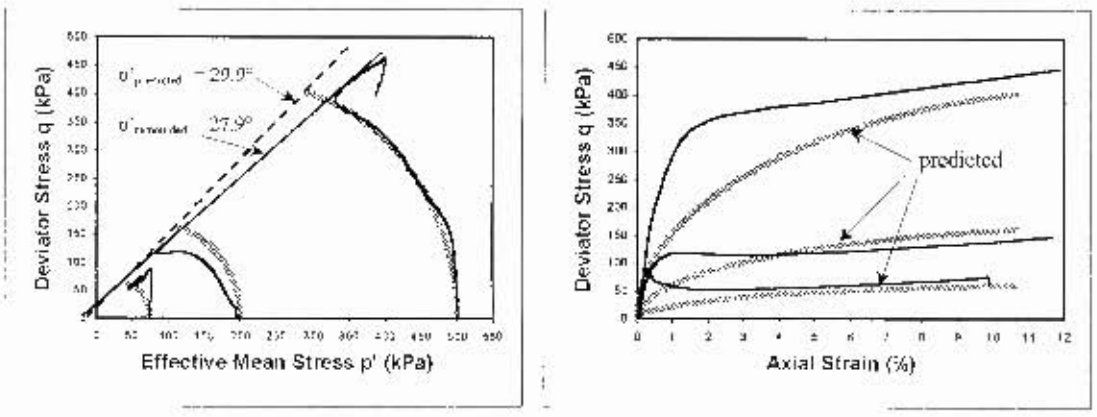

Figure 6.11 Comparison between remoulded CTC stress path test and the back prediction

The internal angle of friction for the back-prediction ($\phi'_{predicted}$) is equal to 29.9°, while the cohesion intercept is derived as 10 kPa. The Mohr-Coulomb shear strength parameters for the predicted triaxial compression test were computed from conversion equations 2.3 in *Chapter 2*.

The comparison between the conventional triaxial compression test data of remoulded Maguga clay and the back-predicted data is good. The effective stress paths are almost perfect simulations of the actual experimental results. Although the final failure conditions are similar for the predicted and experimental stress paths, the critical state model cannot adequately express the actual final yielding behaviour of the clay. However, the back-prediction is exceptional in comparison with the undisturbed CTC stress path test where $\phi'_{undisturbed} = 29.8^{\circ}$ (see Section 5.2.2)

The predicted deviator stress-effective mean stress diagram shown in Figure 6.9 is a conventional representation of a normally consolidated, undrained triaxial compression test undertaken at initial effective mean stresses 75 kPa, 200 kPa and 500 kPa. The back-predicted results follow a smooth profile, which ends at specific peak stress conditions. The maximum deviator stress of the back-predicted tests tends to approach the experimental deviator stress at axial strains of 10%

The back-prediction clearly simulates the clay behaviour well at axial strains greater than 10%, but does not define the peak stress conditions at low axial strains. The peak stress conditions could be improved if the critical state parameters, given in Table 6.2, are varied while certain parameters are assumed to remain the same (i.e. by varying the stress ratio M with respect to the other critical state parameters).

CHAPTER 7

CONCLUSIONS

"As our knowledge of the behaviour of real soils increases, so our appreciation of the inadequacy of conventional laboratory testing grows." (Wroth, 1984)

The quote by Wroth (1984) captured the essence of this research work by emphasising the importance of reliable and competent laboratory testing that we, as geotechnical engineers, must interpret to attain an understanding of the soil behaviour.

The conclusions are drawn for this research work in terms of three distinct sections, namely a comparison of conventional and non-conventional testing methods, test material condition ('undisturbed' and remoulded) and finally, the long-term implications of undertaking non-conventional stress path propagation.

Conventional and non-conventional stress path test results have shown that there are stress-strain-strength differences. Although in the case of Maguga clay, the conventional stress path comparisons are miniscule, the results do emphasise that there are differences between 'undisturbed' and remoulded triaxial tests. The shear strength parameters of conventional stress path testing differ by $\Delta\phi' = 2°$ and $\Delta c' = 5.1$ kPa. However, the non-conventional stress path results show a tendency to have a lower ϕ' (1° to 2.5° lower) and a higher c' (8.0 kPa to 18.5 kPa increase) in comparison with the conventional stress path testing. As was mentioned before, the difference in the clay behaviour was the result of the vastly different stress systems that were applied to fail the test specimens.

The fact remains that conventional testing procedures are prone to common errors and uncertainties, which affects the evaluation of the internal angle of friction (ϕ') and the apparent cohesion (c'). Common errors such as the curvature of the failure surface at high pressure ranges, the actual degree of saturation achieved within the sample, the

undetected presence of air bubbles within the drainage lines and the method of preparation of the triaxial test specimens are compounded in conjunction with uncertainties such as the lack of expertise and/or test apparatus.

These common errors are highlighted, to a greater extent, in conventional stress path testing and are alleviated in the non-conventional stress path applications. The main reason why the uncertainties are reduced in non-conventional stress path tests is because the application of stress during non-conventional testing procedures facilitates the applied stress-clay specimen exposure over a longer time interval, thereby improving the reliability of the triaxial test. Also, non-conventional stress path testing can only be undertaken if the experimenter has the expertise and a competent familiarity of the test apparatus.

The conventional stress path tests consolidated at an effective mean stress of 500 kPa are considered to be in a high stress range, hence the reduction of the 500 kPa stress range to that of 300 kPa, which reduced the effect of curvature of the failure surface. The effect of curvature of the failure surface at high stress ranges is further reduced in the q-p' diagram by using experimental discretion in deciding the orientation of the failure surface, rather than a least squares regression analysis. Experimental discretion enables an allowance to be made for poor individual test results and the general curvature of the failure surface.

Considerable care is taken to ensure that all visible air bubbles are dissolved into the water. The removal of air bubbles from within the stiff structure of Maguga clay is uncertain. Although the Skempton saturation (B) values indicated that the clay specimens were 98% saturated at the end of the saturation stage, it is felt by the experimenter that since saturation was measured from the base of the test samples, the degree of saturation of the top half of the stiff clay specimen may have been different. Also, the extent to which air is dissolved into the water within the drainage lines is uncertain. The non-conventional testing procedure eliminates any misconceptions of

saturation by ensuring that the clay specimen is kept under applied stress conditions for longer periods of time. The fact that the clay specimen is anisotropically loaded facilitates the saturation process by introducing another stress dimension to the stress application.

The method of test sample preparation affects the compaction efficiency of the soil structure resulting in varied, conventional triaxial test results. Applying a stress 'history' to a test sample can improve the condition of the material and induce different responses that could otherwise not be foreseen in conventional triaxial tests. The affect of simulating a stress 'history' ensures that saturation is achieved, but also manages to simulate a better representation of *in-situ* stress conditions.

Non-conventional stress path testing may seem too sophisticated for practical application, but perhaps an important consideration is being 'camouflaged' by the sophisticated terms and procedures. Non-conventional stress path tests are undertaken in a limited stress space region in this thesis, but what is shown highlights the fact that remoulded clay material can be manipulated to simulate realistic soil behaviour, otherwise not represented or simply unattainable in conventional triaxial tests. The non-conventional stress path tests improve the soil behaviour by altering the soil structure via stress manipulation.

A thorough undertaking of non-conventional stress path tests (on different soil types) may improve the understanding of what or how stress conditions (stress paths) interact within the field applications. The predictive behaviour of soil can now be taken to a new level of awareness. Models such as the Critical State, (which were formulated from isotropic soil behaviour), neglected the non-conventional or anisotropic stress path applications. The models do not incorporate anisotropic soil behaviour because the models were developed a few decades ago, before the progression of sophisticated stress path equipment made non-conventional stress path simulation possible. The major attribute of such models is the fact that proper soil relationships (rather than spurious

relationships) can be expressed in dimensionless variables so that advantage can be taken of the scaling laws of continuum mechanics.

The research work focused on only a few sequential combinations of stress paths limited to a particular region of stress space associated with stiff, slightly silty clay. This seems rather inadequate when one thinks of the diverse classification of soil types and their possible stress path characteristics. Undertaking non-conventional stress path testing on different soil types may seem daunting, but may improve the understanding of how the soil structure changes and adapts when subjected to an applied stress 'history'. Non-conventional stress path tests provide a means of attaining meaningful simulations of stress-strain-strength characteristics from otherwise 'inferior' remoulded material. The non-conventional stress-strain characteristics of remoulded Maguga clay replicated a stiffer clay material than that, which was observed in the conventional stress-strain characteristics. The internal soil re-structuring is attributed to the non-conventional stress preconditioning. The preconditioning sequence of common stress paths breaks the particle bonds at particular yield surfaces, hence different failure conditions are observed at unrelated axial strains (as shown in the non-conventional stress path tests).

In conclusion, the following question arises: If the same care and time is spent on conventional stress path testing, why bother to do non-conventional stress path testing? Realistically, *in-situ* soil masses are subjected to complex stress histories involving an interaction of different stress paths. The stress history of different stress paths can be accurately simulated in the computer-controlled triaxial device, providing sensitive simulations of existing stress conditions as well as possible long-term alteration of the soil structure. The sophisticated stress path device enables investigations with respect to past, present and future stress conditions, which are unable to be simulated by any other material testing device in the 'modern' laboratory.

REFERENCES

Atkinson, J.H. (1993), ***An Introduction to the Mechanics of Soils and Foundations through Critical State Soil Mechanics***, McGraw-Hill Book Company, pp. 103-150

Brink, A.B.A. (1985), ***Engineering Geology of Southern Africa***, Volume 4:Post-Gondwana Deposits, CTP Book Printers, South Africa.

Desai, C.S. and Siriwardane, H.J. (1984), ***Constitutive Laws for Engineering Materials with emphasis on geological materials***, Prentice-Hall, United States of America.

Fell, R. MacGregor, P. and Stapleton, D. (1992), ***Geotechnical Engineering of Embankment Dams***, Balkema Publishers, Netherlands.

Fredlund, D.G. and Rahardjo, H. (1993), ***Soil Mechanics for Unsaturated Soils***, John Wiley and Sons, pp 39-249

Hoeg, K. Dyvik, R. and Sendbekken, G. (2000), ***Strength of Undisturbed versus Reconstituted Silt and Silty Sand Specimens***, Journal of Geotechnical and Geoenvironmental Engineering, pp. 606-617.

Head, K.H. (1980), ***Manual of Soil Laboratory Testing***, Volume 1: Soil Classification and Compaction Tests, Pentech Press Limited, London.

Head, K.H. (1986), ***Manual of Soil Laboratory Testing***, Volume 3: Effective Stress Tests, Pentech Press, London.

Jaky, J. (1944), ***The Coefficient of Earth Pressure at Rest***, Journal of the Society of Hungarian Architects and Engineers, pp. 355-358.

Komati Joint Ventures (2000), ***On-Site Laboratory Report on Maguga Dam Soil Classification***, Swaziland.

Lambe, T.W. (1967), ***Stress Path Method***, Journal of the Soil Mechanics and Foundations Division, Proceedings of the American Society of Civil Engineers, pp. 309-331.

Lambe, T.W. and Marr, W.A. (1979), ***Stress Path Method: Second Edition***, Journal of the Geotechnical Engineering Division, ASCE, pp. 727-738.

Lambe, T.W. and Whitman, R.V. (1979), ***Soil Mechanics,*** SI version, Wiley.

Malangraki, V. and Toll D.G. (2000), ***Triaxial Tests on Weakly Bonded Soil with Changes in Stress Path***, Journal of Geotechnical and Geo-environmental Engineering, pp. 282-291.

Mitchell, J.K. (1976), ***Fundamentals of Soil Behaviour***, Wiley, New York.

Ninham Shand Consulting Engineering (2001), ***Report on Particle Size Distribution of Maguga Dam Soils***, Ninham Shand Geotechnical Laboratory, Cape Town

Parry, R.H.G (1958), Correspondence ***On the Yielding of Soils***, Geotechnique, Volume 4, pp.183-186

Pender, M. J. (1980), ***Discussion on Stress Path Method***, Journal of the Geotechnical Engineering Division, September 1980, pp. 1068-1077.

Prieman, R.A. (1982), Annual Book of ASTM Standards, Volume 04.08. ***Soil, Rock and Building Stones***, Easton, USA

Roscoe, K.H. (1958), ***On the Yielding of Soils***, Geotechnique, London, Volume 8, pp. 22-53.

Schofield, A.N. and Wroth, C.P. (1968), ***Critical State Soil Mechanics***, McGraw-Hill Book Co., London, pp. 282-291.

Terzaghi, K. (1936), ***The Shearing Resistance of Saturated Soils and the Angle between the Planes of Shear***, Proceedings of the 1st International Conference Soil Mechanics & Foundation Engineering, Volume 1, Cambridge, USA, pp. 54-56.

Toll, D.G. (1993), ***A computer control system for stress path triaxial testing***, Developments in civil and construction engineering computing, B. H. V. Topping, ed., Civil-Comp Press, Edinburgh, pp. 107-113.

Van Koersveld, A. (2001), ***Critical State and Maguga Dam Material Behaviour***, B. Sc. Thesis, University of Cape Town, Department of Civil Engineering.

Wood, D.M. (1990), ***Soil Behaviour and Critical State Soil Mechanics***, Cambridge University Press, pp. 310-353.

Wroth, C.P. (1984), ***Predictive Soil Mechanics***, Thomas Telford, London.

APPENDICES

STANDARD TEST METHOD FOR ATTERBERG LIMITS OF SOILS

Determination of the Atterberg Limits of Soils (BS 1377:1975, Test 2B and BS 1377:1975, Test 3)

Liquid Limit: The water content at the boundary between liquid and plastic states, expressed as a percentage of the oven-dried soil mass

Plastic Limit: The water content at the boundary between the plastic and semisolid, expressed as a percentage of the oven-dried soil mass.

Apparatus

- Liquid limit device consisting of Casagrande device and cone penetrometer.
- Grooving tool conforming to specification dimensions.
- Containers, spatulas and miscellaneous equipment used in test procedure.
- Analytical balance sensitive to 0,01 g.

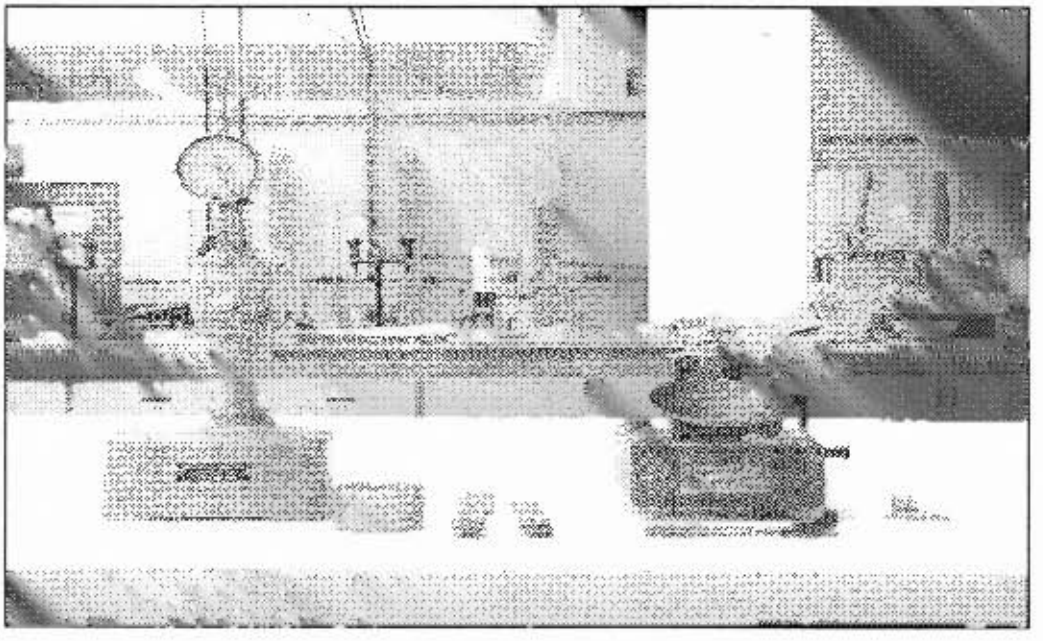

Cone penetrometer and Casagrande liquid limit devices

Testing Procedure

LIQUID LIMIT

- Inspect the liquid limit devices to determine that the devices are in good working order and conform to the specification dimensions.

- A sufficient quantity of air-dried soil material is placed in an evaporation dish (or on suitable surface) and thoroughly mixed with 20 to 30 ml of de-aired water by kneading and stirring with a spatula.

- **Casagrande:** When sufficient water has been thoroughly mixed with the soil to produce a consistency that will require 20 to 30 drops of the brass cup, a portion of the mixture is squeezed down and spread into position with as few strokes of the spatula as possible.

  Cone Penetrometer: Similarly, for the cone penetrometer test, the mixture is squeezed into a cup until the mixture is flush with the edge of the cup.

- **Casagrande:** The soil in the brass cup is divided into two equal halves by firm strokes of the grooving tool along the centre-line of the cup. Tearing or slipping of the surface should be avoided. The cup is lifted and dropped at approximately 2 rps, until the two halves come into contact with each other along a distance of approximately 10 mm. The process is repeated until a reliable range of results is established.

  Cone Penetrometer: The cup containing the mixture is placed onto the pedestal and the cone tip is carefully positioned in contact with the surface of the mixture and an initial displacement reading is recorded. The release switch is released and the cone penetrates the mixture. After five seconds the release switch is pressed to a stop position and another displacement reading as well as a representative moisture content sample is taken. The process is repeated until the displacement readings are within 0.5 mm of each other.

PLASTIC LIMIT

- A small quantity of dry soil material is mixed with a minuscule quantity of de-aired water and squeezed into an ellipsoidal shape between the fingers. This mass is rolled on an appropriate flat surface with sufficient pressure to roll the mass into a thread of uniform diameter.

- When the diameter of the thread becomes approximately 5 mm and the thread crumbles under the pressure required for rolling (can no longer be rolled into a thread). This shall be considered the end point and the portions of the crumbled soil are weighed and oven-dried to attain the moisture content.

FINAL CALCULATION

Plasticity Index (PI) = Liquid Limit (LL) – Plastic Limit (PL)

STANDARD TEST METHOD FOR SPECIFIC GRAVITY OF SOIL

Determination of the Specific Gravity (BS 1377:1975, Test 6B)

Specific gravity is the ratio of the weight in air of a given volume of a material at a constant temperature, to the weight in air of an equal volume of distilled water at a constant temperature.

Apparatus

- Density bottles (50 ml) with stoppers, numbered and calibrated.
- Constant-temperature water-bath maintained at 25 °C, with shelf for holding density bottles.
- Vacuum desiccator suitable for three density bottles per soil sample.
- Vacuum pump and vacuum tubing.
- Wash bottle, small glass funnel and small spatula.
- Analytical balance sensitive to 0,001 g.

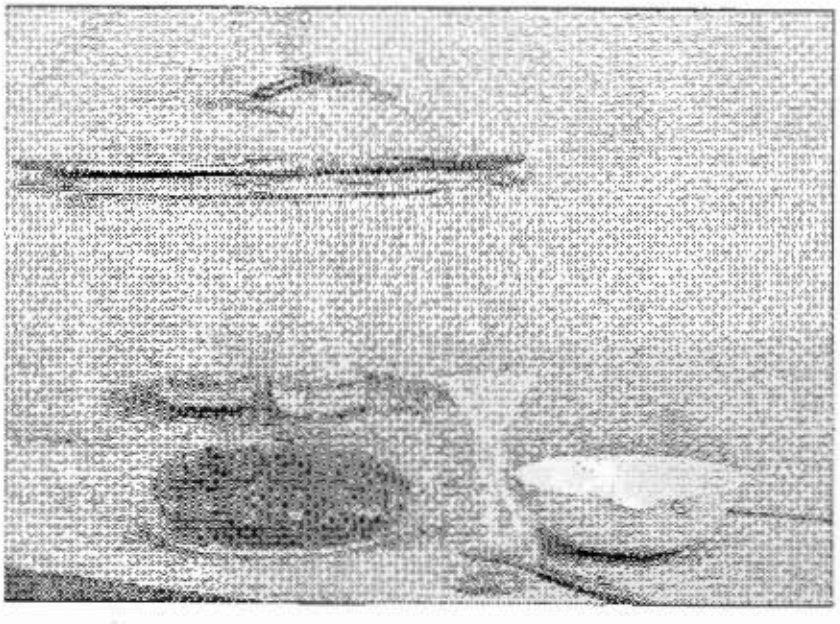

Specific gravity apparatus-density bottles in dessicator

Testing Procedure

PRE-INITIATION OF SPECIFIC GRAVITY TEST

- Calibration of the density bottles is necessary before the test can commence, as the bottles are prone to weight distortions when dried in an oven. The density bottles and stoppers are weighed individually (M_b). The bottles are filled with water and placed under vacuum in the desiccator

- When the extraction of the oxygen in the density bottle ceases, the bottles are removed from the desiccator and filled carefully with distilled water to the rim of the bottle. The stopper is inserted and the excess water is carefully wiped away

- The density bottles are placed in the constant warm-bath maintained at 25 °C for 1 hour. The bottles are then removed from the bath and wiped dry carefully and quickly so as to avoid changes in temperature. They are then weighed to the nearest 0,001g ($M_b + M_{wt}$). The volume of the beaker with respect to the water (V_{bb}) is then recorded as $V_{bb} = M_{wt}/\rho_{wt}$.

INITIATION OF SPECIFIC GRAVITY TEST

- A sample of 50 – 100g of the dry soil material, together with a representative proportion of the gravel-sized particles is prepared. The soil is ground with a pestle and mortar and the dry material that passes through the 425 μm sieve is collected. During the oven-drying of the test material it is essential that the oven is maintained at a temperature of 40 °C or below, for a time period deemed long enough by the tester. Oven-drying at a temperature of 40 °C instead of the standard 105 – 110 °C minimises the chemical changes that would affect the specific gravity value.

- Place approximately 5 g of the fine test material, directly from the cooling desiccator, into each density bottle (three bottles used for test) and weigh the bottle together with the stopper and the soil ($M_1 = M_b - M_d$). Add the distilled

water, by running the liquid carefully down the side of the bottle, until the soil is covered (about half-full) and there is no visible entrapped air. Place the bottles in the vacuum desiccator (without stoppers) and apply the vacuum pressure gradually.

- The vacuum is maintained until there is no air left to 'bubble' out of the soil. The bottles can be removed individually and agitated frequently by the tester. Care must be taken to ensure that particles in suspension are not lost through the bottle opening while the bottle is agitated.

- The agitation process is repeated until the complete removal of air has taken place. The complete elimination of air within the soil is necessary for obtaining consistent results. If the tester is undecided whether the air has been exhausted in the soil (due to murkiness on the sides of the bottle), then place the bottles in the vacuum desiccator for a longer period of time.

- Remove the density bottles once satisfied with air extraction and fill the bottles with further distilled water. Insert the stopper carefully and wipe away any excess water that exudes from the capillary tube within the stopper.

- Place the stoppered density bottle in the constant temperature bath so that it is immersed up to the neck of the bottle. The density bottles should be placed in the bath until they have attained the temperature of the bath (a time period of 1 hour is specified in BS 1377:1975, Test 6B).

- Remove each bottle from the bath and carefully wipe away any water that adheres to the outside of the bottles. Prolonged contact with the air and hands must be avoided as this may raise the temperature of the bottle.

- The density bottles are weighed individually to the nearest 0,001g and recorded as $M_2 = M_d + M_b + M_w$.

FINAL PROCEDURAL CALCULATIONS

- Mass of water in density bottle (M_{wt}) = $M_2 - M_1$
- Volume of water in bottle (V_{wt}) = $\frac{M_{wt}}{\rho_{wt}}$
- Volume of specimen (V_s) = $V_{bti} - V_{wt}$
- Mass of specimen (M_s) = $M_1 - M_b$
- Density of specimen (ρ_s) = $\frac{M_s}{V_s}$

Hence specific gravity (G_s) = $\frac{\rho_s}{\rho_{wt}}$ [where ρ_{wt} = 1.000g/cm^3]

STANDARD TEST METHOD FOR PROCTOR COMPACTION OF SOIL

Determination of Moisture-Dry Density relations of Soils (BS 1377:1983, Test 12)

Proctor Compaction tests deal with the determination of the relationship between the density of soils and the moisture content for a certain degree of compaction effort. The moisture conditions that produce the most efficient compaction at an optimum dry density are determined.

Apparatus

- Cylindrical steel moulds 101.6 mm in diameter, having a capacity 944cm^3 ± 11 cm^3 and conforming to specifications. The moulds are fitted with removable extension collars.
- A manual rammer with a mass of 2,5 kg ±25g and a circular contact face with a diameter of 50 mm, conforming to specifications. The rammer is equipped with a guide-sleeve that will not restrict the free-fall of the rammer.
- Extracting platform so that the sample can be extruded from the mould.
- Evaporating dishes necessary for moisture content determination.

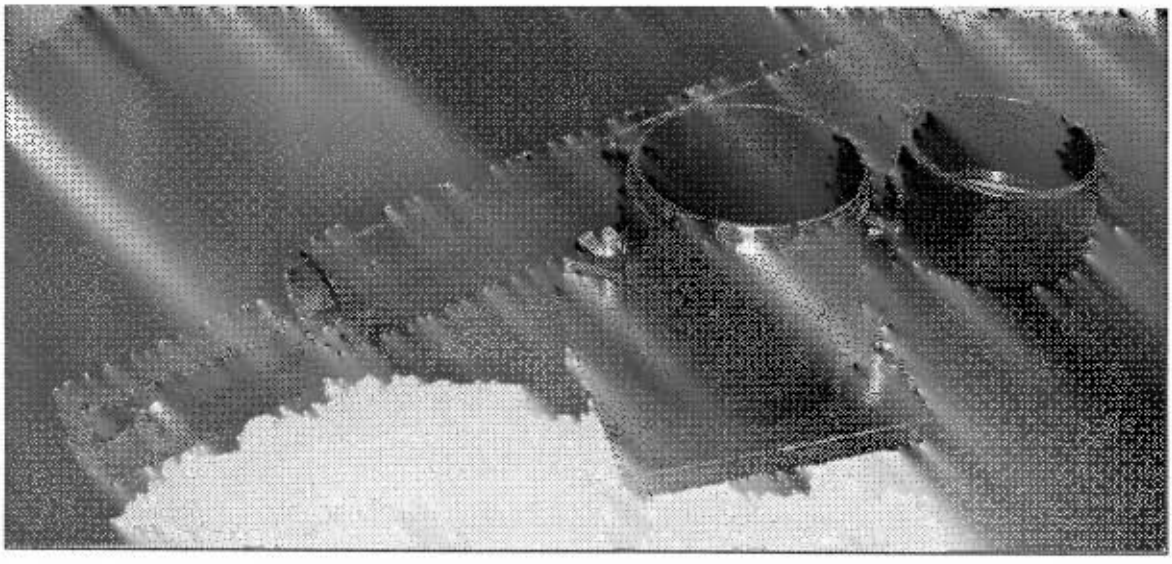

Proctor compaction apparatus – steel mould with 2,5 kg rammer

Testing Procedure

SAMPLE PREPARATION

- The original bulk sample is sieved through a 19 mm sieve and all soil particles retained on the sieve are removed. A representative portion of the bulk sample is taken, an amount weighing approximately 10 kg.

- A series of five specimens are prepared by adding increasing amounts of water to each sample (one specimen is available as an extra test). The moisture contents of the specimens are selected so that the optimum moisture relationships are bracketed within the predetermined moisture contents.

- The specimens are thoroughly mixed to ensure an even distribution of moisture. They are then placed in a sealed container and allowed to stand for 24 hours, so that the full hydration process can take place.

SPECIMEN COMPACTION

- Check that the steel mould, extension collar and base plate are clean, dry and conform to the specifications shown in BS 1377:1975. Calculate the volume of the mould and record the weight of the mould including the base plate

- Place the steel mould on a rigid base and add the first of three soil layers. The soil is compacted by applying 25 blows of the rammer from a height of 300mm. The surface of the first two compacted layers should be lightly scrapped to facilitate bonding of the layers. To ensure an efficient compaction effort a systematic sequence should be applied.

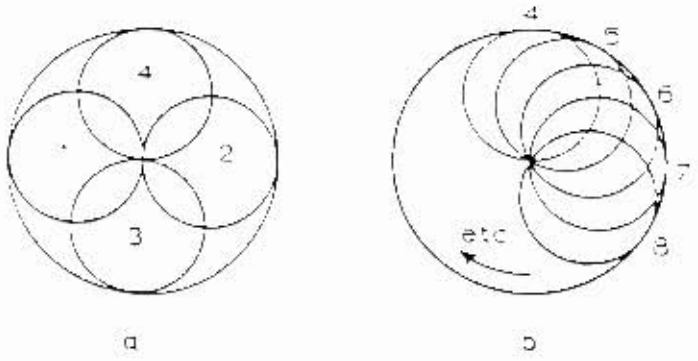

Systematic application of blow sequence

- On completion of the layered compaction effort, the extension collar is removed carefully and the excess soil is trimmed away until the surface of the compacted soil is flush with the edges of the mould. The base plate, mould and compacted soil is then weighed.

- The compacted sample is extracted and placed on a tray. The extracted sample is then cut into quarters and a representative portion (preferably the core) is taken for moisture content determination.

- On completion of all the moisture content determinations, a graph showing the relationship of dry density (kg/m^3) versus moisture content (%) can be plotted and the maximum dry density at optimum moisture content can be extrapolated from it.

STANDARD TEST METHOD FOR ONE-DIMENSIONAL CONSOLIDATION PROPERTIES OF SOILS

Determination of the Consolidation Properties of Soils (ASTM-D2435-80)

This method covers the procedure for determining the rate and magnitude of consolidation of soil when it is restrained laterally and loaded and drained axially.

Apparatus

- Load device suitable for applying vertical loads to the specimen.
- Consolidometer device to hold the specimen in a ring, which is fixed to the base.
- Analytical balance sensitive to 0,1 g of the total mass of the test specimen.
- Dry oven that is maintained at 110 ± 5°C.
- Miscellaneous equipment including compaction block, hammer, trimming device and vernier caliper, used in the preparation of the specimen.

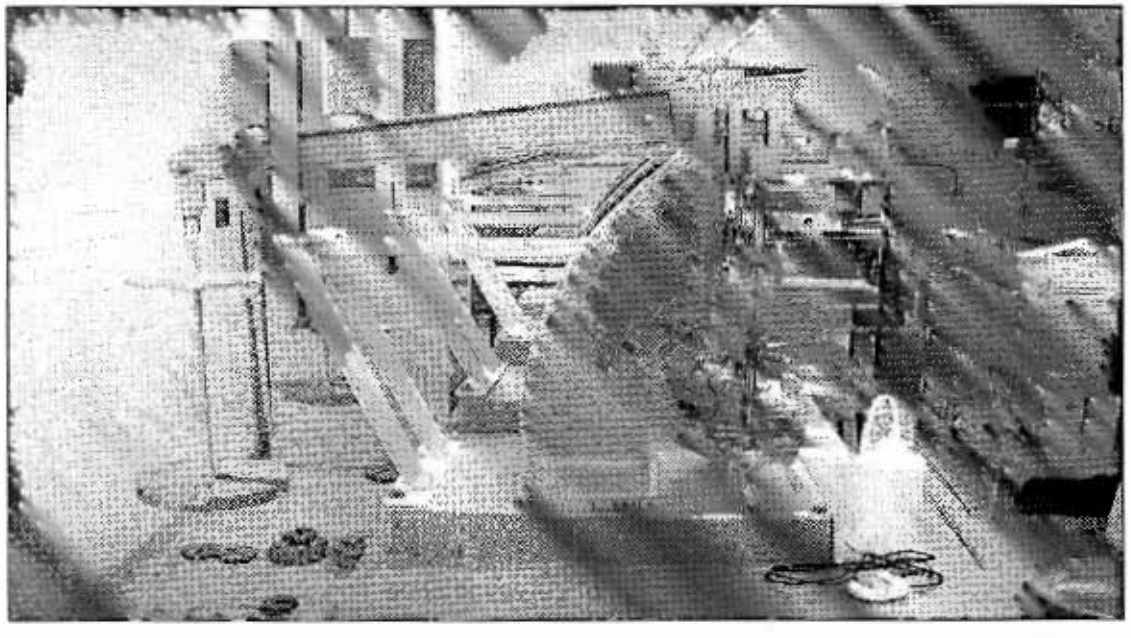

Consolidometer platform showing loading device and consolidation cell in place

Testing Procedure

PREPARATION OF APPARATUS

- Check the consolidation cell is clean and not distorted, that the o-ring seal is in good condition. Assemble the cell components of the consolidation cell to ensure that they fit together properly. Once satisfied with the components of the consolidation cell, dis-assemble the components and moisten the inside surfaces of the cell as well as the porous discs

- Check loading beam can move freely and the loading hanger is fitted in the correct position.

- With the loading hanger in the vertical position, adjust the counterbalance as necessary so that the beam and hanger assembly is in balance Make sure all screwed connections are tightly secured.

PREPARATION, PLACEMENT and LOADING OF SPECIMEN

- Compaction is done by hand tamping with a wooden rod until a specified, consistent compaction effort is attained. After compaction the specimens are trimmed and weighed, then stored for approximately 24 hours. The mass of the test sample is measured before and after to ensure that no loss in moisture content occurred.

- The porous stones and the filter paper are wetted and the sample (in a steel ring) is placed into position. The steel consolidometer rings are tightened and the specimen is enclosed The consolidation cell is placed on the loading platform.

- The loading hanger is again adjusted to accommodate the imbalance of the consolidation cell (and water, which will be added). The displacement dial is adjusted so that contact with the consolidation cell is established and the dial reading is recorded. The loading and unloading procedure is then followed and the deformation for each load application is recorded.

APPENDIX D-6 Predicted Soil Response of Maguga Clay consolidated at 75 kPa

	η^*	$\{(M^2+\eta^2)/(M^2+\eta_{(c)}^2)\}^{0.786}$	δp (kPa)	p' (kPa)	$\delta p'$ (kPa)	$\delta p-\delta p'=u$ (kPa)	q (kPa)	Plastic Volumetric Strain (%)	Plastic Shear Strain (%)	Shear Strain (%)
10	0.00	1.000	75.00	75.00	0.00	0.00	0.00	0.000	0.000	0.00
11	0.00	1.000	75.25	75.00	0.00	0.25	0.75	0.001	0.001	0.00
12	0.00	1.000	75.50	74.99	0.01	0.52	1.50	0.004	0.003	0.00
13	0.00	1.000	75.76	74.97	0.02	0.79	2.25	0.007	0.005	0.01
14	0.00	1.001	76.01	74.95	0.02	1.06	3.00	0.010	0.007	0.02
15	0.00	1.001	76.27	74.92	0.03	1.35	3.75	0.013	0.009	0.03
16	0.00	1.001	76.53	74.89	0.03	1.64	4.49	0.016	0.011	0.04
17	0.00	1.002	76.79	74.85	0.04	1.94	5.24	0.019	0.013	0.05
18	0.01	1.003	77.05	74.81	0.05	2.25	5.98	0.021	0.015	0.07
19	0.01	1.003	77.32	74.75	0.05	2.57	6.73	0.024	0.017	0.08
20	0.01	1.004	77.59	74.70	0.06	2.89	7.47	0.027	0.019	0.10
21	0.01	1.005	77.85	74.63	0.06	3.22	8.21	0.030	0.021	0.12
22	0.01	1.006	78.13	74.56	0.07	3.56	8.95	0.033	0.023	0.15
23	0.02	1.007	78.40	74.49	0.08	3.91	9.68	0.035	0.025	0.17
24	0.02	1.008	78.67	74.41	0.08	4.26	10.42	0.038	0.027	0.20
25	0.02	1.009	78.95	74.32	0.09	4.63	11.15	0.041	0.029	0.23
26	0.03	1.010	79.23	74.23	0.09	5.00	11.88	0.044	0.031	0.26
27	0.03	1.012	79.51	74.13	0.10	5.38	12.60	0.046	0.033	0.29
28	0.03	1.013	79.79	74.03	0.10	5.76	13.32	0.049	0.035	0.33
29	0.04	1.015	80.07	73.92	0.11	6.15	14.04	0.051	0.037	0.37
30	0.04	1.016	80.36	73.80	0.11	6.56	14.76	0.054	0.039	0.41
31	0.04	1.018	80.65	73.68	0.12	6.96	15.47	0.057	0.041	0.45
32	0.05	1.020	80.94	73.56	0.13	7.38	16.18	0.059	0.043	0.49
33	0.05	1.021	81.23	73.42	0.13	7.80	16.89	0.062	0.044	0.53
34	0.06	1.023	81.52	73.29	0.14	8.23	17.59	0.064	0.046	0.58
35	0.06	1.025	81.82	73.15	0.14	8.67	18.29	0.067	0.048	0.63
36	0.07	1.027	82.12	73.00	0.15	9.12	18.98	0.069	0.050	0.68
37	0.07	1.030	82.42	72.85	0.15	9.57	19.67	0.071	0.051	0.73
38	0.08	1.032	82.72	72.69	0.16	10.03	20.35	0.074	0.053	0.78
39	0.08	1.034	83.03	72.53	0.16	10.50	21.03	0.076	0.055	0.84
40	0.09	1.036	83.33	72.36	0.17	10.97	21.71	0.078	0.056	0.89
41	0.10	1.039	83.64	72.19	0.17	11.45	22.38	0.081	0.058	0.95
42	0.10	1.041	83.96	72.02	0.18	11.94	23.05	0.083	0.060	1.01
43	0.11	1.044	84.27	71.84	0.18	12.43	23.71	0.085	0.061	1.07
44	0.12	1.047	84.59	71.65	0.18	12.93	24.36	0.087	0.063	1.13
45	0.12	1.050	84.91	71.46	0.19	13.44	25.01	0.089	0.064	1.20
46	0.13	1.052	85.23	71.27	0.19	13.96	25.66	0.091	0.066	1.26
47	0.14	1.055	85.55	71.07	0.20	14.48	26.30	0.093	0.067	1.33
48	0.14	1.058	85.88	70.87	0.20	15.01	26.93	0.095	0.068	1.40
49	0.15	1.061	86.21	70.66	0.21	15.54	27.56	0.097	0.070	1.47
50	0.16	1.065	86.54	70.45	0.21	16.08	28.18	0.099	0.071	1.54
51	0.17	1.068	86.87	70.24	0.21	16.63	28.80	0.101	0.072	1.61
52	0.18	1.071	87.21	70.02	0.22	17.19	29.41	0.102	0.074	1.69
53	0.18	1.074	87.55	69.80	0.22	17.75	30.01	0.104	0.075	1.76
54	0.19	1.078	87.89	69.58	0.22	18.31	30.61	0.106	0.076	1.84
55	0.20	1.081	88.24	69.35	0.23	18.89	31.21	0.107	0.077	1.91
56	0.21	1.085	88.58	69.12	0.23	19.47	31.79	0.109	0.078	1.99
57	0.22	1.089	88.93	68.88	0.23	20.05	32.37	0.110	0.079	2.07
58	0.23	1.093	89.29	68.64	0.24	20.64	32.95	0.112	0.081	2.15
59	0.24	1.096	89.64	68.40	0.24	21.24	33.52	0.113	0.082	2.23
60	0.25	1.100	90.00	68.16	0.24	21.84	34.08	0.115	0.083	2.32
61	0.26	1.104	90.36	67.91	0.25	22.45	34.64	0.116	0.084	2.40
62	0.27	1.108	90.73	67.66	0.25	23.06	35.18	0.118	0.085	2.48
63	0.28	1.113	91.09	67.41	0.25	23.68	35.73	0.119	0.085	2.57

54	0 29	1.117	91.46	67.16	0.26	24.31	36.26	0.120	0.086	2.66
55	0.30	1.121	91.84	66.90	0.26	24.94	36.79	0.121	0.087	2 74
56	0.31	1.125	92.21	66.64	0.26	25.58	37.32	0.122	0.088	2.83
57	0 32	1.130	92.59	66.38	0.26	26.22	37.83	0.123	0.089	2.92
58	0.34	1.134	92.98	66.11	0.26	26.86	38.34	0.125	0.090	3.01
59	0 35	1.139	93.36	65.84	0.27	27.52	38.85	0.126	0.090	3.10
60	0.36	1.144	93.75	65.57	0.27	28.18	39.34	0.127	0.091	3.19
61	0.37	1.148	94.14	65.30	0.27	28.84	39.84	0.127	0.092	3.28
62	0.38	1.153	94.54	65.03	0.27	29.51	40.32	0.128	0.092	3.37
63	0.40	1 158	94.94	64.76	0.27	30.18	40.80	0 129	0.093	3.47
64	0.41	1.163	95.34	64.48	0 28	30.86	41 27	0.130	0.094	3.56
65	0.42	1 168	95.74	64.20	0.28	31.54	41.73	0.131	0 094	3.66
66	0.44	1.173	96 15	63.92	0 28	32 23	42.19	0.131	0.095	3.75
67	0.45	1.178	96.57	63.64	0.28	32.92	42.64	0.132	0.095	3.85
68	0.46	1.184	96.98	63.36	0.28	33.62	43.09	0.133	0.096	3.94
69	0.48	1.189	97.40	63.08	0.28	34 33	43 52	0.133	0 096	4.04
70	0.49	1.194	97.83	62.79	0.28	35.03	43.95	0.134	0 096	4.13
71	0.50	1.200	98.25	62.51	0.29	35.75	44.38	0.135	0.097	4.23
72	0.52	1.205	98.68	62.22	0.29	36.46	44.80	0.135	0.097	4.33
73	0.53	1.211	99.12	61.93	0.29	37.19	45.21	0.135	0.097	4.42
74	0.55	1.217	99.56	61.64	0.29	37.91	45 62	0.136	0.098	4 52
75	0.56	1.222	100.00	61 35	0.29	38.65	46.01	0 136	0 098	4.62
76	0.58	1.228	100.45	61.06	0.29	39.38	46.41	0.137	0.098	4.72
77	0.59	1.234	100.90	60.77	0.29	40.12	46.79	0.137	0.099	4.82
78	0.61	1.240	101.35	60.48	0.29	40.87	47 17	0.137	0.099	4 92
79	0.62	1.246	101.81	60.19	0.29	41 62	47.55	0.137	0.099	5.01
80	0.64	1.252	102.27	59.90	0.29	42.38	47.92	0.138	0.099	5.11
81	0.66	1.258	102.74	59.60	0.29	43.14	48.28	0.138	0.099	5.21
82	0.67	1.265	103.21	59.31	0.29	43.90	48 63	0.138	0.099	5.31
83	0.69	1.271	103.69	59.02	0.29	44.67	48.98	0.138	0.099	5.41
84	0.71	1.277	104.17	58.72	0.29	45.45	49.33	0.138	0.099	5.51
85	0.72	1.284	104.65	58.43	0.29	46.22	49.66	0 138	0.100	5 61
86	0.74	1.290	105 14	58.13	0.29	47.01	49.99	0.138	0.100	5.71
87	0.76	1.297	105 63	57.84	0.29	47.79	50.32	0 138	0.100	5.81
88	0.77	1.303	106.13	57.55	0.29	48.59	50.64	0.138	0.100	5.91
89	0.79	1.310	106.64	57.25	0.29	49.38	50.95	0.138	0.100	6.01
90	0.81	1.317	107.14	56.95	0.29	50.19	51.26	0.138	0.100	6.11
91	0.83	1.324	107.66	56.66	0.29	50.99	51.56	0.138	0.099	6.21
92	0.85	1.331	108.17	56.37	0.29	51.80	51.86	0 138	0.099	6.31
93	0.86	1 337	108 70	56 08	0.29	52.62	52.15	0.138	0 099	6.41
94	0.88	1.344	109.22	55.78	0.29	53.44	52.44	0.138	0.099	6.51
95	0.90	1.352	109.76	55.49	0.29	54.27	52.72	0.138	0.099	6.60
96	0 92	1 359	110.29	55.20	0.29	55 10	52.99	0.137	0.099	6.70
97	0.94	1.366	110.84	54.91	0.29	55.93	53.26	0.137	0.099	6.80
98	0 96	1.373	111.39	54.62	0.29	56.77	53.52	0.137	0.099	6.90
99	0.98	1.381	111.94	54.33	0.29	57.61	53.78	0.137	0 098	7.00
100	1.00	1 388	112.50	54.04	0.29	58.46	54.04	0.136	0.098	7 10
101	1.02	1.395	113.07	53.75	0.29	59 32	54 28	0.136	0.098	7.20
102	1 04	1.403	113.64	53.46	0.29	60.18	54.53	0.136	0.098	7.29
103	1 06	1.411	114.21	53.17	0 29	61.04	54.76	0.136	0.098	7.39
104	1.08	1.418	114.80	52.88	0.29	61.91	55.00	0.135	0 097	7.49
105	1.10	1.426	115.38	52.60	0.29	62.79	55 23	0.135	0.097	7.59
106	1.12	1.434	115.98	52.31	0 29	63.67	55 45	0.134	0.097	7.68
107	1.14	1.442	116.58	52.03	0.28	64.56	55.67	0.134	0 096	7.78
108	1.17	1.450	117.19	51.74	0.28	65.45	55.88	0.134	0.096	7.87
109	1.19	1.457	117.80	51.46	0.28	66.34	56.09	0.133	0.096	7.97
110	1.21	1.466	118.42	51.18	0.28	67.25	56.29	0 133	0.096	8.07
111	1.23	1.474	119.05	50.89	0.28	68.15	56.49	0.132	0.095	8 16
112	1.25	1.482	119.68	50.61	0.28	69.07	56.69	0.132	0.095	8.26
113	1.28	1 490	120 32	50 34	0 28	69 99	56.88	0.131	0 095	8.35

4	1 30	1.498	120.97	50.06	0.28	70.91	57.07	0.131	0.094	8.44
5	1.32	1.507	121.62	49.78	0.28	71.84	57.25	0.130	0.094	8.54
6	1.35	1.515	122.28	49.50	0.28	72.78	57.43	0.130	0.093	8.63
7	1.37	1.523	122.95	49.23	0.27	73.72	57.60	0.129	0.093	8.72
8	1.39	1.532	123.63	48.96	0.27	74.67	57.77	0.129	0.093	8 82
9	1.42	1.541	124.31	48.68	0.27	75.63	57.93	0.128	0.092	8.91
0	1.44	1.549	125.00	48.41	0.27	76.59	58.09	0.128	0.092	9.00
1	1.46	1.558	125.70	48.14	0.27	77.56	58.25	0.127	0.091	9.09
2	1.49	1.567	126.40	47.87	0.27	78.53	58.40	0.127	0.091	9.18
3	1.51	1.575	127.12	47 60	0.27	79.51	58.55	0.126	0.091	9.27
4	1.54	1.584	127.84	47.34	0.27	80.50	58.70	0.125	0.090	9.37
5	1.56	1.593	128.57	47.07	0.27	81.50	58.84	0.125	0.090	9.45
6	1.59	1.602	129.31	46.81	0.26	82.50	58.98	0.124	0.089	9.54
7	1.61	1 611	130.06	46.55	0 26	83.51	59.11	0 124	0.089	9.63
8	1.64	1.620	130.81	46.28	0.26	84.53	59.24	0.123	0.089	9.72
9	1.66	1.630	131.58	46.02	0.26	85.55	59.37	0.122	0.088	9.81
0	1.69	1.639	132.35	45.77	0.26	86.59	59.50	0.122	0.088	9.90
1	1.72	1.648	133.14	45.51	0.26	87.63	59.62	0.121	0.087	9.98
2	1.74	1.657	133.93	45.25	0.26	88.68	59.73	0.121	0.087	10.07
3	1.77	1.667	134.73	45.00	0.25	89.73	59.85	0.120	0.086	10.16
4	1.80	1.676	135.54	44.74	0.25	90.80	59.96	0.119	0.086	10.24
5	1.82	1.686	136.36	44.49	0.25	91.87	60.06	0.119	0 085	10.33
6	1.85	1.695	137.20	44.24	0.25	92.95	60.17	0.118	0 085	10.41
7	1.88	1.705	138.04	43.99	0.25	94.05	60.27	0.117	0.084	10.50
8	1.90	1.715	138.89	43.74	0.25	95.15	60.37	0.117	0.084	10 58
9	1.93	1.724	139.75	43.50	0.25	96.26	60.46	0.116	0.084	10.67